IMPERIAL

John Adams Institute for Accelerator Science

Betatron Radiation - Applications

Eupraxia-Doctoral Network Camp III: Innovation

Zulfikar Najmudin

7th October 2025, University of Pecs

EuPRAXIA Doctoral Network

X-ray Sources

X-ray sources

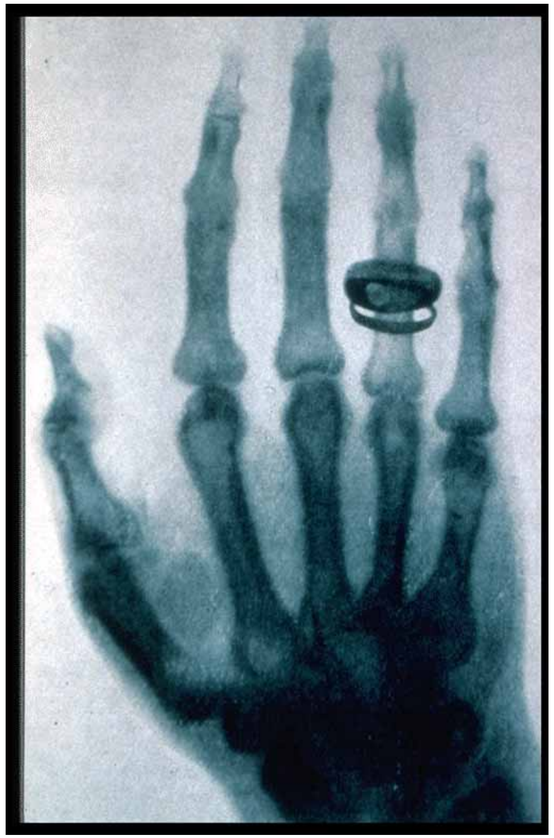

Roentgen’s first radiograph

Röntgen discovers the x-ray (1895) and immediately realises its use for taking medical radiographs.

Röntgen awarded first Nobel Prize for discovery of x-rays (1901).

Conventional x-ray sources limited by maximum current (~ 100 mA due to melting) and minimum source size

Radiation from bending magnets predicted by Ivanenko and Pomeranchuk (1944) and Schwinger (1945), and observed by F.R. Elder, A.M. Gurewitsch, R.V. Langmuir, and H.C. Pollock in a synchrotron accelerator (1947)

“The radiation is seen as a small spot of brilliant white light by an observer looking into the vacuum tube tangent to the orbit and toward the approaching electrons.”

Synchrotrons and Free Electron Lasers

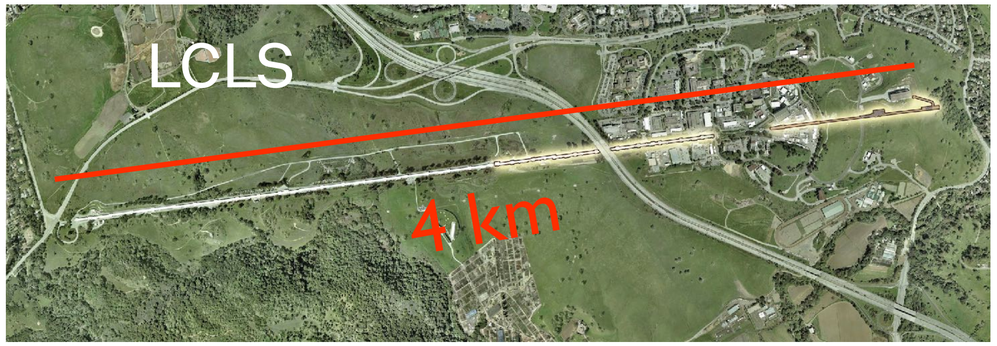

Brilliance of x-ray source increases with electron energy. Most synchrotron light sources now run with electron energy » GeV (ESRF runs at 6 GeV).

4th generation x-ray source (such as ESRF-EBS) offer brightness > 10^{22} ph s^{-1} mm^{-2} $mrad^{-2}$ $(0.1\%\ BW)^{-1}$

Higher quality beams and longer undulators can lead to feedback and coherent gain → free electron lasers

X-ray FELs (such as LCLS and Euro XFEL) offer brightness > 10^{33} ph s^{-1} mm^{-2} $mrad^{-2}$ $(0.1\%\ BW)^{-1}$

LCLS-II runs at up to 15 GeV

“bubble” plasma wave

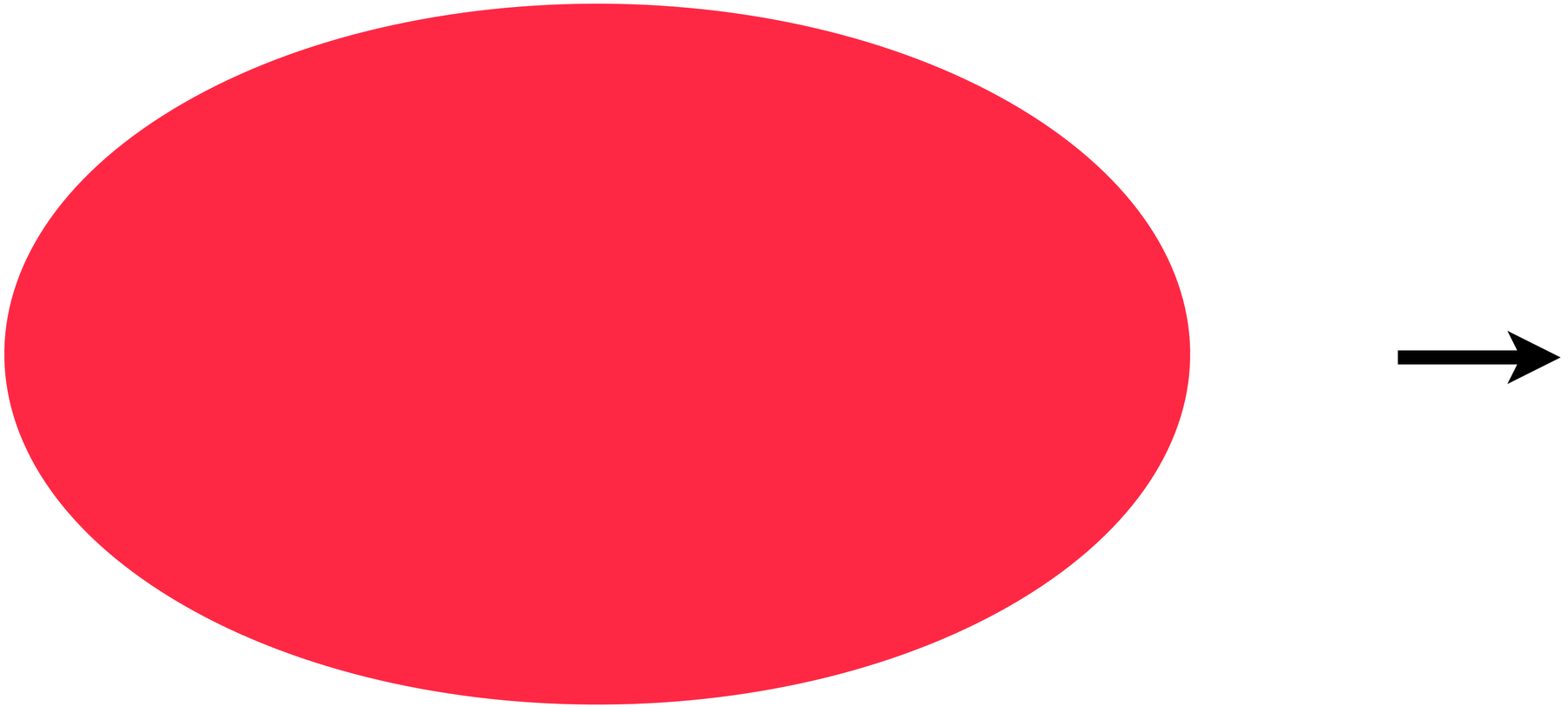

“bubble” plasma wave

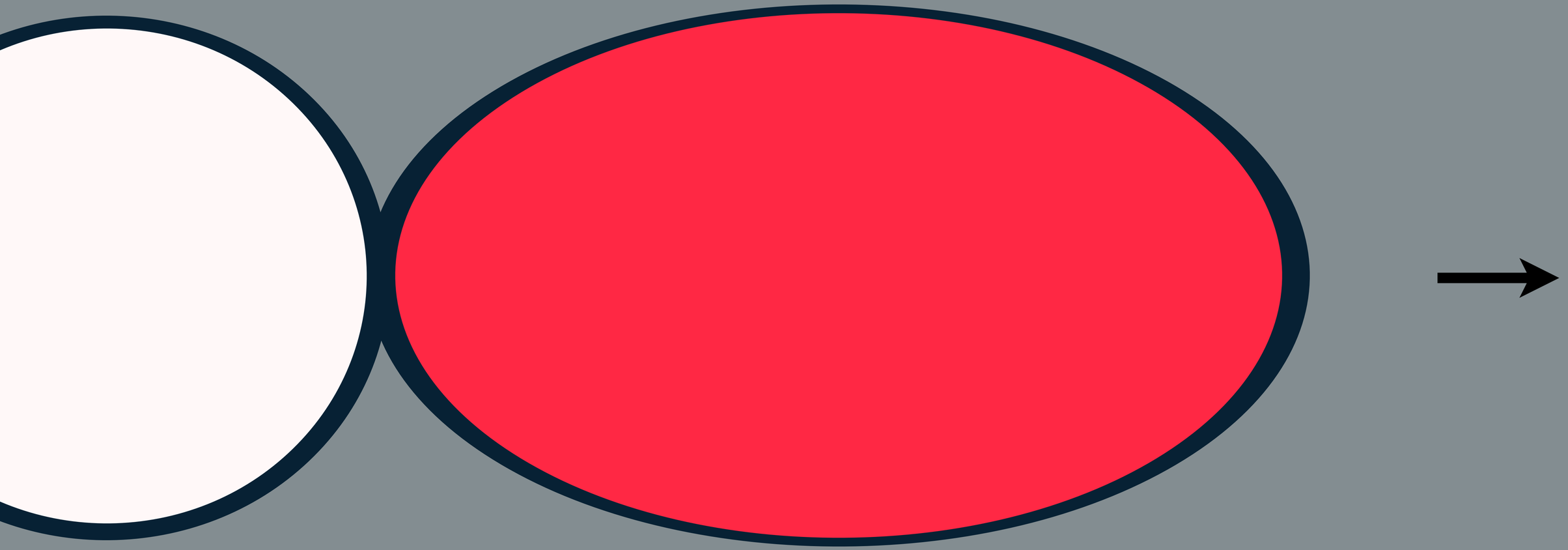

“bubble” plasma wave

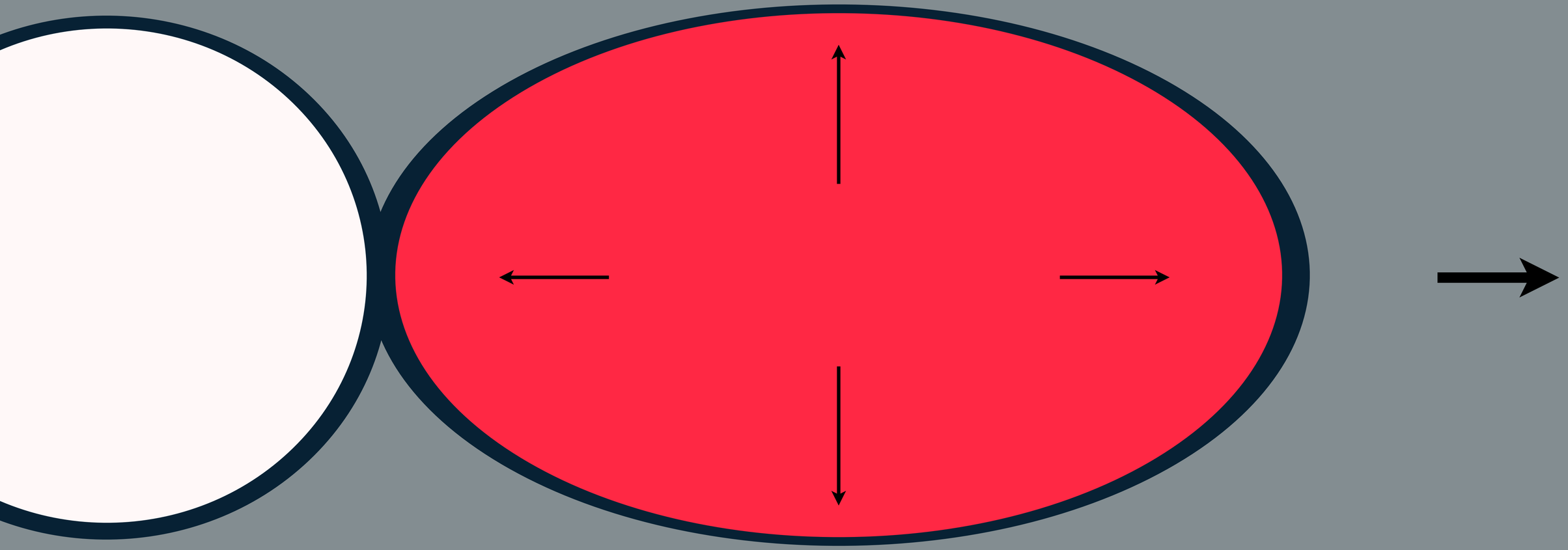

$$E = 10^{11}\ \mathrm{Vm}^{-1}$$

trapping

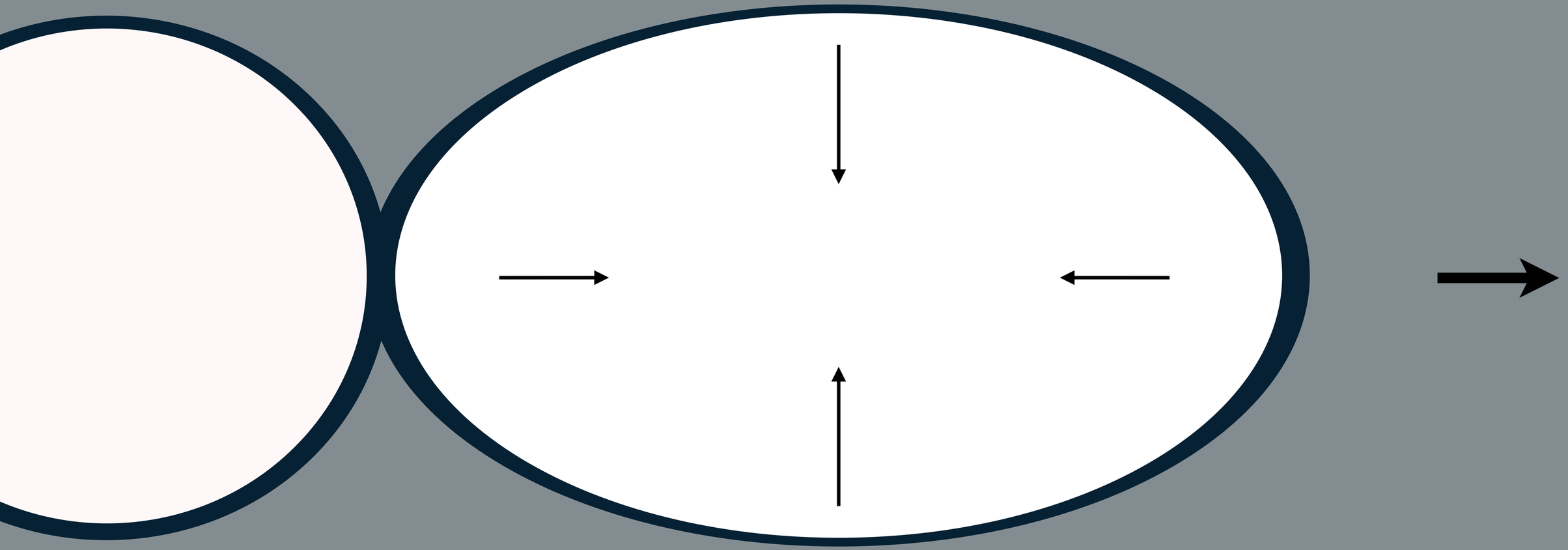

trapping

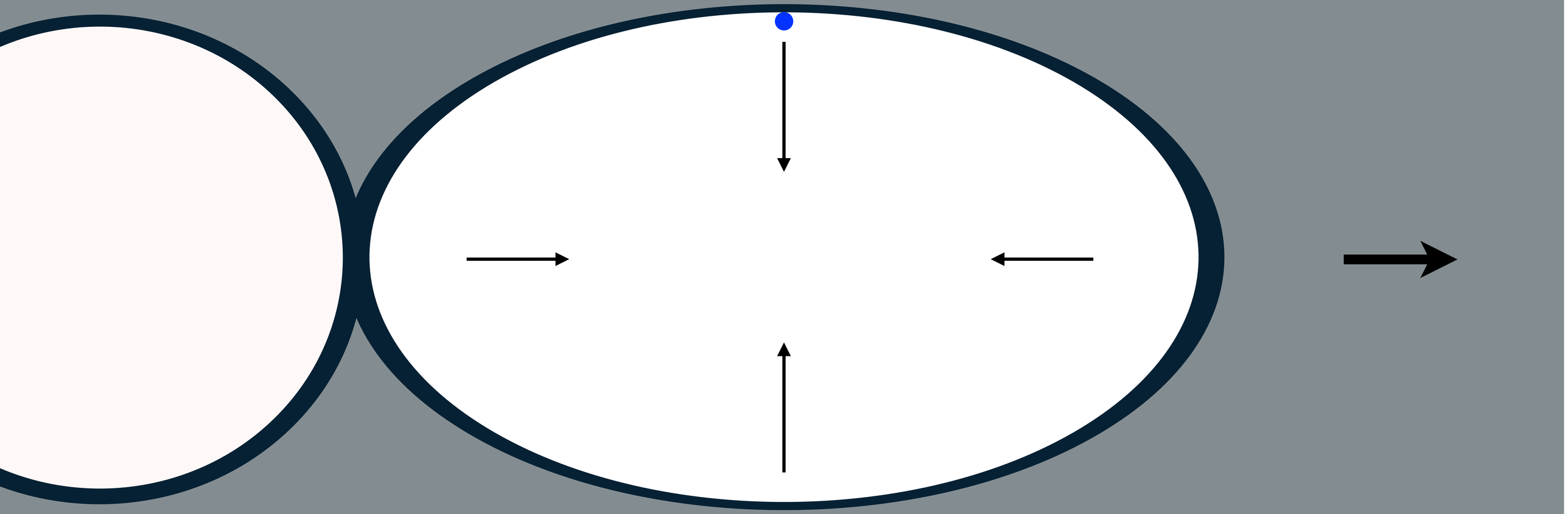

trapping

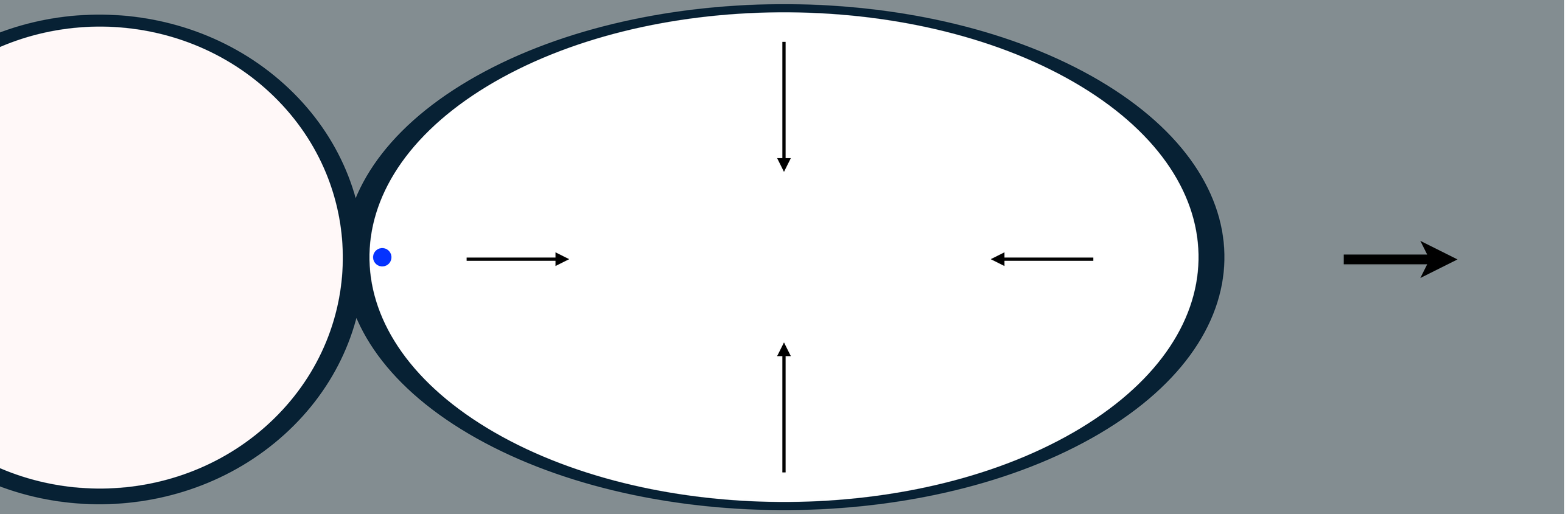

acceleration and undulation

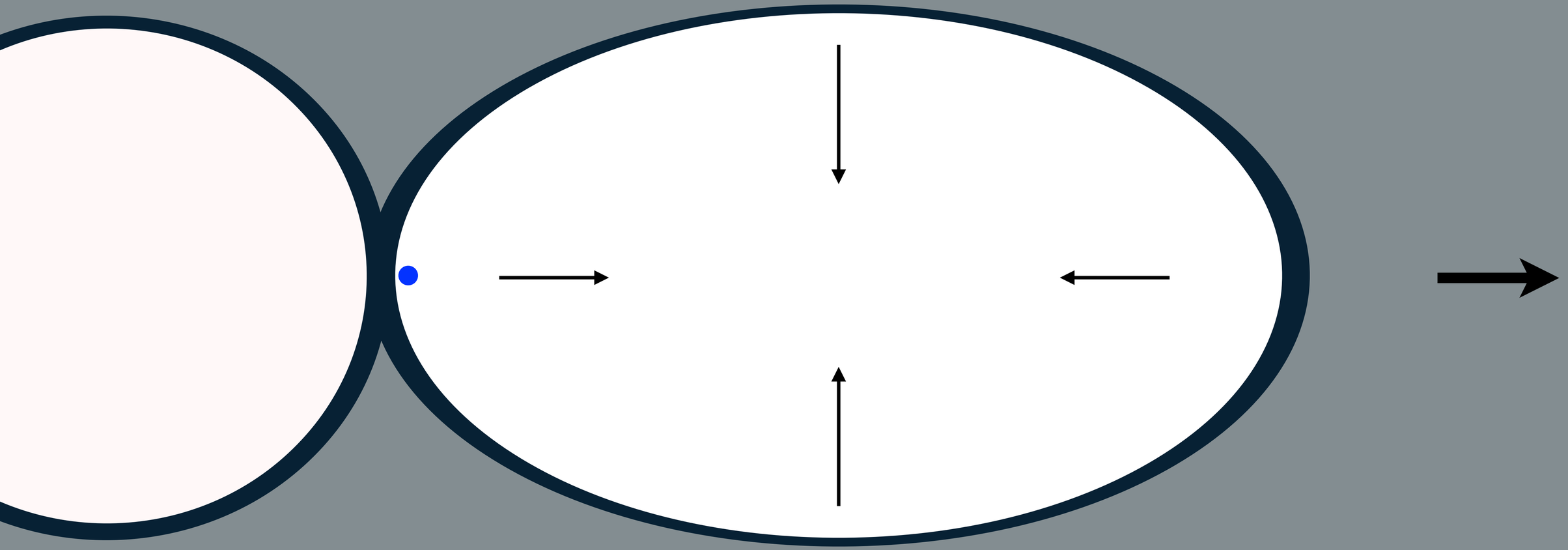

acceleration and undulation

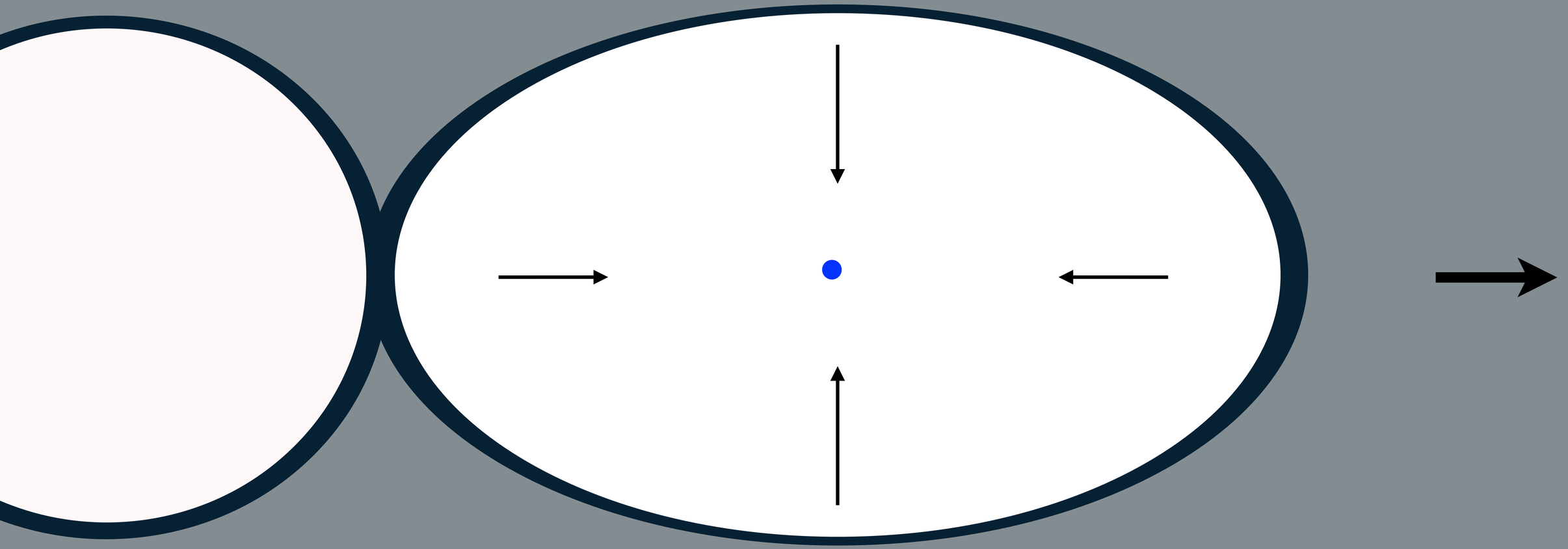

acceleration and undulation

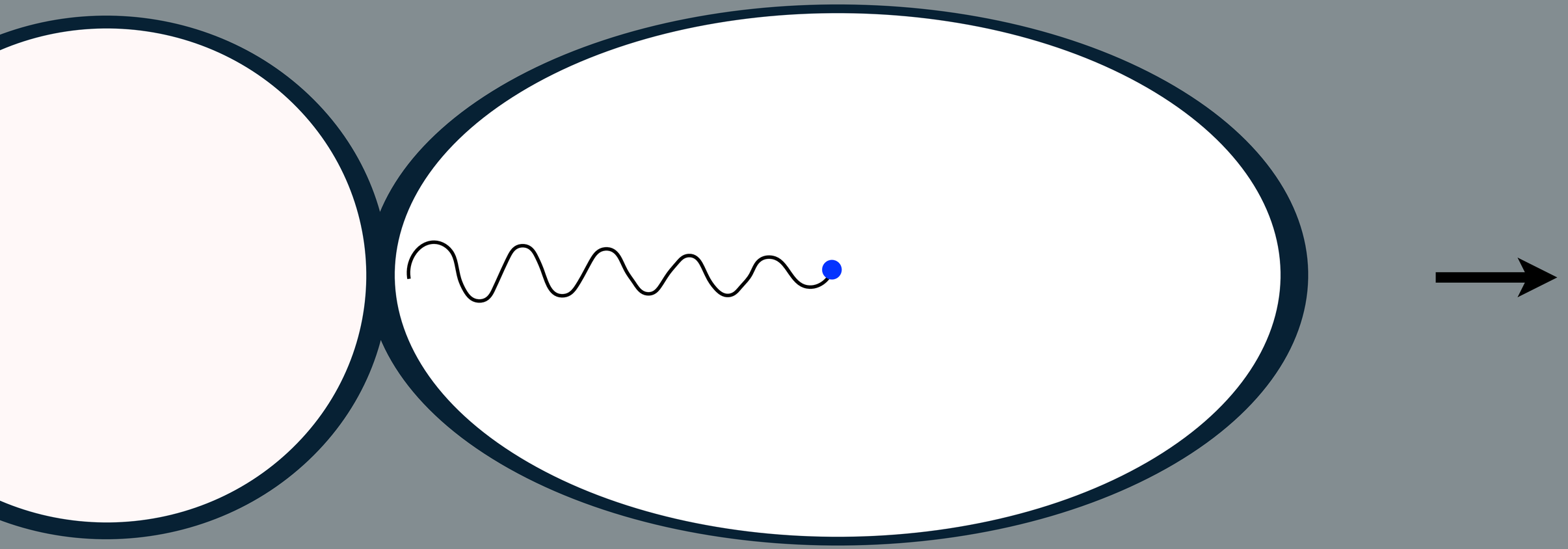

radiation

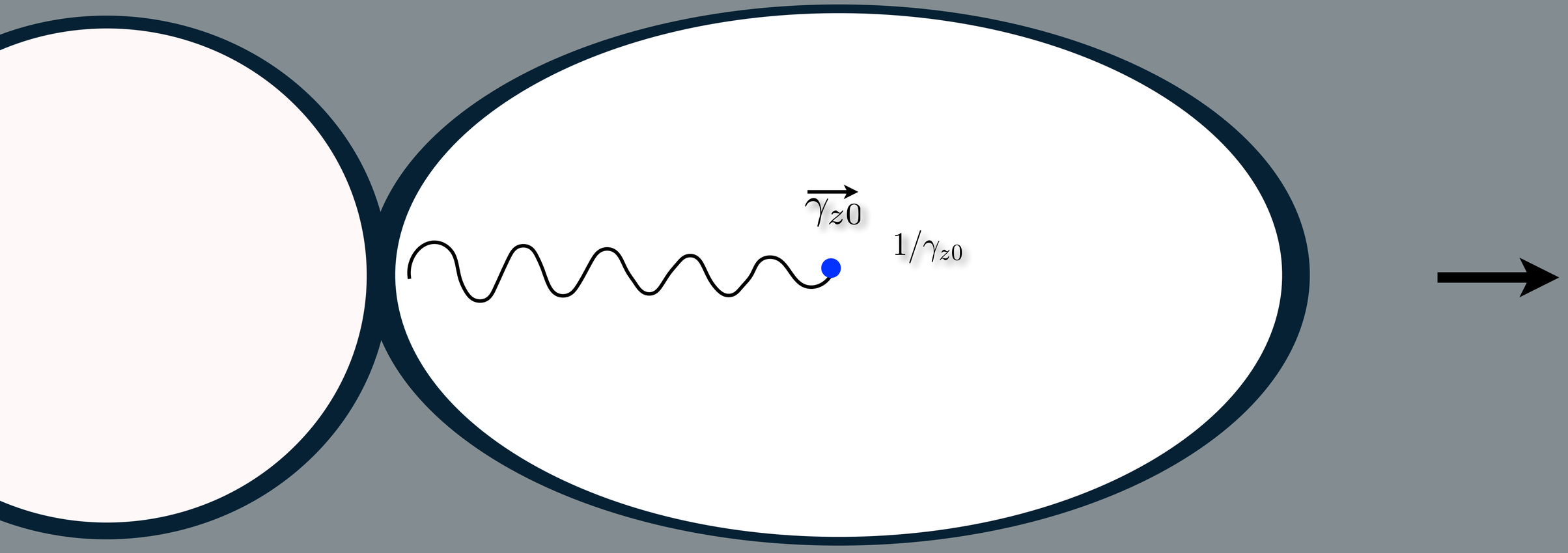

radiation

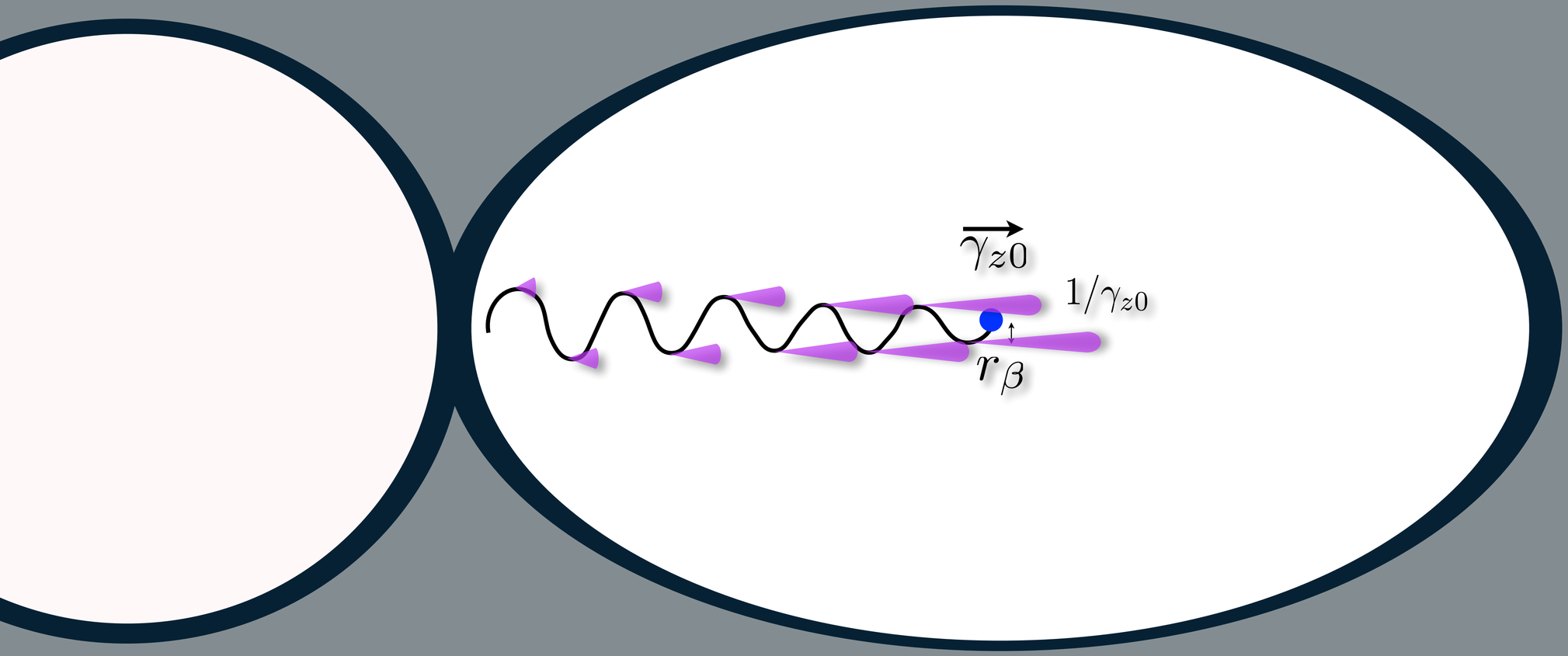

$$P_s = \frac{e^2 c}{12\pi\epsilon_0}\gamma_{z0}^2 k_\beta^2 a_\beta^2$$

$$a_\beta = \gamma_{z0} r_\beta k_\beta$$

$$\omega_c = 3\gamma^3 \omega_\beta^2 r_\beta / c$$

E Esarey PRE 65, 056505 (2002)

Synchrotron radiation from laser wakefield accelerators

plasma wakefield acceleration

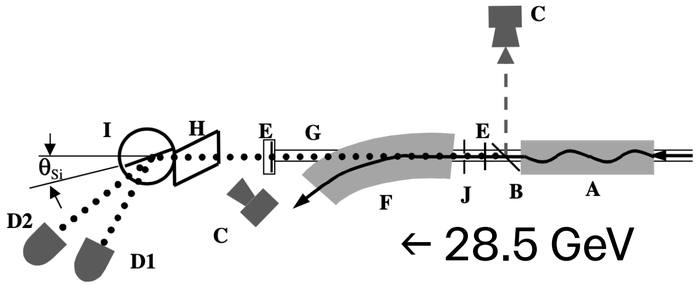

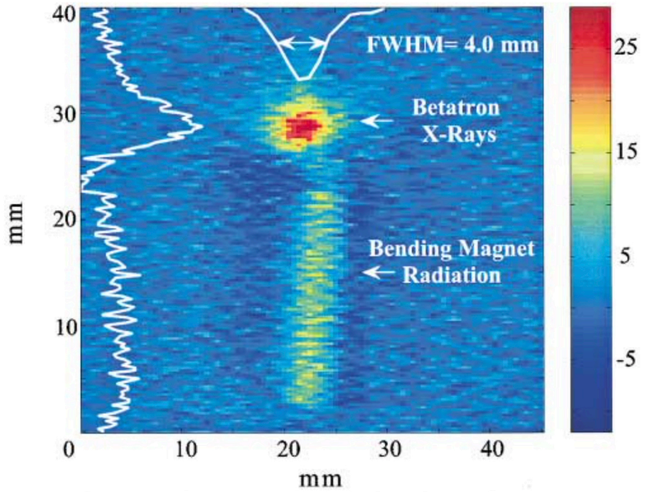

Wang, S. et al. X-Ray Emission from Betatron Motion in a Plasma Wiggler. Physical Review Letters 88, 135004 (2002).

laser wakefield acceleration

e-beam upto 200 MeV

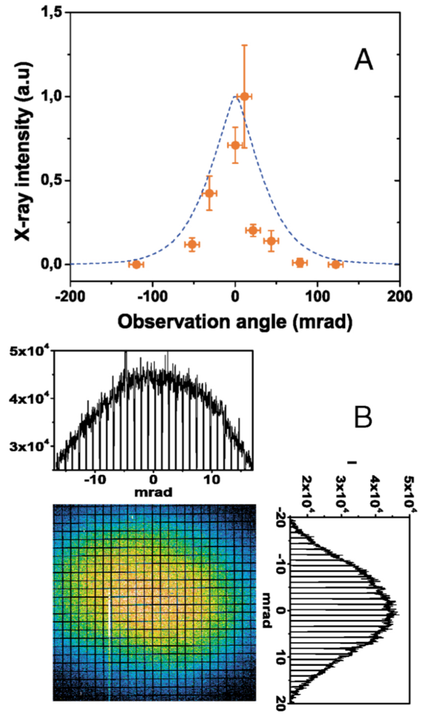

Rousse, A. et al. Production of a keV X-Ray Beam from Synchrotron Radiation in Relativistic Laser-Plasma Interaction. Phys. Rev. Lett. 93, 135005 (2004).

direct laser acceleration

e-beam upto 300 MeV

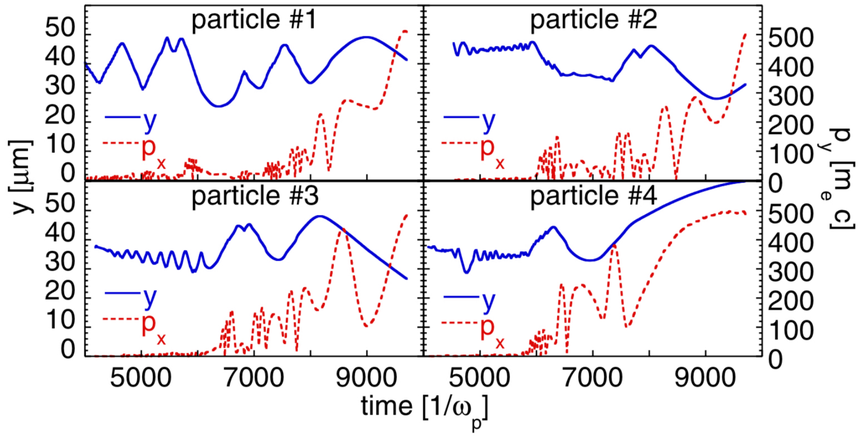

Kneip, S. et al. Observation of Synchrotron Radiation from Electrons Accelerated in a Petawatt-Laser-Generated Plasma Cavity. Phys. Rev. Lett. 100, 105006 (2008).

Betatron setup on Astra Gemini at Rutherford Laboratory

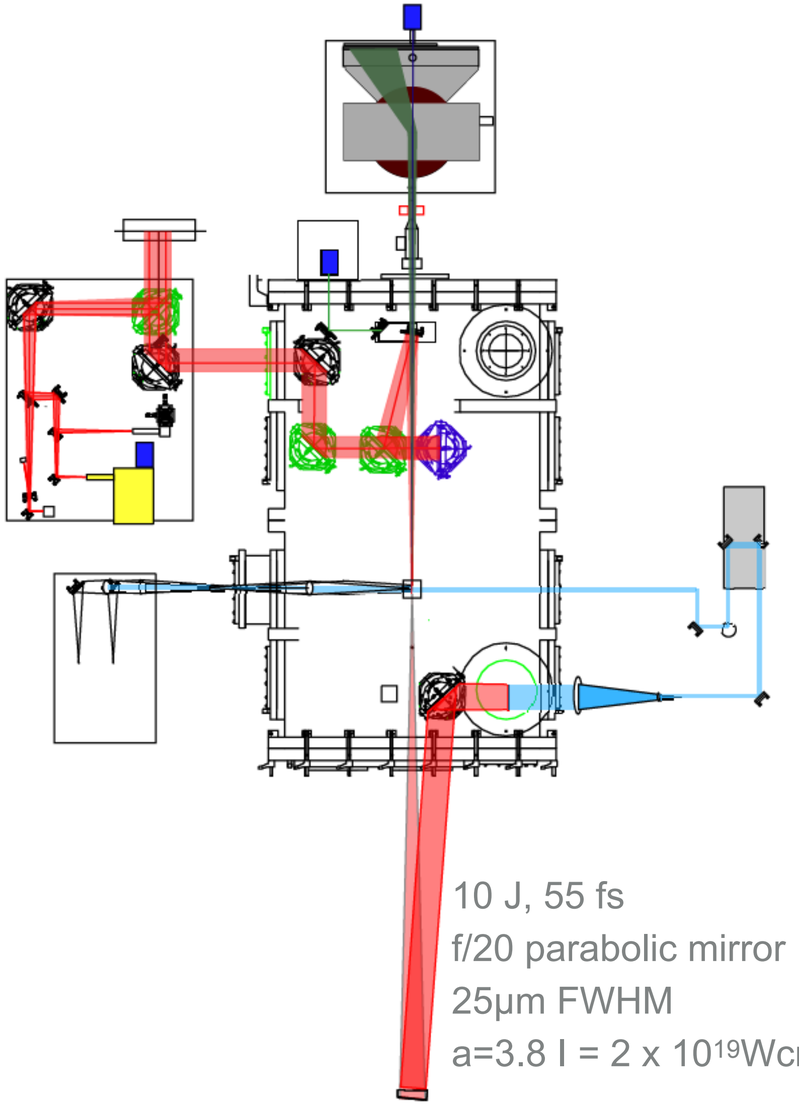

10 J, 55 fs
f/20 parabolic mirror
25μm FWHM
$a=3.8$ $I = 2 \times 10^{19} Wcm^{-2}$

Betatron setup on Astra Gemini at Rutherford Laboratory

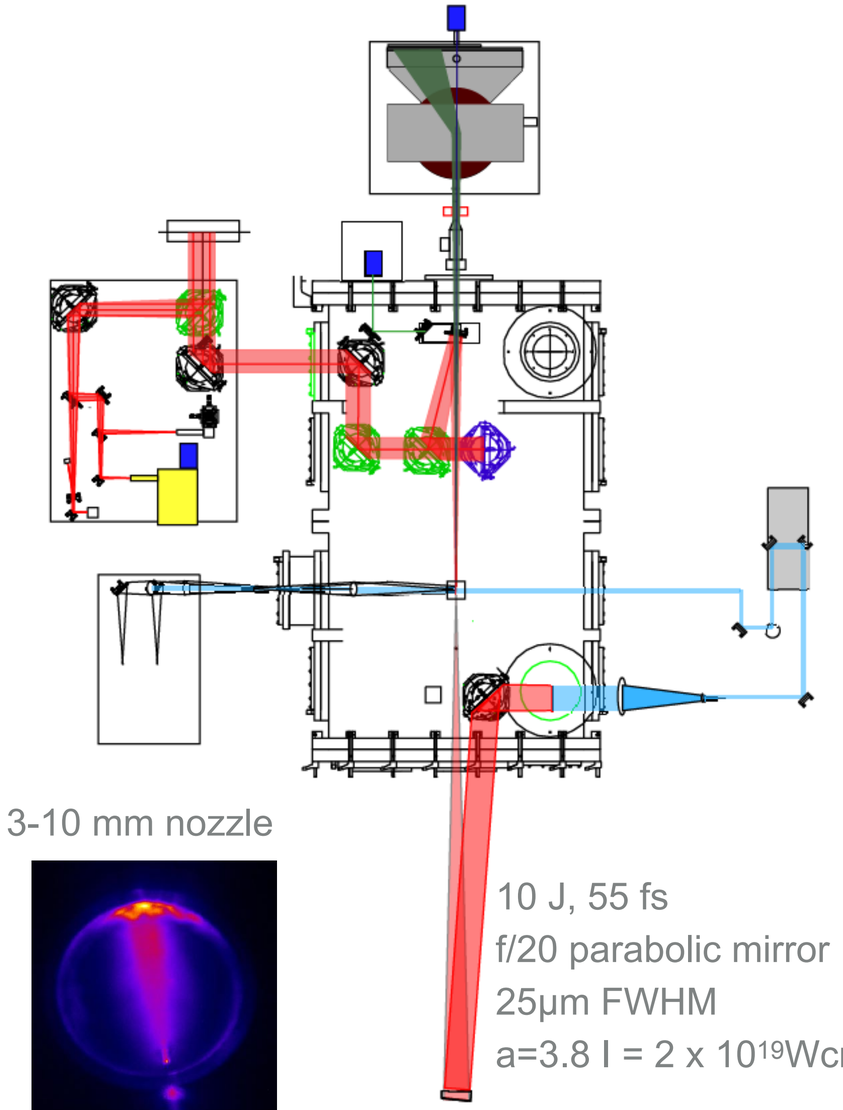

3-10 mm nozzle

10 J, 55 fs
f/20 parabolic mirror
25μm FWHM
$a=3.8$ $I = 2 \times 10^{19} Wcm^{-2}$

Betatron setup on Astra Gemini at Rutherford Laboratory

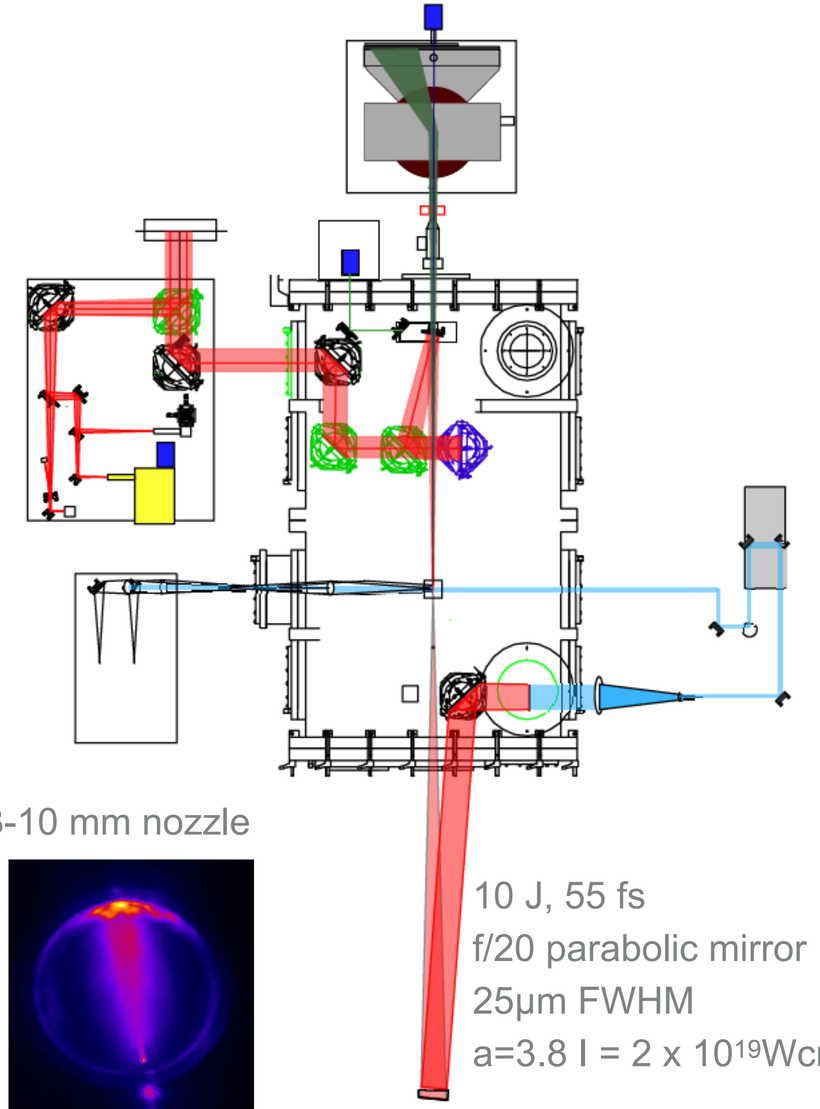

centimetre scale channel

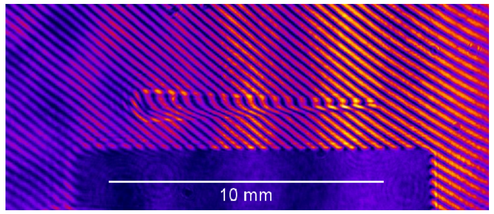

3-10 mm nozzle

10 J, 55 fs
f/20 parabolic mirror
25μm FWHM
a=3.8 I = 2 x 10^{19}Wcm^{-2}

Betatron setup on Astra Gemini at Rutherford Laboratory

Self-guiding >10mm

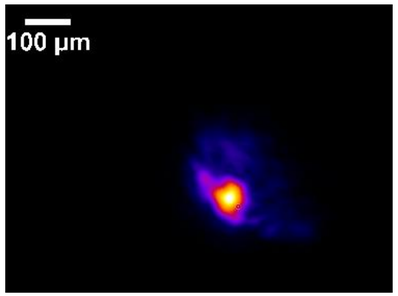

centimetre scale channel

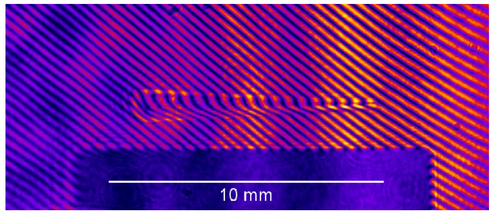

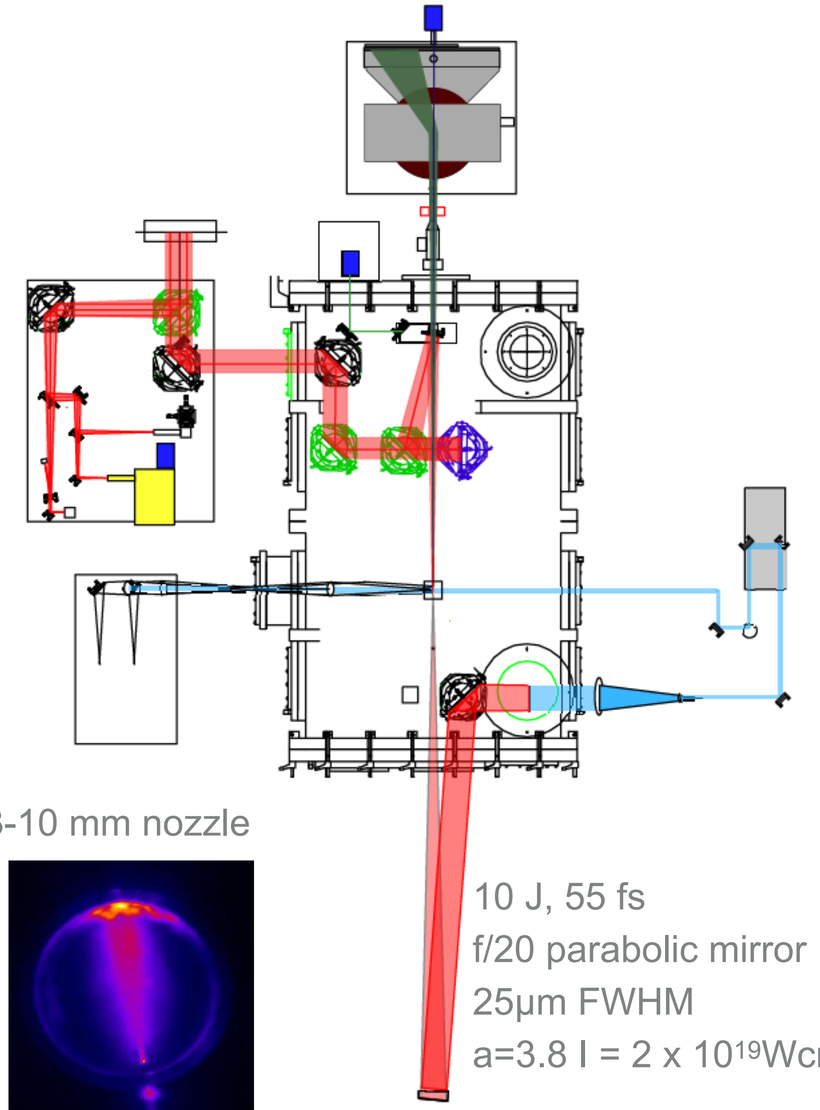

3-10 mm nozzle

10 J, 55 fs
f/20 parabolic mirror
25µm FWHM
$a=3.8$ $I = 2 \times 10^{19} Wcm^{-2}$

Betatron setup on Astra Gemini at Rutherford Laboratory

Self-compression <20fs

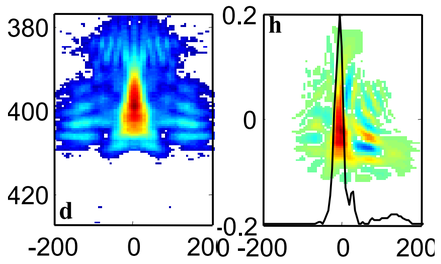

Self-guiding >10mm

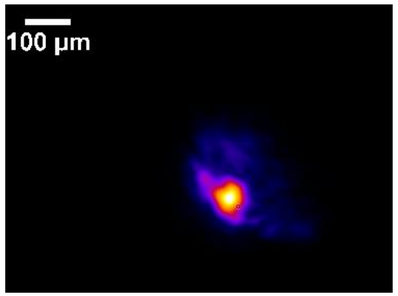

centimetre scale channel

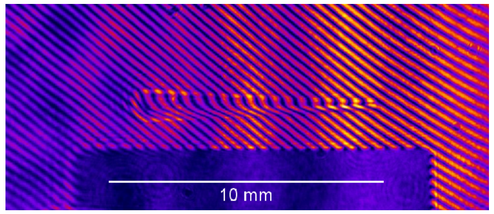

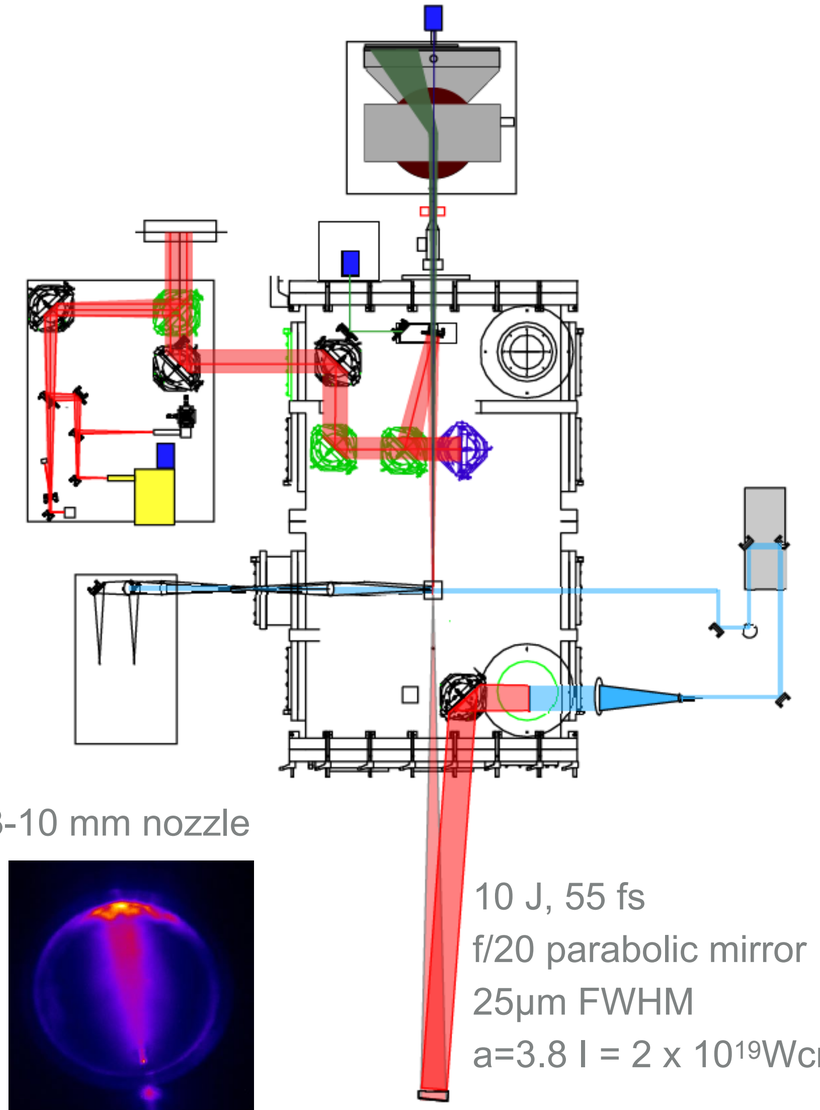

3-10 mm nozzle

10 J, 55 fs
f/20 parabolic mirror
25µm FWHM
a=3.8 I = 2 x 10^{19}Wcm^{-2}

Betatron setup on Astra Gemini at Rutherford Laboratory

Self-compression <20fs

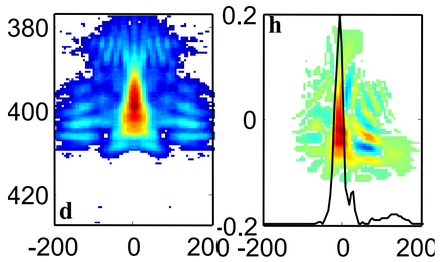

Self-guiding >10mm

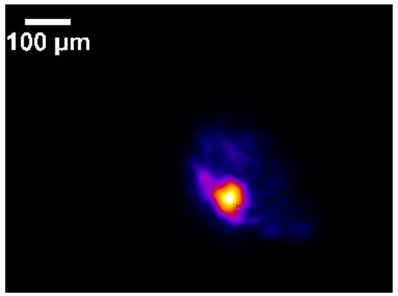

centimetre scale channel

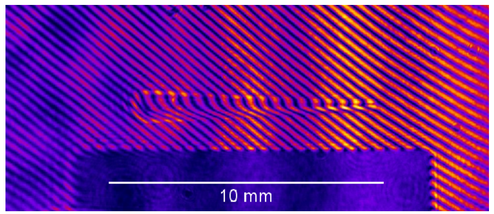

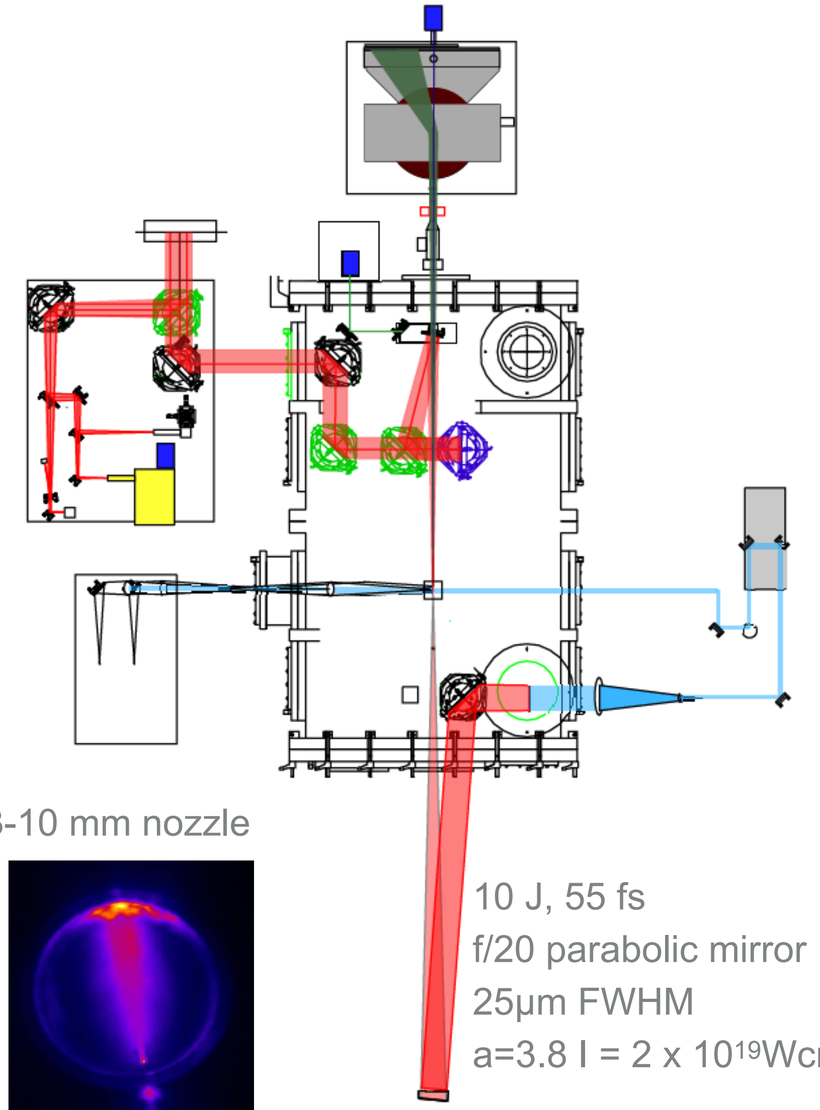

3-10 mm nozzle

10 J, 55 fs
f/20 parabolic mirror
25µm FWHM
a=3.8 I = 2 x 10^{19}Wcm^{-2}

>90% e-beams
< 4 mrad

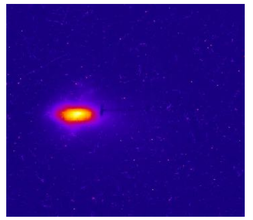

Betatron setup on Astra Gemini at Rutherford Laboratory

Self-compression <20fs

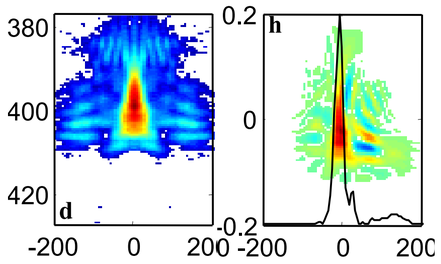

Self-guiding >10mm

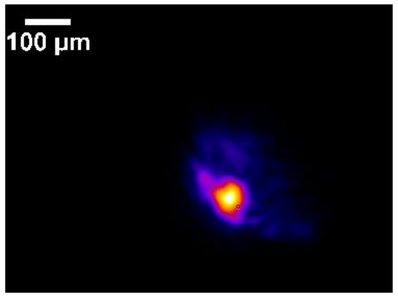

centimetre scale channel

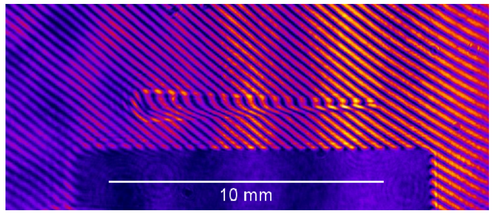

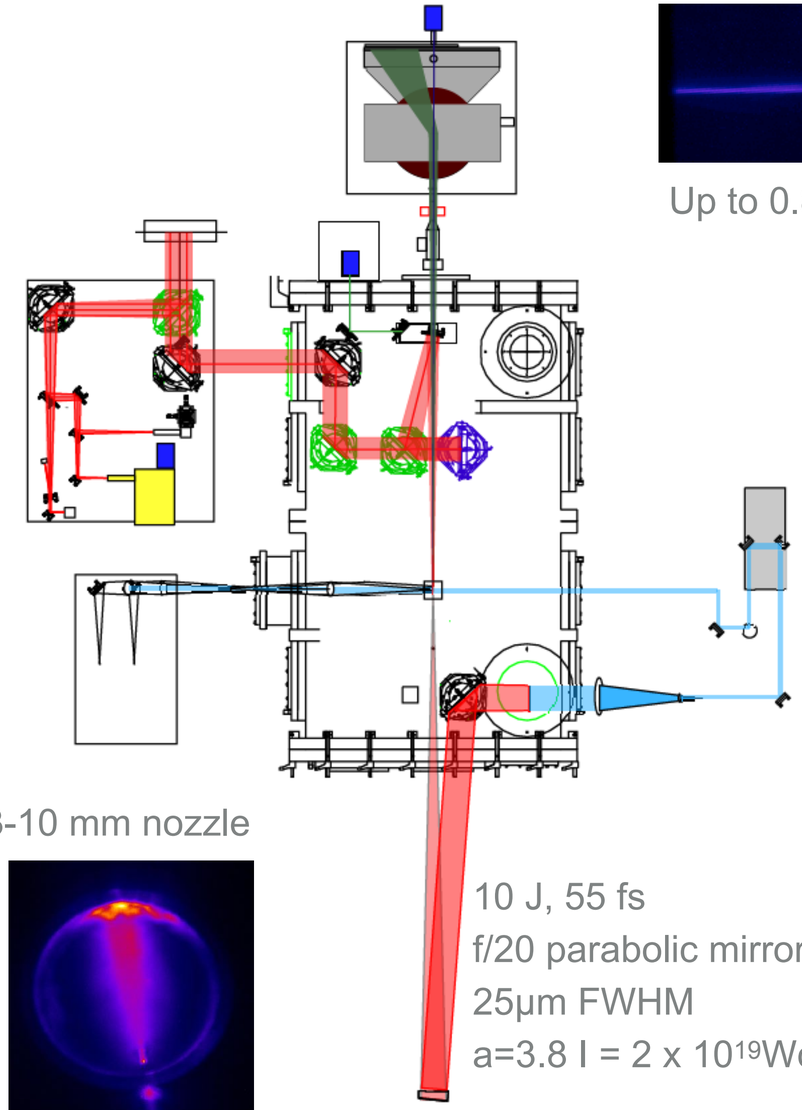

3-10 mm nozzle

10 J, 55 fs
f/20 parabolic mirror
25µm FWHM
a=3.8 I = 2 x 10^{19}Wcm^{-2}

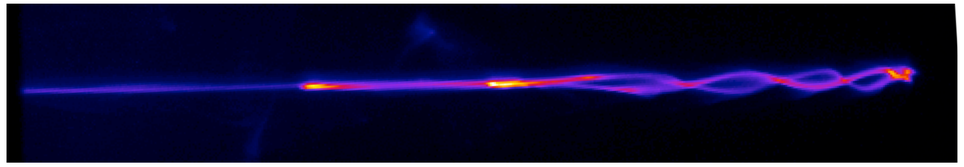

Up to 0.8 GeV e-beams

energy →

>90% e-beams
< 4 mrad

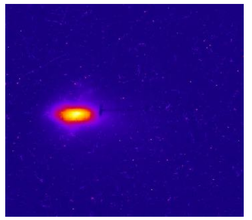

Betatron setup on Astra Gemini at Rutherford Laboratory

Self-compression <20fs

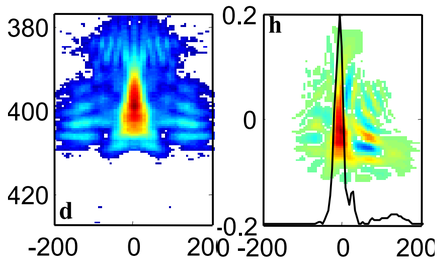

Up to 0.8 GeV e-beams

energy →

>90% e-beams

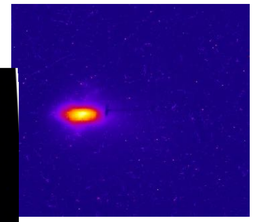

Self-guiding >10mm

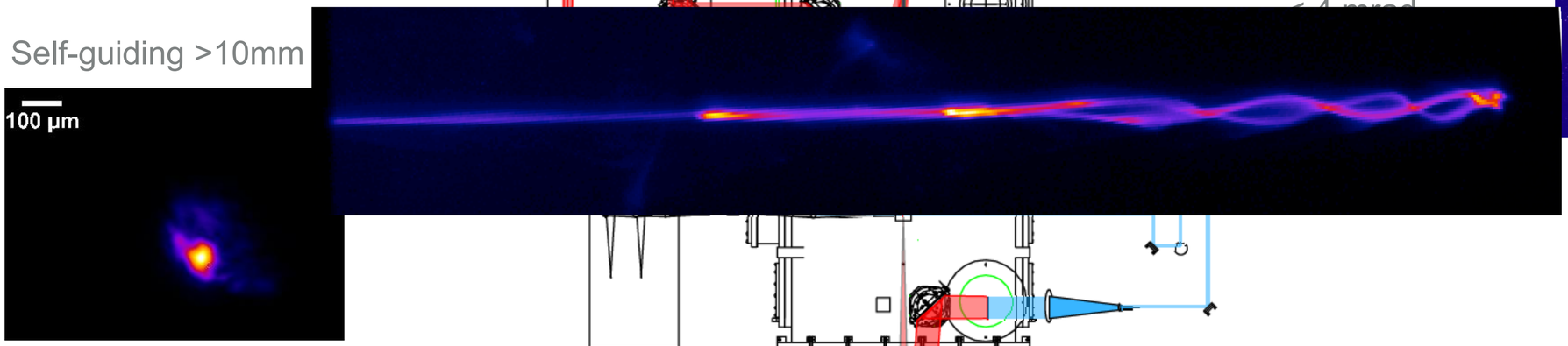

centimetre scale channel

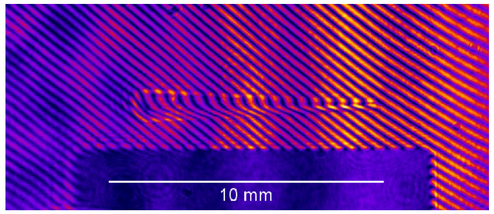

3-10 mm nozzle

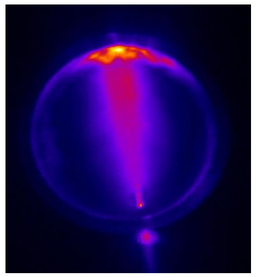

10 J, 55 fs
f/20 parabolic mirror
25µm FWHM
a=3.8 I = 2 x 10^{19}Wcm^{-2}

Betatron setup on Astra Gemini at Rutherford Laboratory

Self-compression <20fs

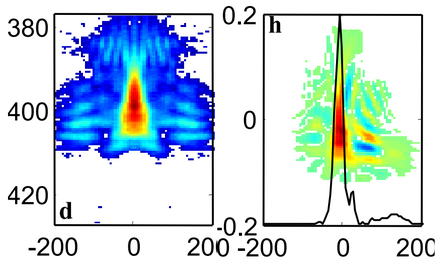

Self-guiding >10mm

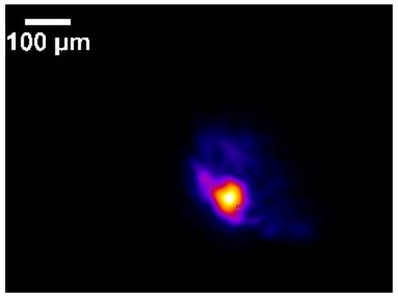

centimetre scale channel

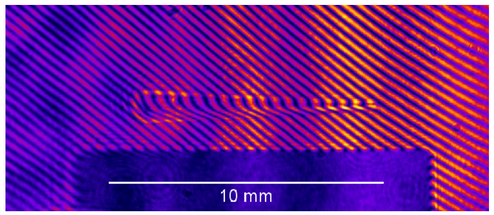

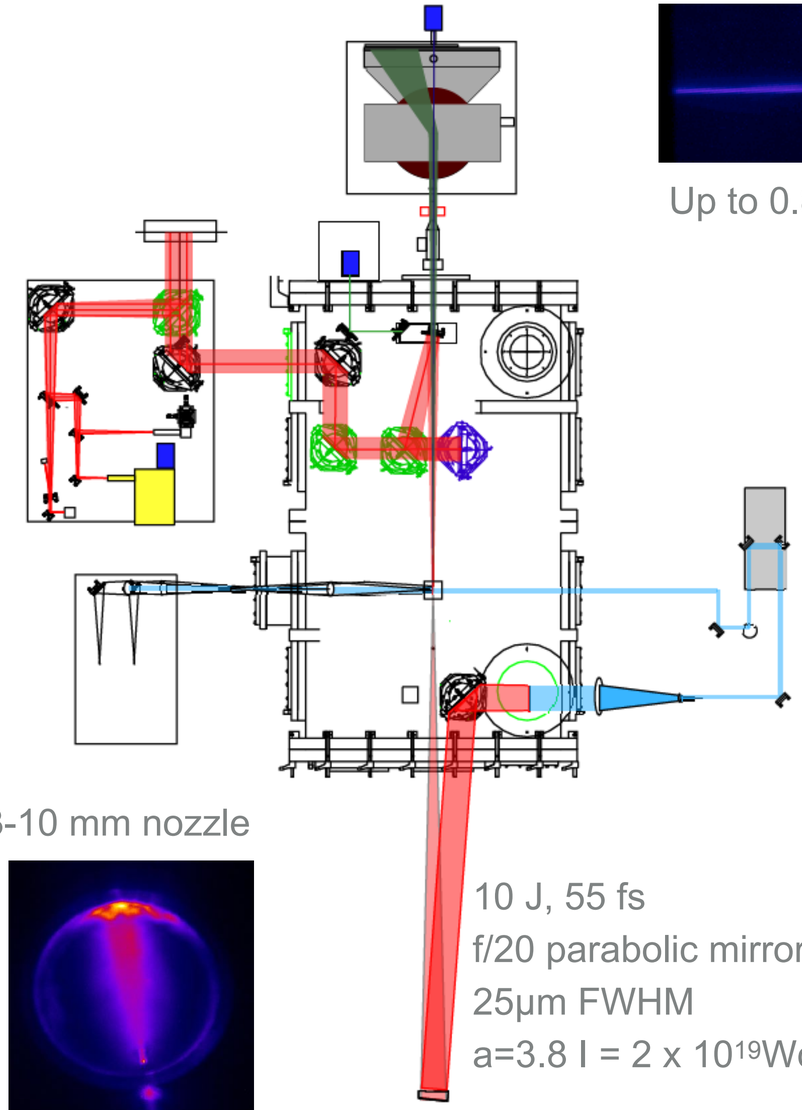

3-10 mm nozzle

10 J, 55 fs
f/20 parabolic mirror
25µm FWHM
a=3.8 I = 2 x 10^{19}Wcm^{-2}

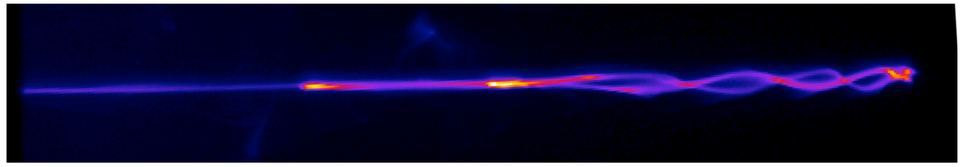

Up to 0.8 GeV e-beams

energy →

>90% e-beams
< 4 mrad

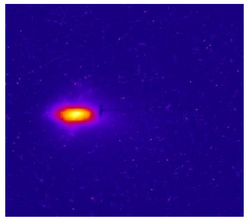

Betatron setup on Astra Gemini at Rutherford Laboratory

Self-compression <20fs

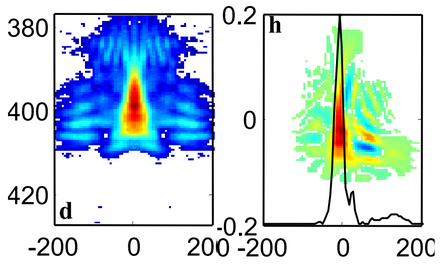

Self-guiding >10mm

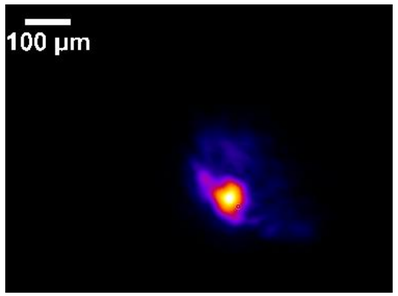

centimetre scale channel

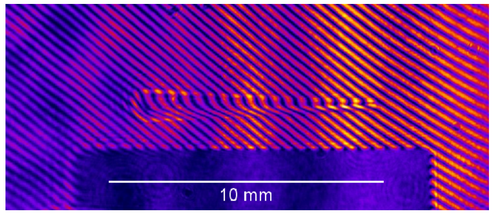

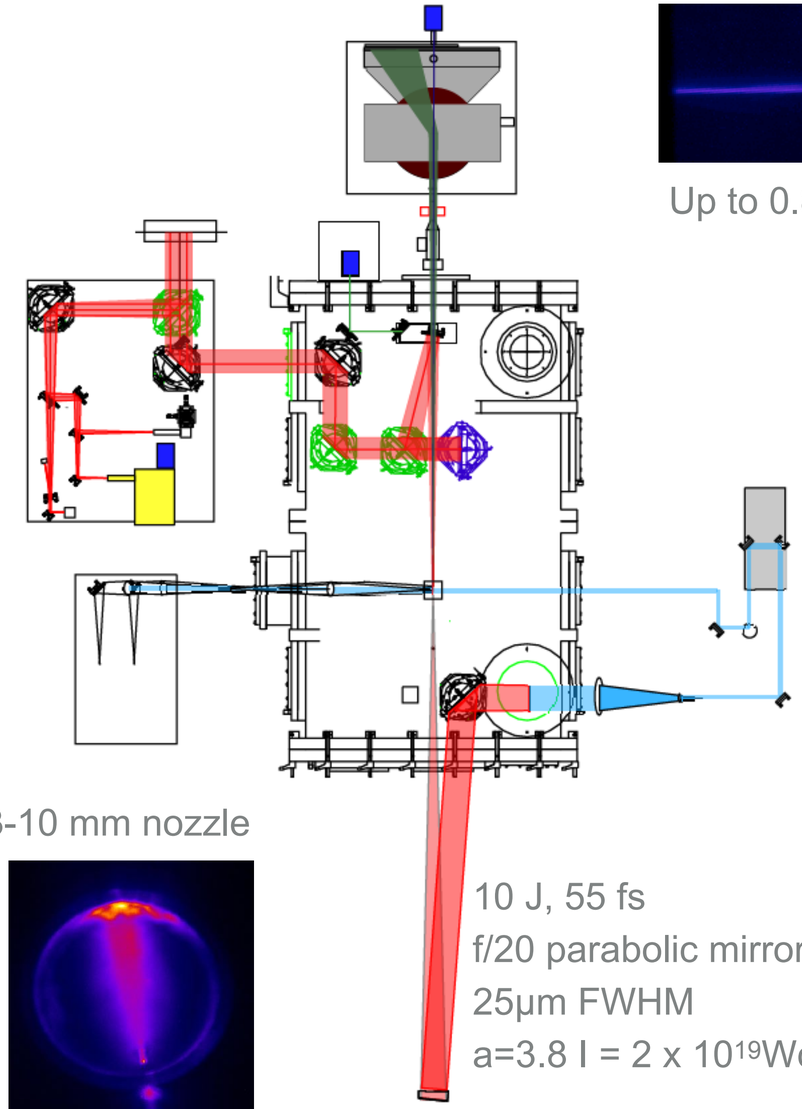

3-10 mm nozzle

10 J, 55 fs
f/20 parabolic mirror
25µm FWHM
a=3.8 I = 2 x 10^{19}Wcm^{-2}

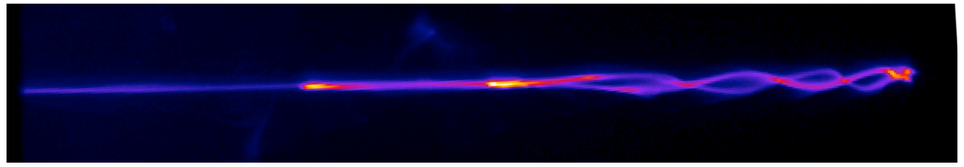

Up to 0.8 GeV e-beams

energy →

>90% e-beams
< 4 mrad

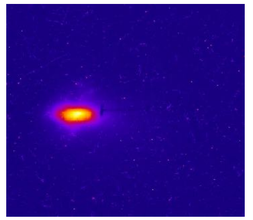

bright x-rays

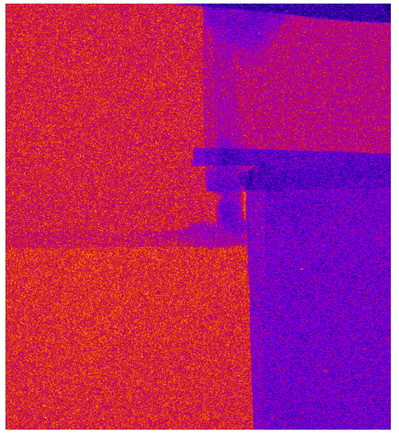

Betatron setup on Astra Gemini at Rutherford Laboratory

Self-compression <20fs

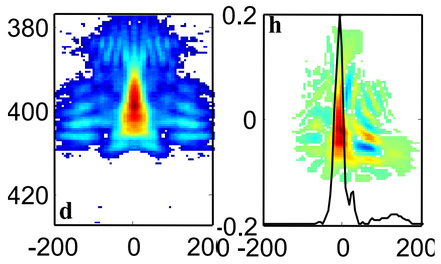

Self-guiding >10mm

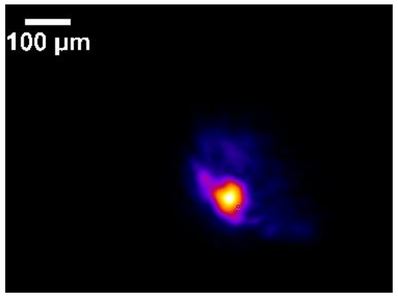

centimetre scale channel

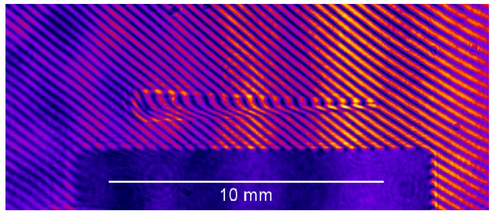

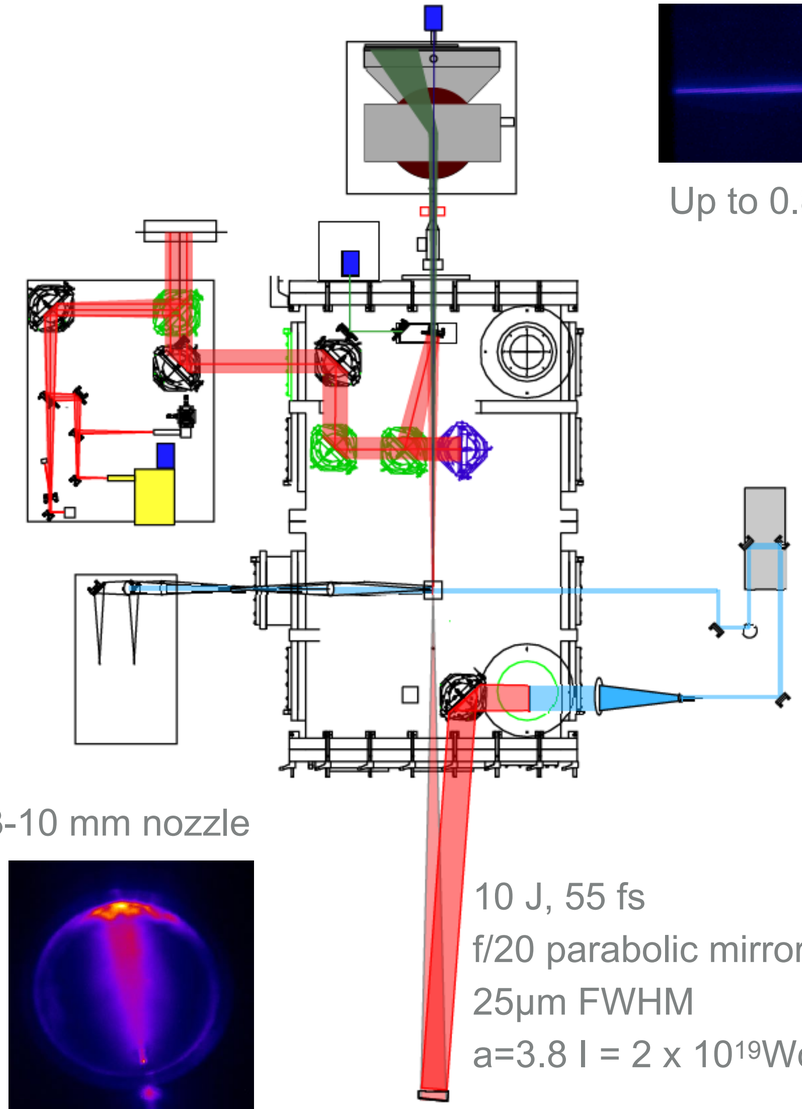

3-10 mm nozzle

10 J, 55 fs
f/20 parabolic mirror
25µm FWHM
a=3.8 I = 2 x 10^{19}Wcm^{-2}

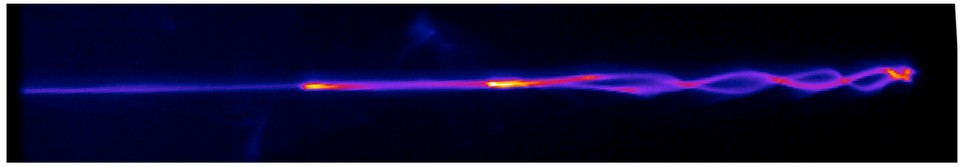

Up to 0.8 GeV e-beams

energy →

>90% e-beams
< 4 mrad

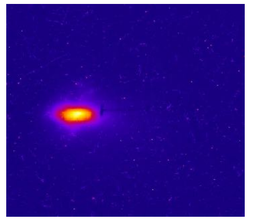

bright x-rays

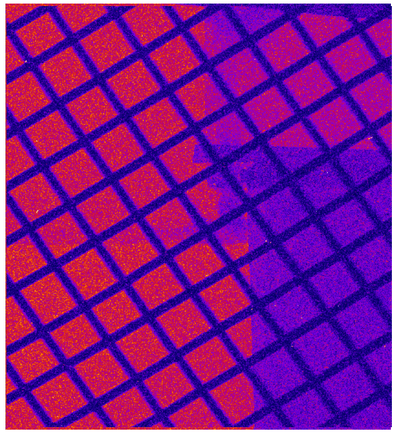

20 µm

Betatron setup on Astra Gemini at Rutherford Laboratory

Self-compression <20fs

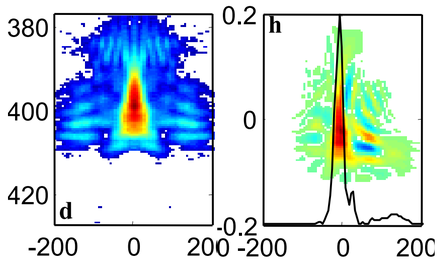

Self-guiding >10mm

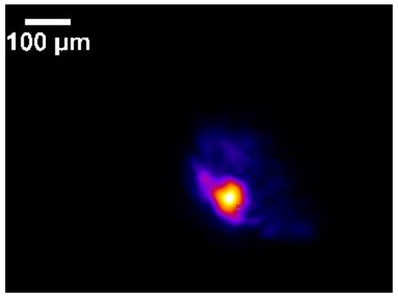

centimetre scale channel

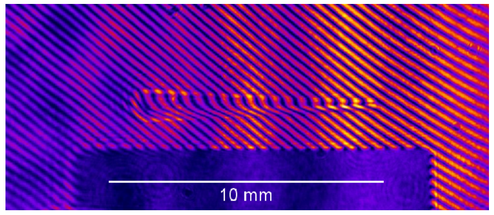

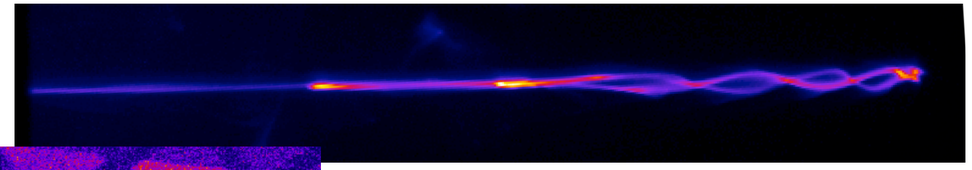

beams

energy →

e-beams

rad

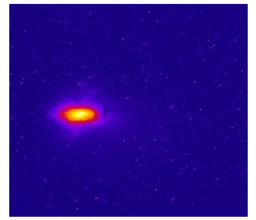

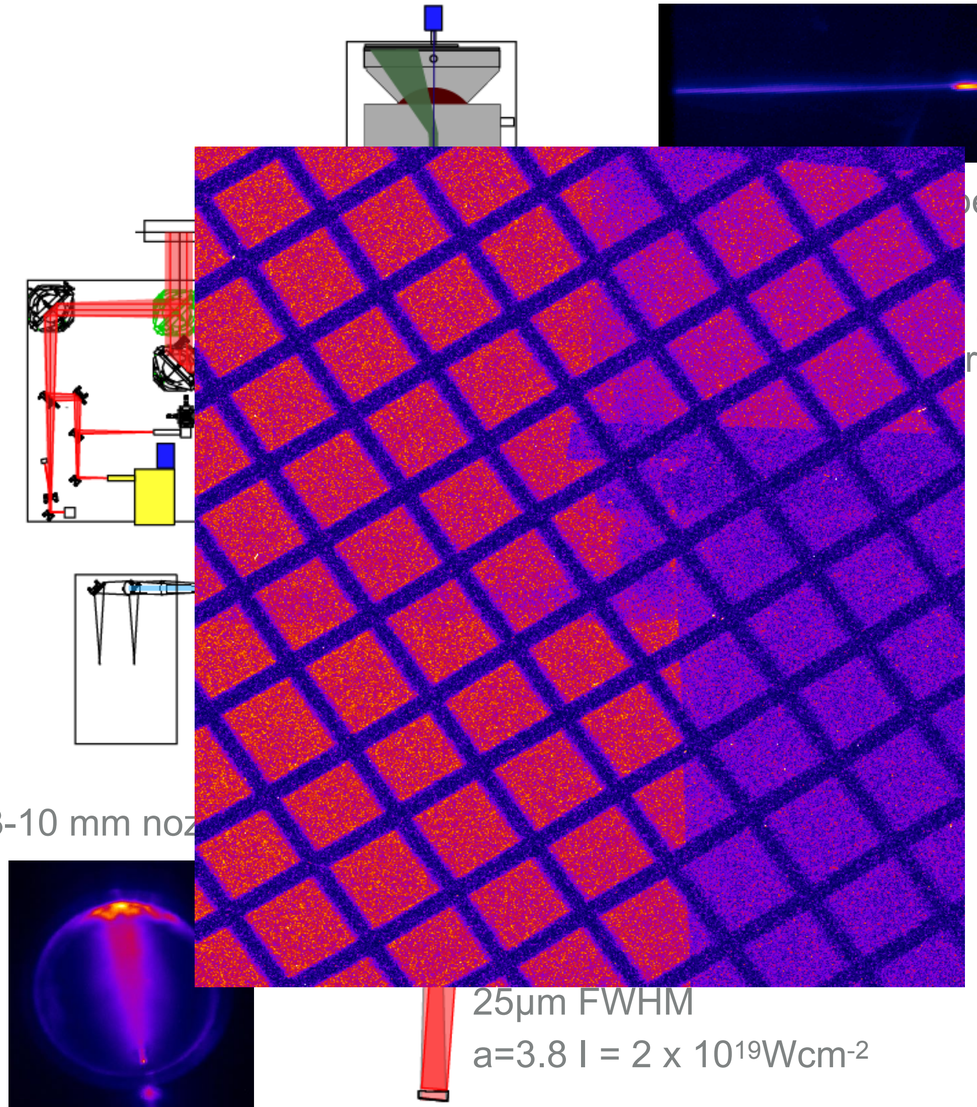

3-10 mm noz

25µm FWHM

a=3.8 I = 2 x 10^{19}Wcm^{-2}

bright x-rays

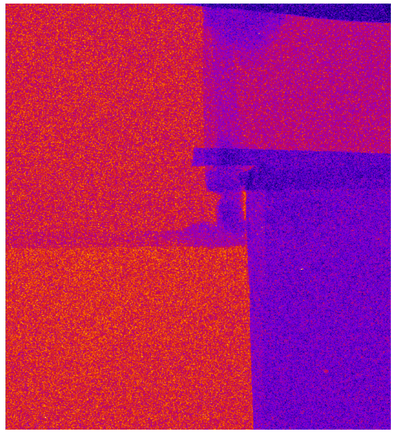

20 µm

Source Size measurements

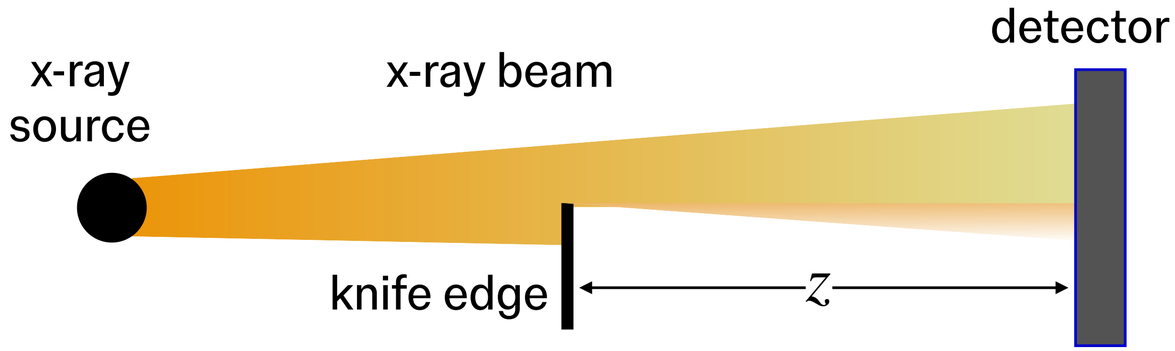

Transmission across a knife edge gives (performed on experiments on Hercules Laser at U. Michigan)

Source sizes on the order of μm measured (factor of 100× improvement on standard x-ray tubes and 10× better than micro focus tubes).

Knife-edge images show fringes - signs of spatial coherence

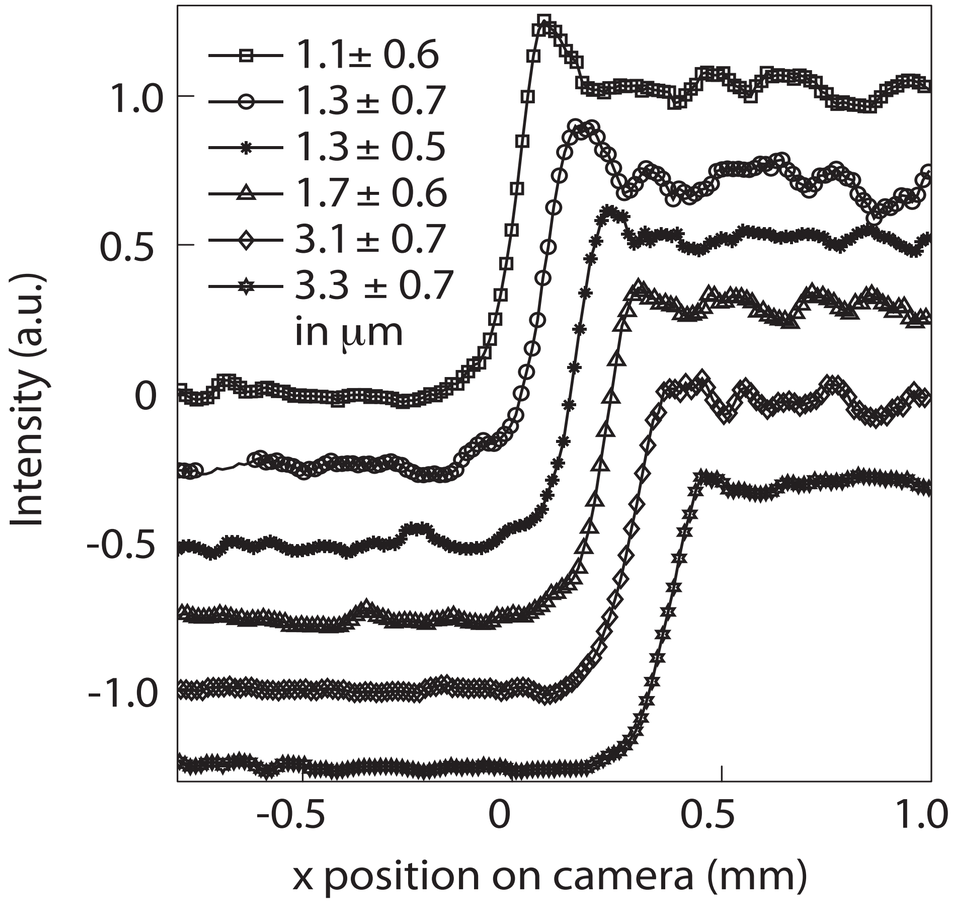

Fresnel Diffraction

Incoherent source produces exposure like an Error function, to model observed exposure use Fresnel formalism

Fresnel Diffraction occurs when wave passes through aperture and diffracts in near field

Diffraction pattern differs in size and shape depending on object and image distance, source profile and spectrum

Treatment necessary if Fresnel Number $N_F = a^2/(s\lambda) \approx 1$

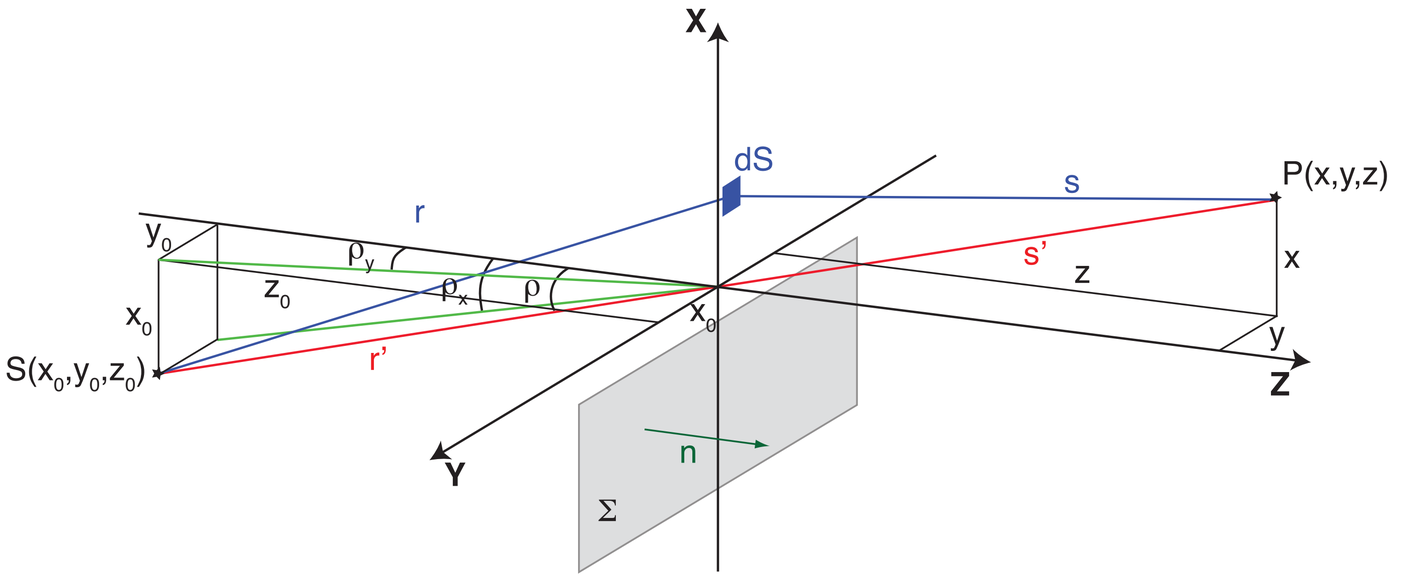

for knife edge, integrate over half plain only:

$$E(P) = A \cdot \int_{\eta=-\infty}^{\infty} \int_{\xi=-\infty}^{x_0} \exp\left(\frac{2\pi}{\lambda}\frac{1}{2} \cdot \left(\frac{1}{r'} + \frac{1}{s'}\right)\left(\xi^2 \cos^2\rho + \eta^2\right)\right) d\xi d\eta$$

Fresnel Diffraction Modeling

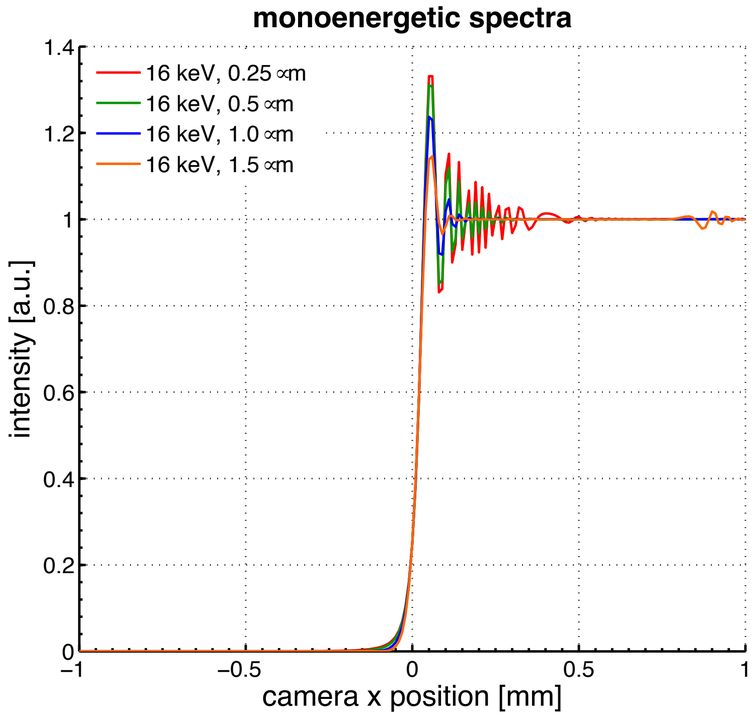

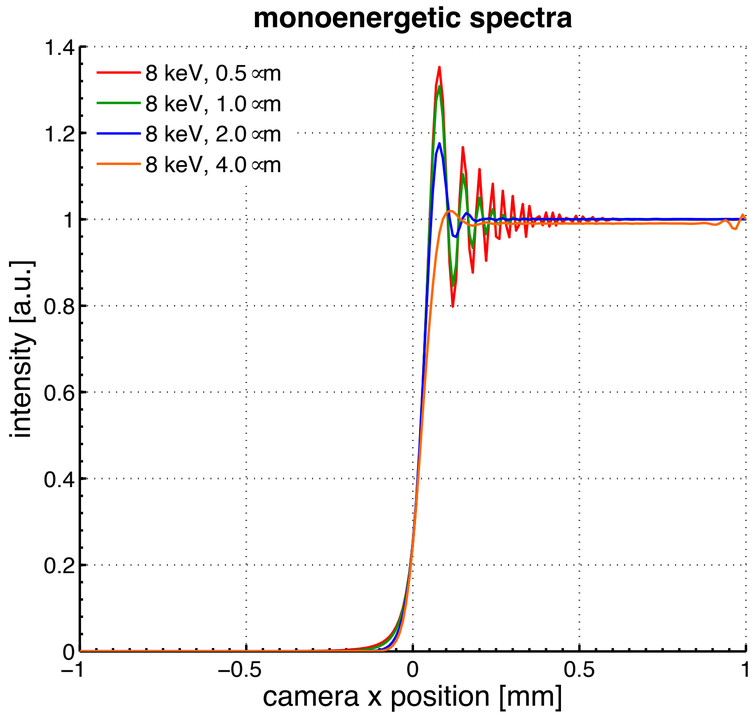

Increase source size
→ Reduction of number of fringes
→ Steepening of rising edge

Increase wavelength
→ fewer fringes
→ less steep rising edge

Fresnel Diffraction Modeling

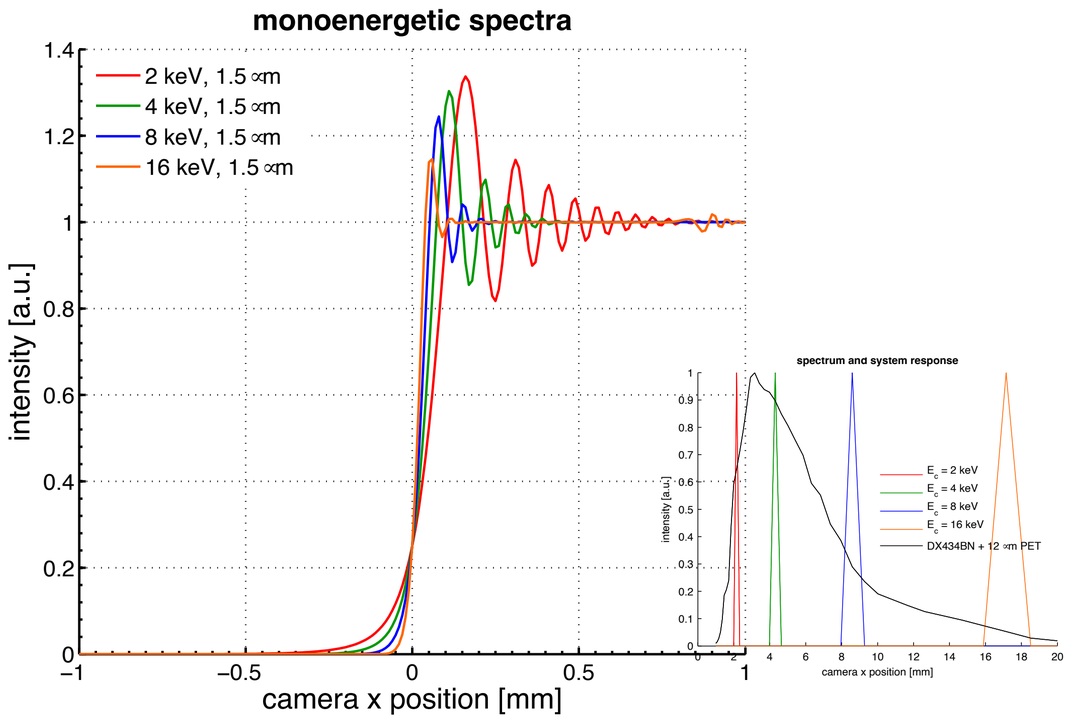

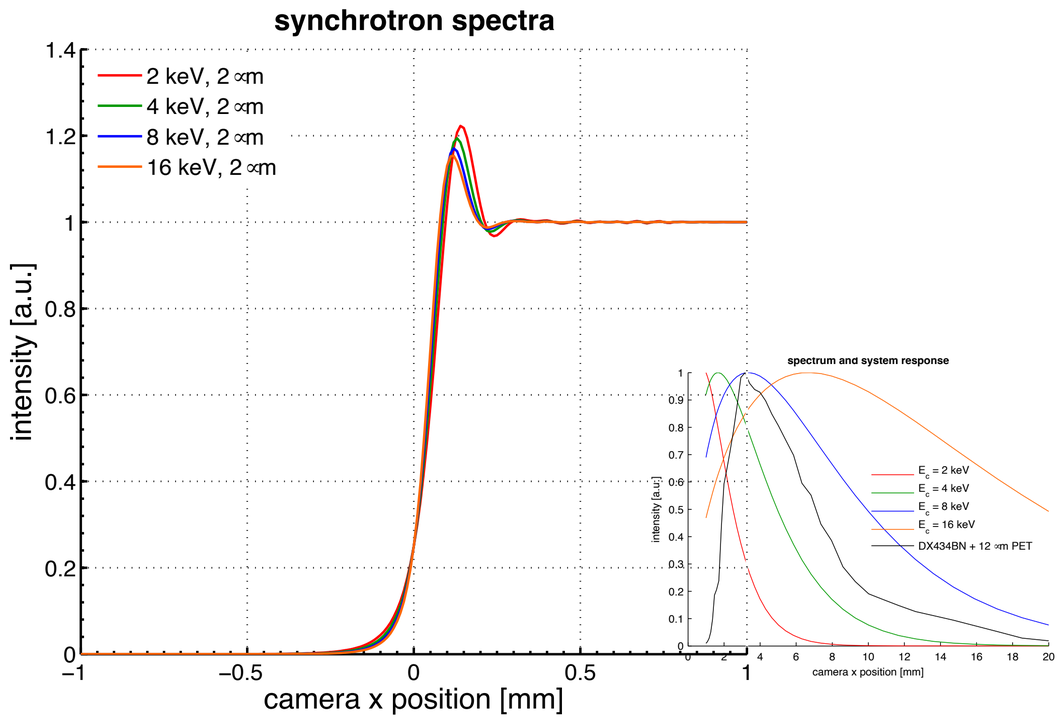

Use quantum efficiency (QE) of Andor DX434BN CCD

→ spectrum dominated by wavelength at which QE is highest

Using full synchrotron spectrum shows steepening of edge

→ but edge enhancement is similar over wide spectral range

Fresnel Diffraction Data

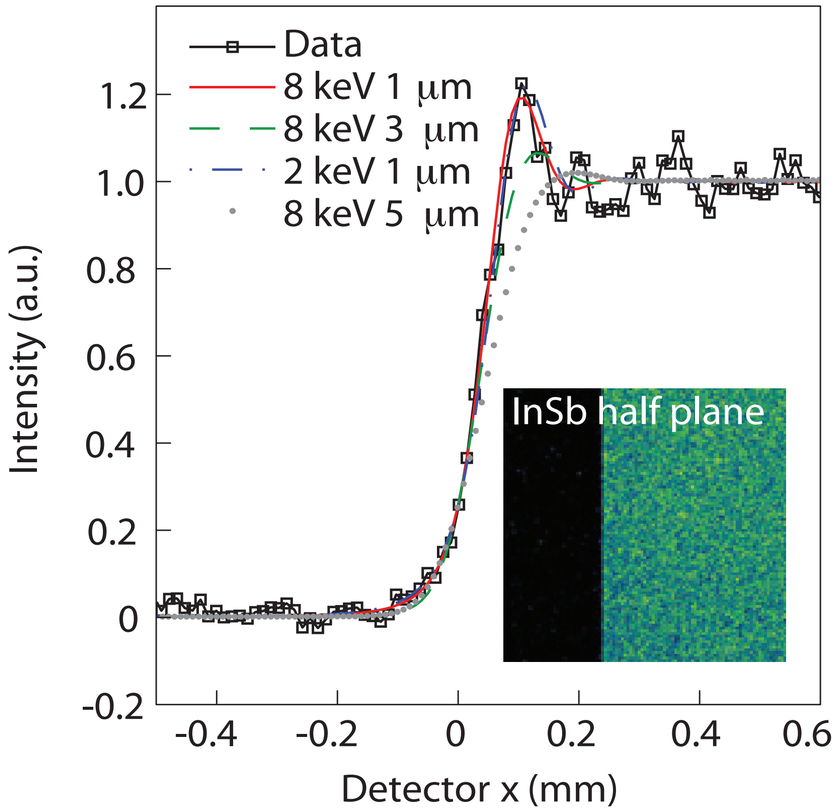

- Use QE of Andor DX434BN CCD
- Filter with 12 um Mylar
- Appearance of single fringe

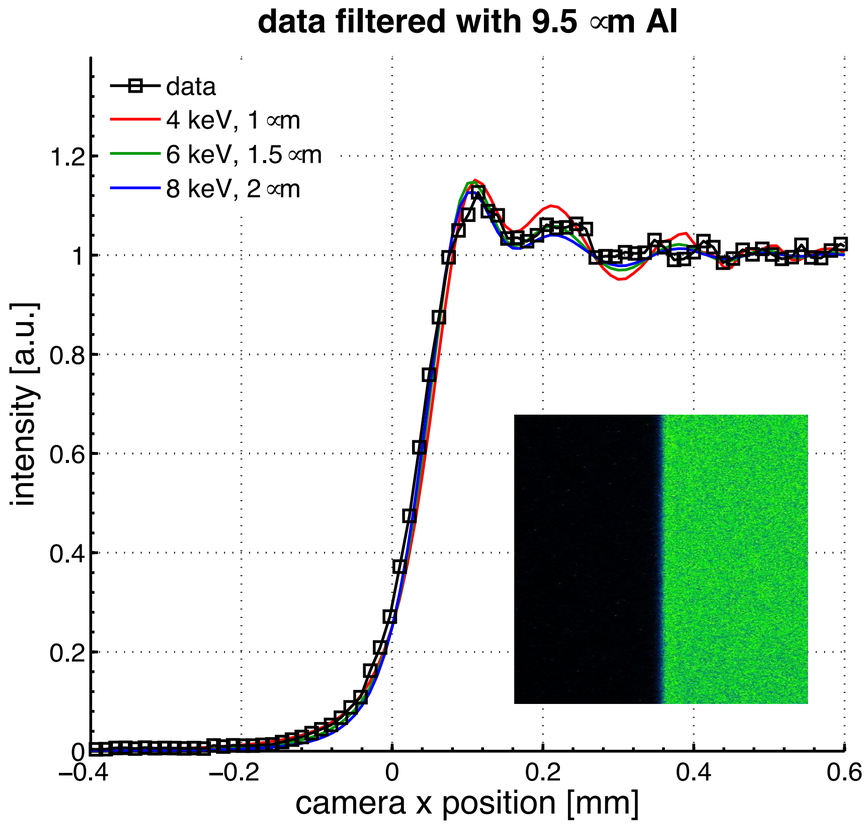

- Use QE of Andor DX434BN CCD
- Filter with 9.5 um Al
- Appearance of additional fringe

S Kneip et al., Nat. Phys. **10**, 980 (2010)

Radiation Spatially Coherent

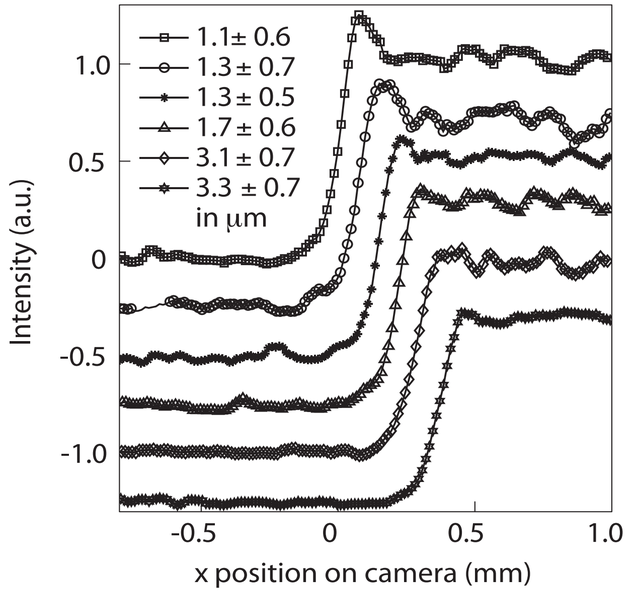

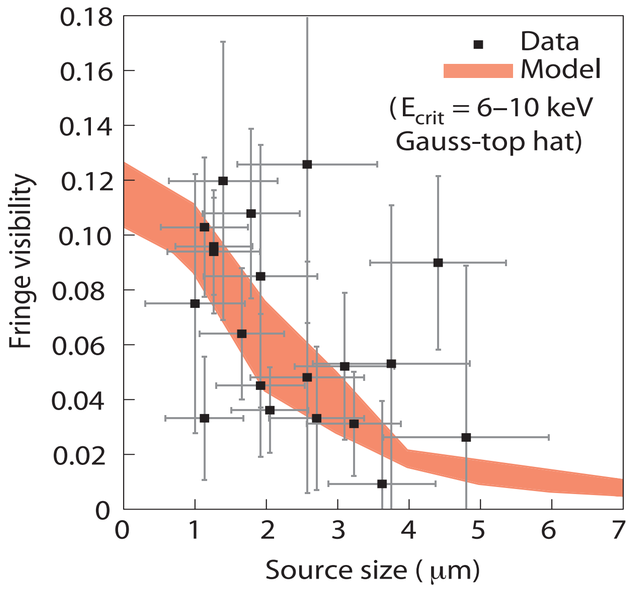

spatial coherence result of small source size

define fringe visibility:

$$v = \frac{I_{\max} - I_{\min}}{I_{\max} + I_{\min}}$$

- observed and modelled fringe visibility agree well for Gauss to flat-top source with ~8 keV synchrotron spectrum
- complex coherence factor: μ~0.88

Betatron Radiation Characteristics

spectrum obtained by differential transmission

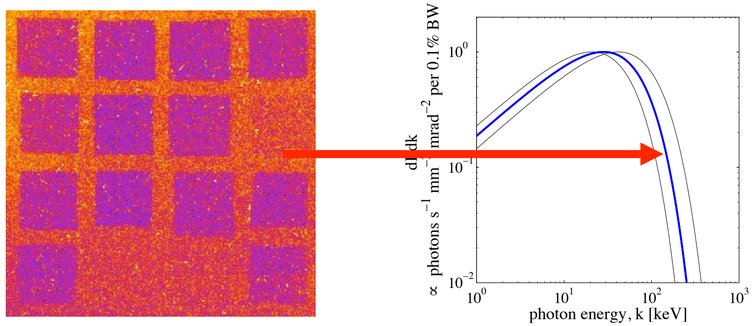

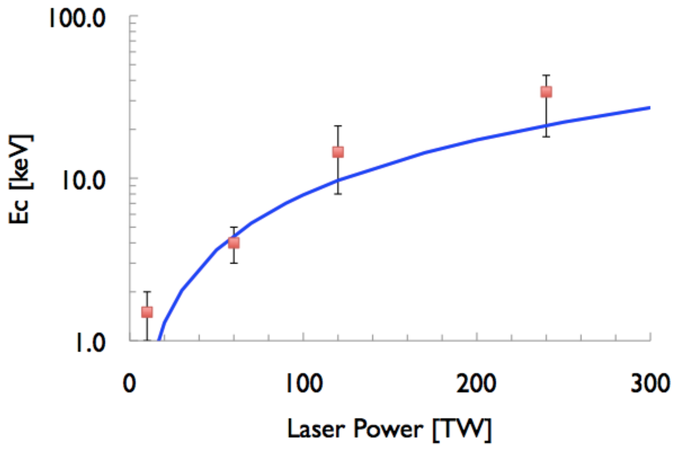

Source size **2.65** μm fwhm

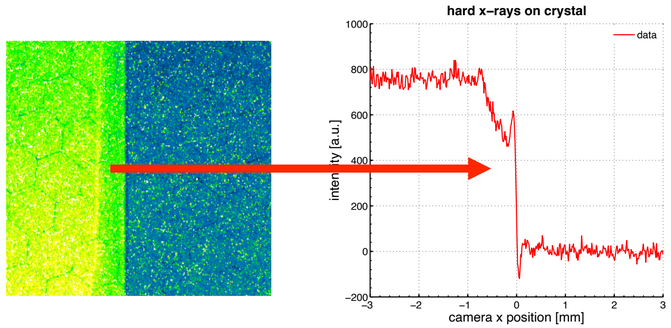

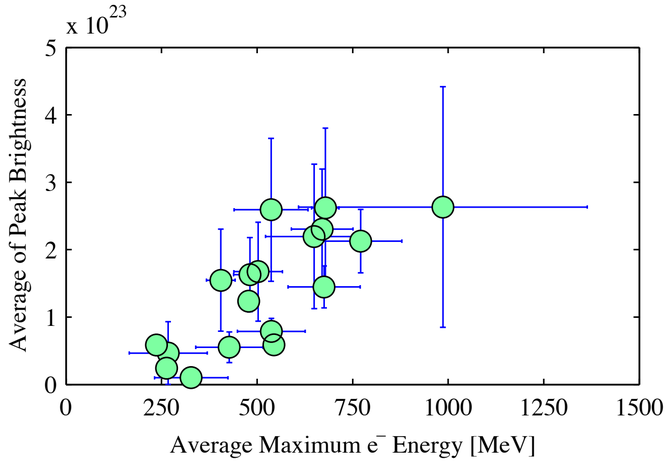

Yield > 10^8 photons > keV → brightness > 10^{22} photons/s/mm²/mrad²/0.1% BW

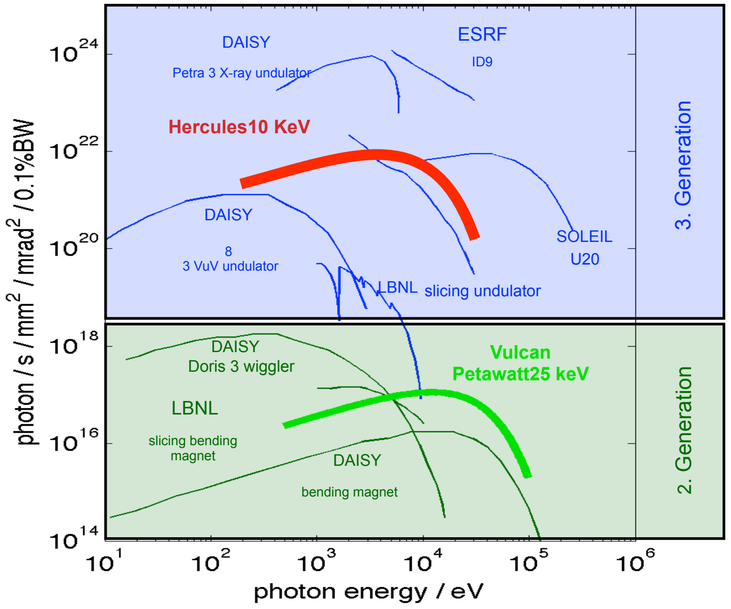

other light sources from A. Rousse *et al*, EPJD, 2008

Peak brightness ~ 3rd generation light source

Gemini setup with folded spot

Focussing to larger focal spot size allows laser to self-compress before injection

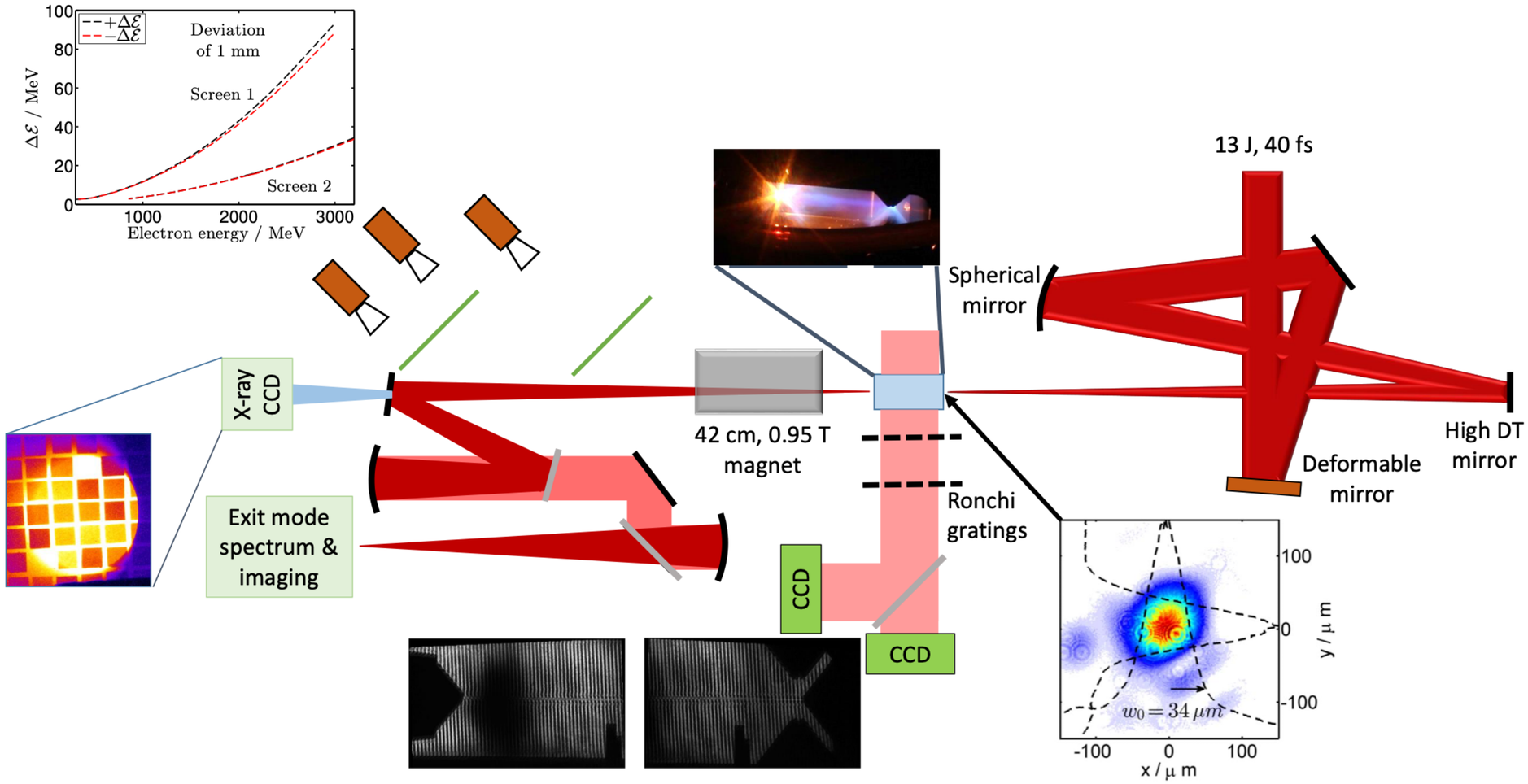

Enhanced betatron emission

A secondary bunch is produced that has strong betatron emission

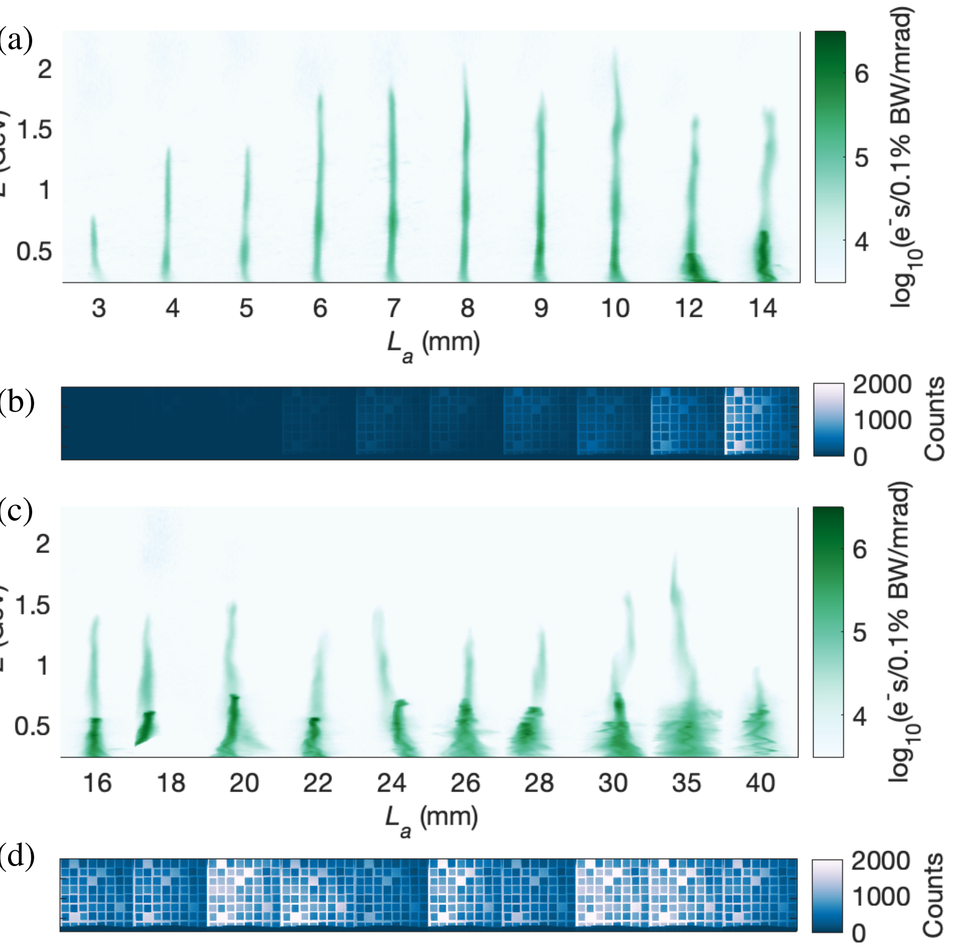

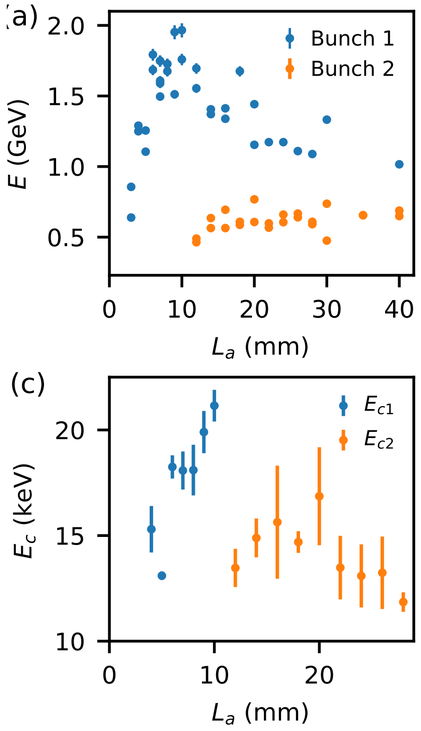

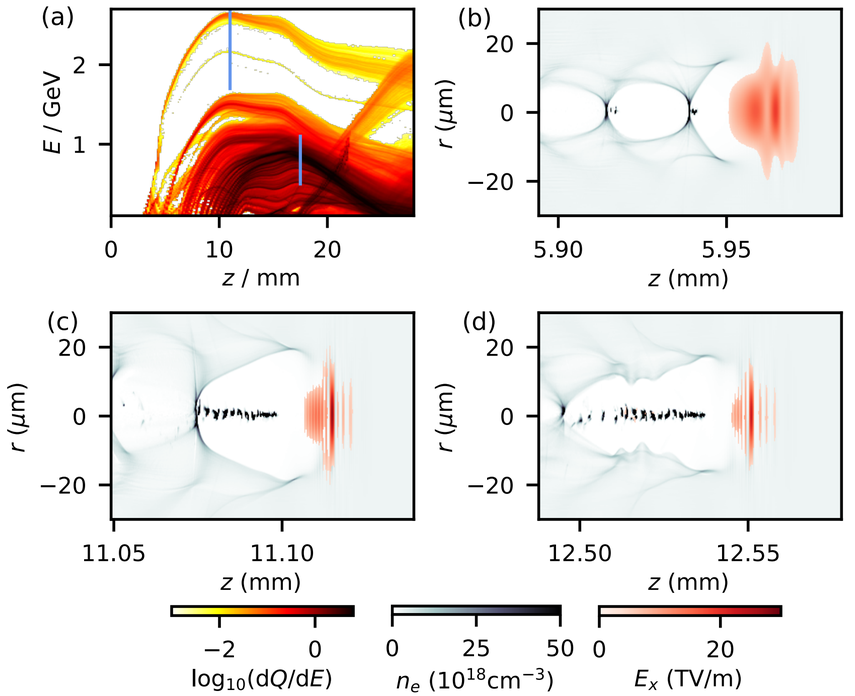

By allowing secondary injection, photon flux can increase by another order of magnitude > 5 ×10^{10} ph with E_c = 12-17 keV and flux 7×10^4 ph/mrad^{2}0.1%BW

J. C. Wood, et al “High Flux X-ray Emission from a Laser Wakefield Accelerator Operated Beyond the Depletion Length” submitted Phys. Rev. Lett. (2025)

Properties of β-tron sources

'Hard' photon energy - E_{crit} > 25 keV
- investigating dense material, biological materials

Small source **size** (~ μm)
- intrinsically high resolution
- exhibits spatial resolution

Small divergence (~ 10 mRad)
- makes beam line

Short pulse (~10s fs)
- suitable for ultrafast dynamics

Bright (>10^9 photons per shot)
- suitable for single shot imaging

All of these things makes for a unique imaging capability

X-ray imaging

(phase contrast imaging)

Phase vs. absorption contrast

Absorption contrast

Contrast through photon absorption

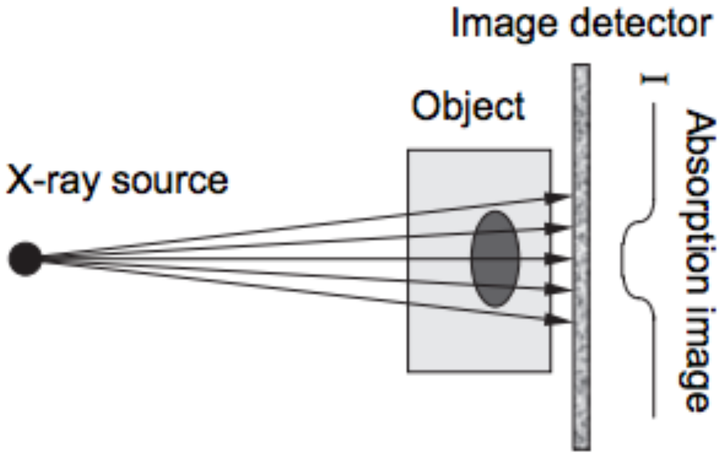

$$\eta = 1 - \delta - i\beta$$

Phase contrast

Object deflects photons, highlighting edges

Propagation-based, works for polychromatic sources

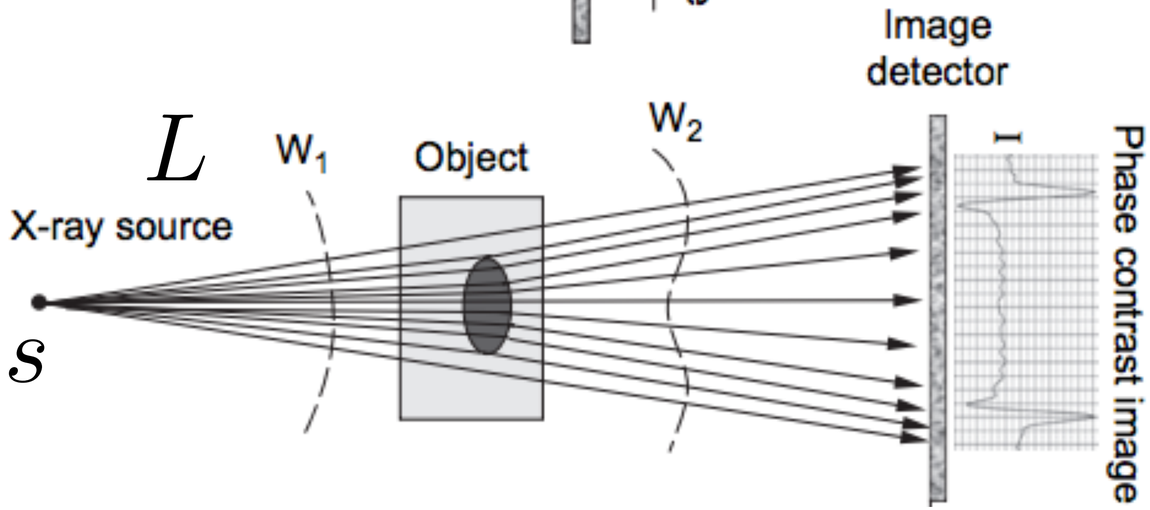

$$l_{coh} = \frac{\lambda L}{s}$$

Zhou S-A and Brahme A, Physica Medica (2008) **24**

Phase vs. absorption contrast

Absorption contrast

Contrast through photon absorption

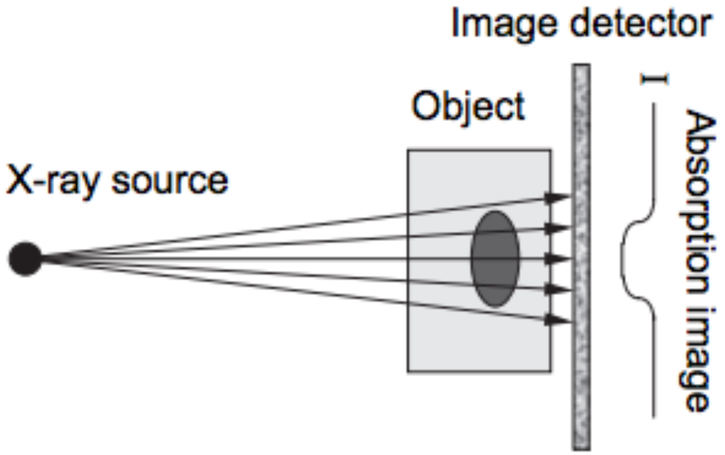

Phase shift Absorption

$$\eta = 1 - \delta - i\beta$$

Phase contrast

Object deflects photons, highlighting edges

Propagation-based, works for polychromatic sources

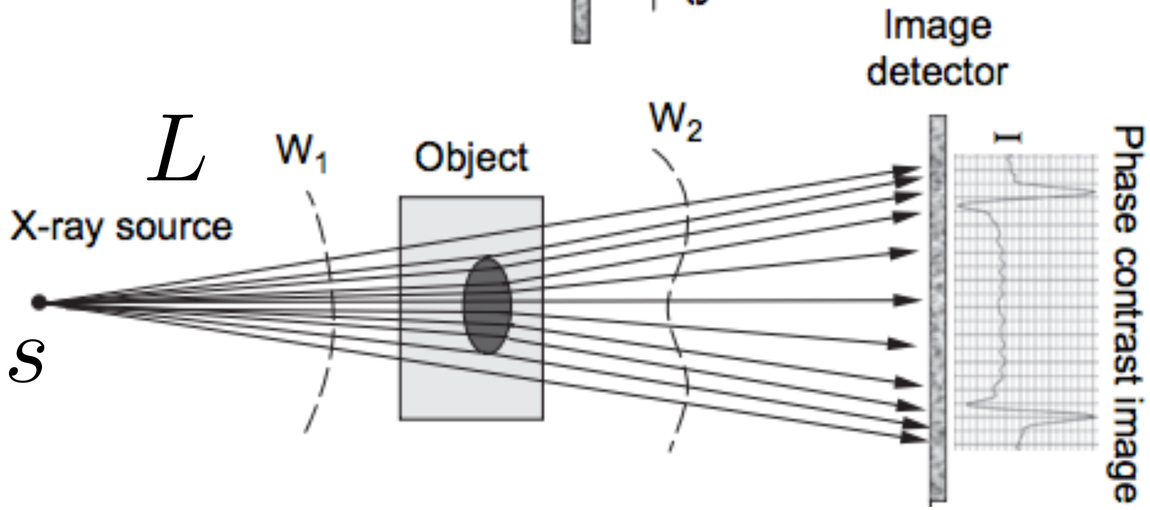

$$l_{coh} = \frac{\lambda L}{s}$$

Zhou S-A and Brahme A, Physica Medica (2008) **24**

Phase contrast imaging ideal for low-dose soft tissue imaging

- Conventional x-ray radiography in soft tissue gives poor contrast
- Phase contrast more sensitive
- Choose optimum photon energy to minimise absorption

Phase contrast method provides superior quality images with a lower dose

- X-ray source requirements:
  - High brightness at high energy (10's keV)
  - High degree of spatial coherence

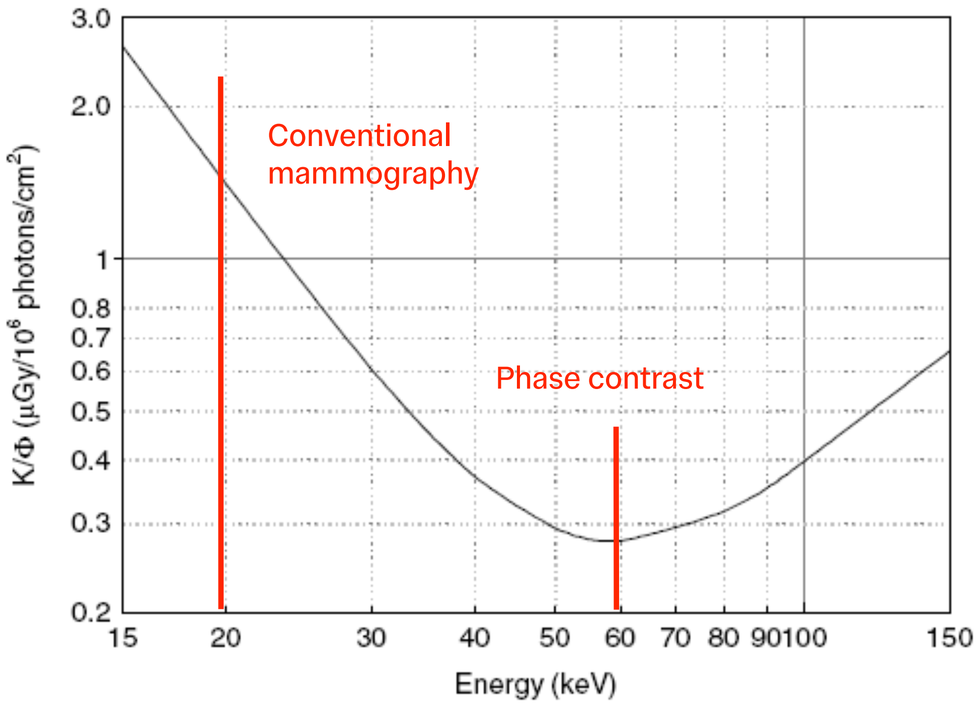

Energy deposition in breast tissue

Lewis Phys Med Biol 2004

Phase contrast for detecting steep gradients

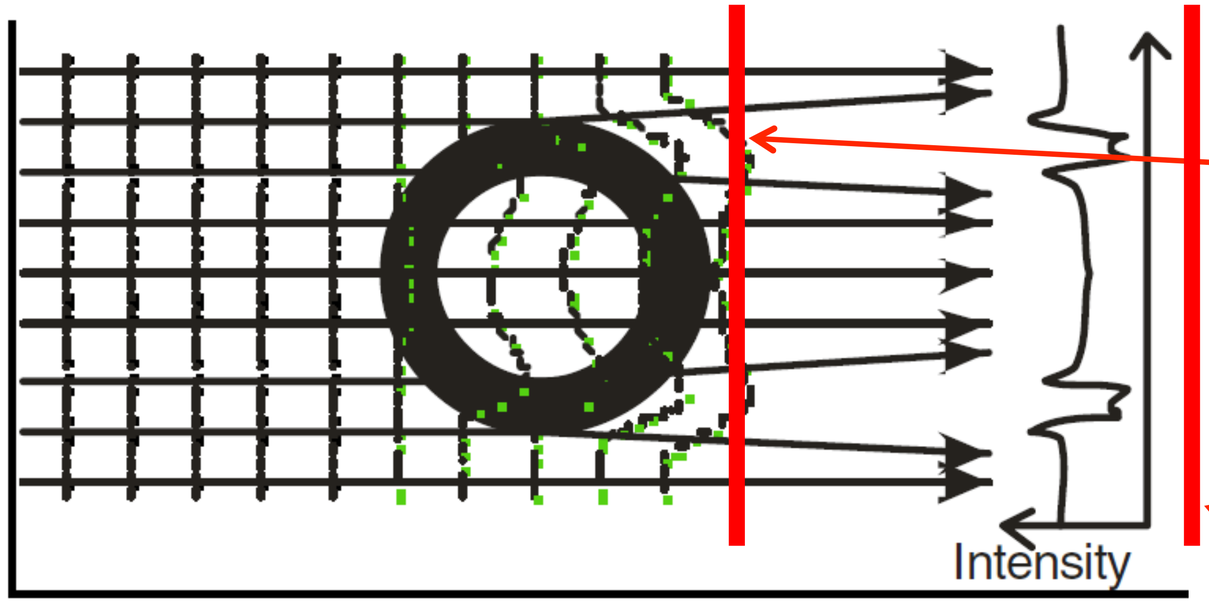

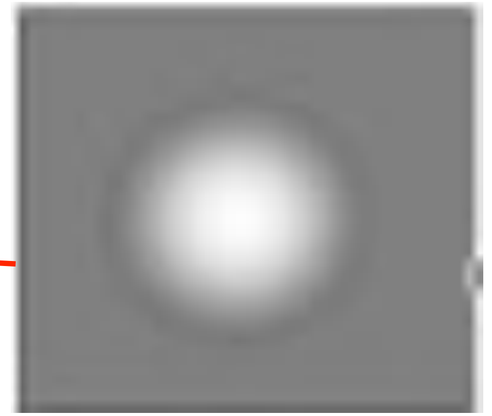

Absorption contrast

Phase contrast

- Conventional radiography shows difference of absorption in material
- Phase contrast generated by deflections of x-rays through material
- Much more sensitive when differences in refractive index are small
- To see diffractive effects, want Fresnel Number $N_F = a^2/L\lambda \lesssim 1$

Lewis Phys Med Biol 2004

Phase contrast imaging: Propagation method

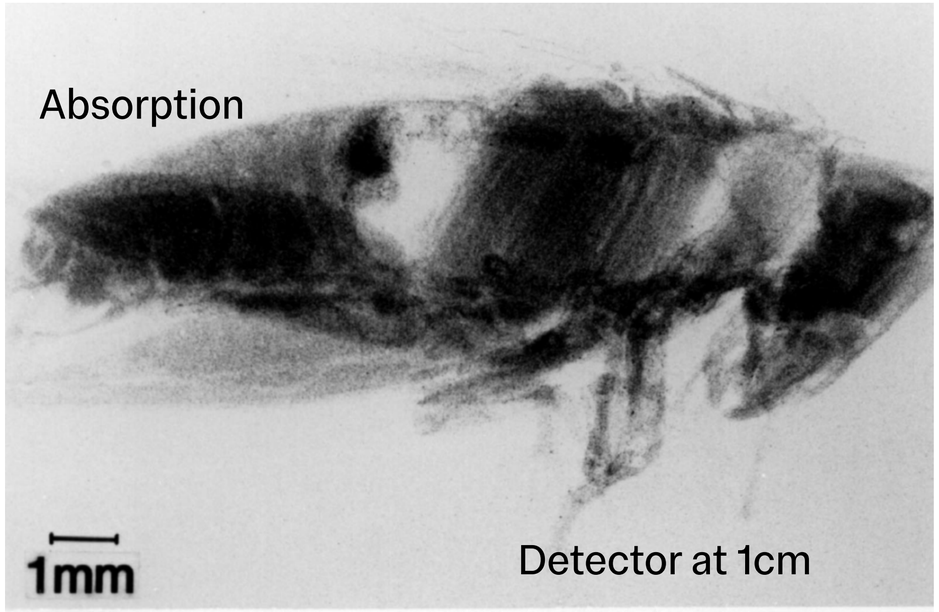

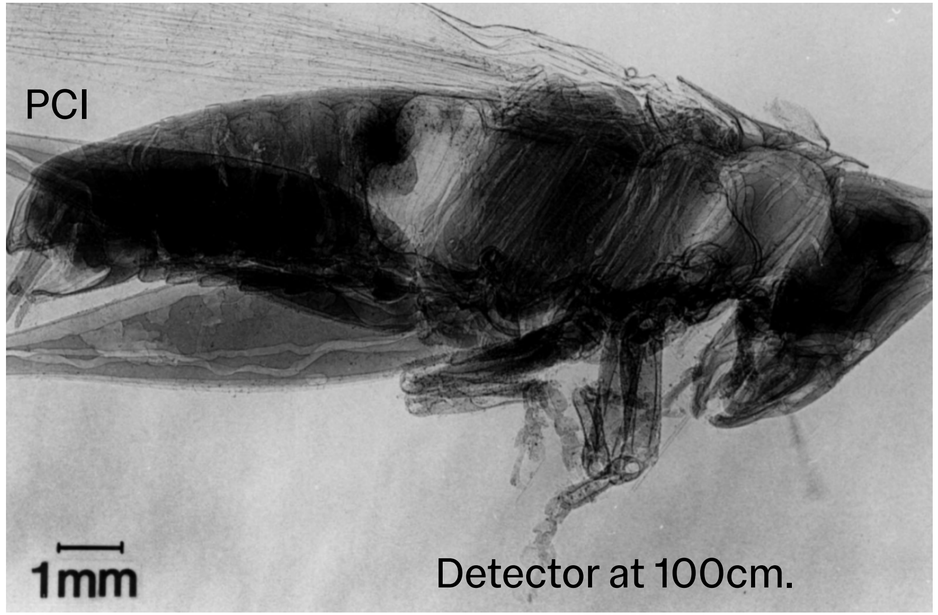

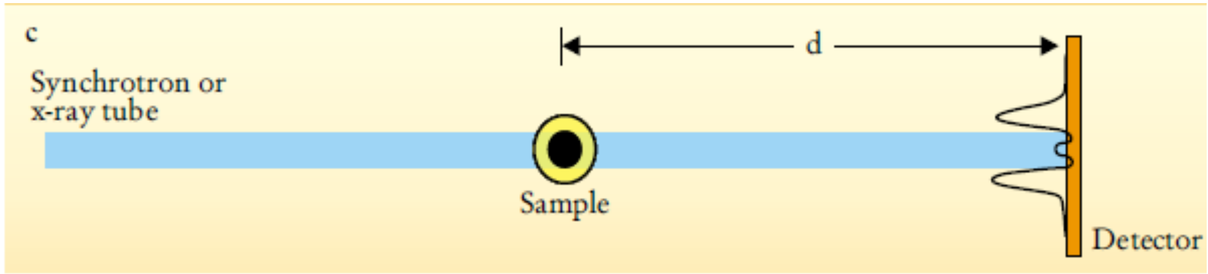

- Deflection of x-rays leads to edge enhancement through interference
- Need to increase sample-detector distance for image to form

Richard Fitzgerald, Phys. Today, July 2000

Phase contrast imaging: Diffraction enhanced imaging

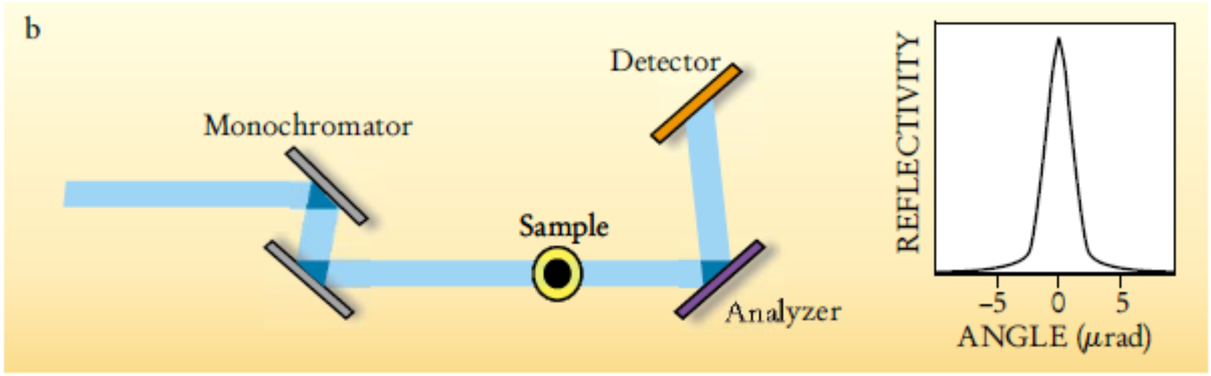

• Reflectivity of the crystal is extremely sensitive to angle (few microrad)

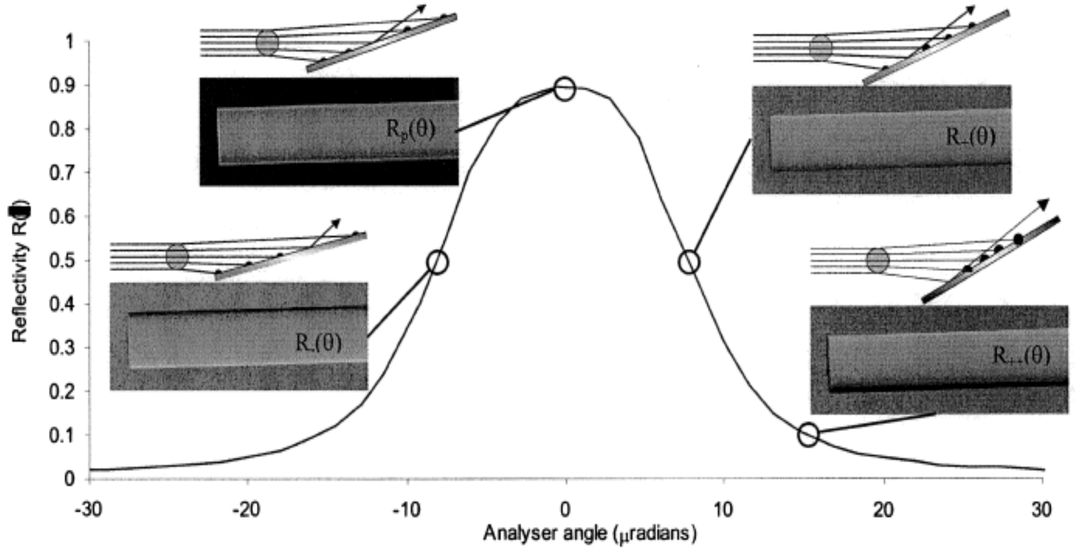

Lewis Proc SPIE 2002

Multiple Image Radiography

- Absorption (zero)
- Refraction (microrad)
- Scatter (millirad)

Richard Fitzgerald, Phys. Today, July 2000

Phase contrast imaging: Grating based interferometry

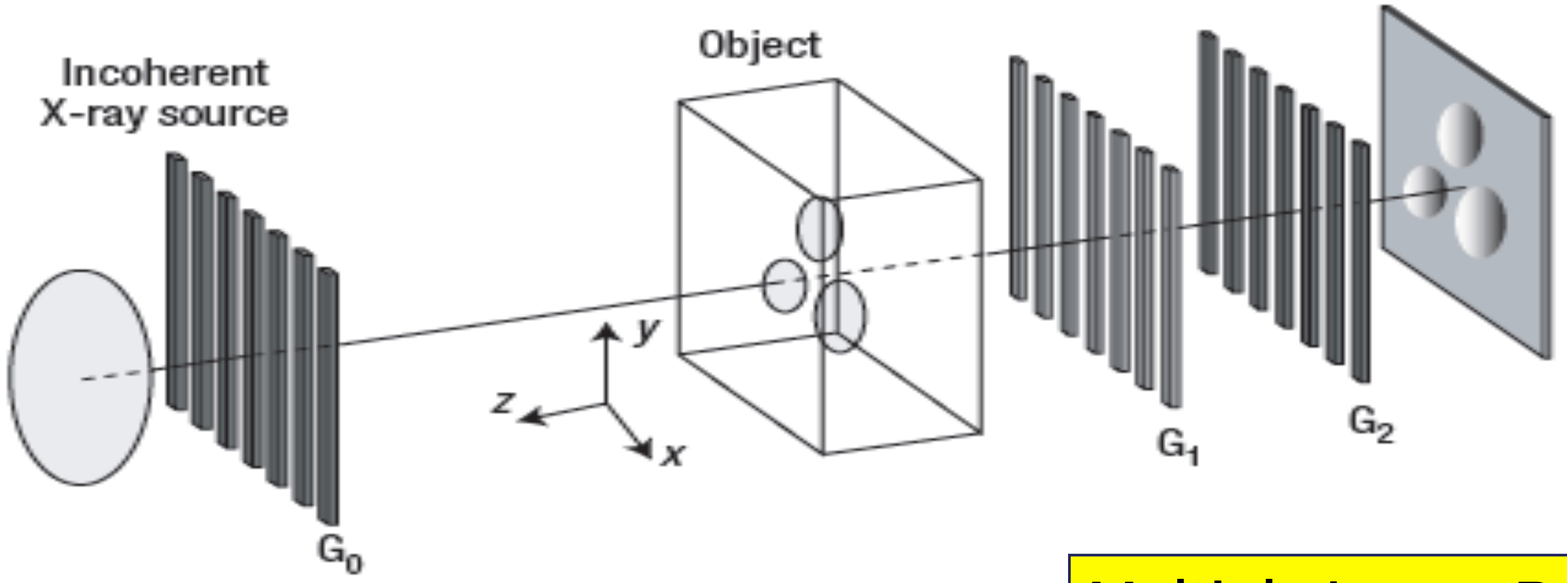

Talbot Lau interferometry

- G0 produces partially coherent source
- “Phase-step” G1 and G2 to separate different deflections

Multiple Image Radiography

•Absorption (zero)

•Refraction (microrad)

•Scatter (millirad)

Pfeiffer Nat. Phys 2006

Crystal and grating based PCI using standard x-ray tubes

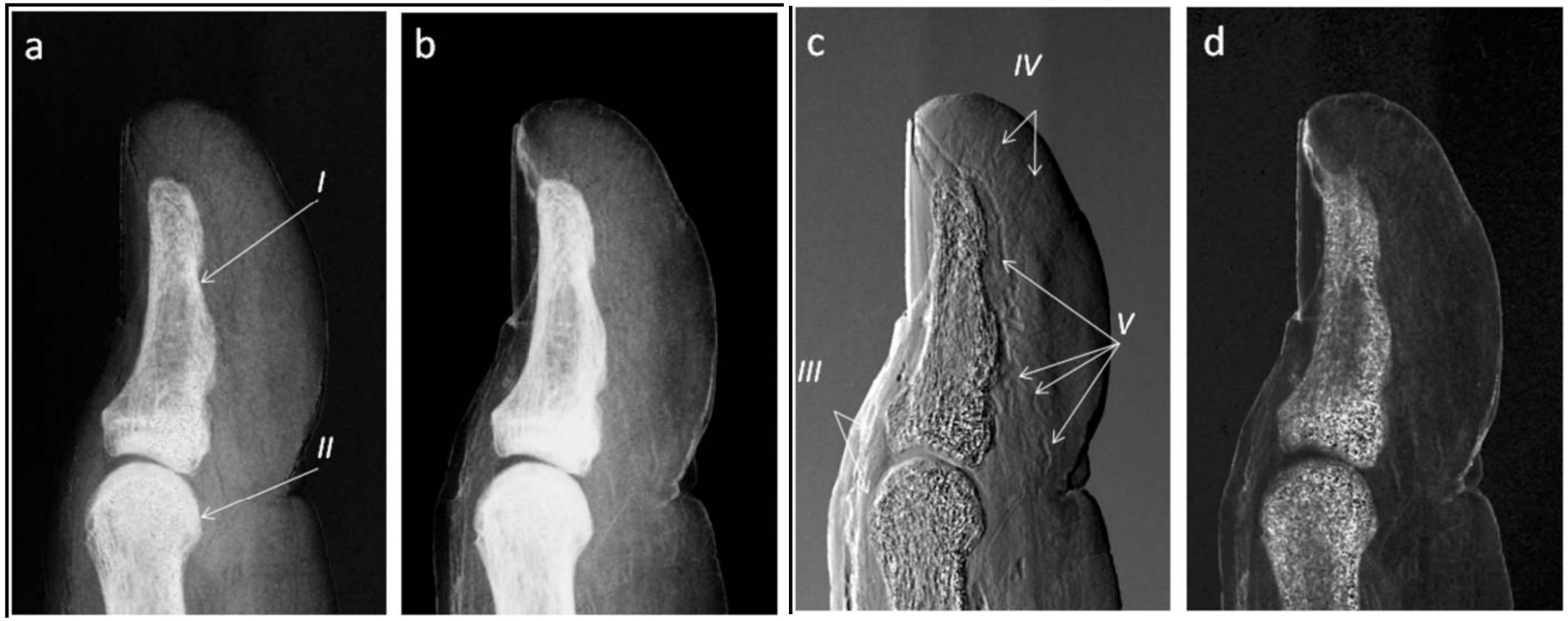

Conventional Radiography	Absorption (zero deflection)	Phase contrast (microrad deflection)	Scatter (millirad deflection)

• Phase contrast allows visualisation of:
III flexor pollicis longus tendon; IV connective tissue; and V blood vessels

http://www.neschllc.com; Nesch Rev Sci Instrum 2009

High flux from synchrotrons makes clinical application possible

Beamlines at several synchrotrons dedicated to phase contrast imaging, eg:
ELETTRA (Trieste) SYRMEP (Synchrotron Radiation for Medical Physics) Project

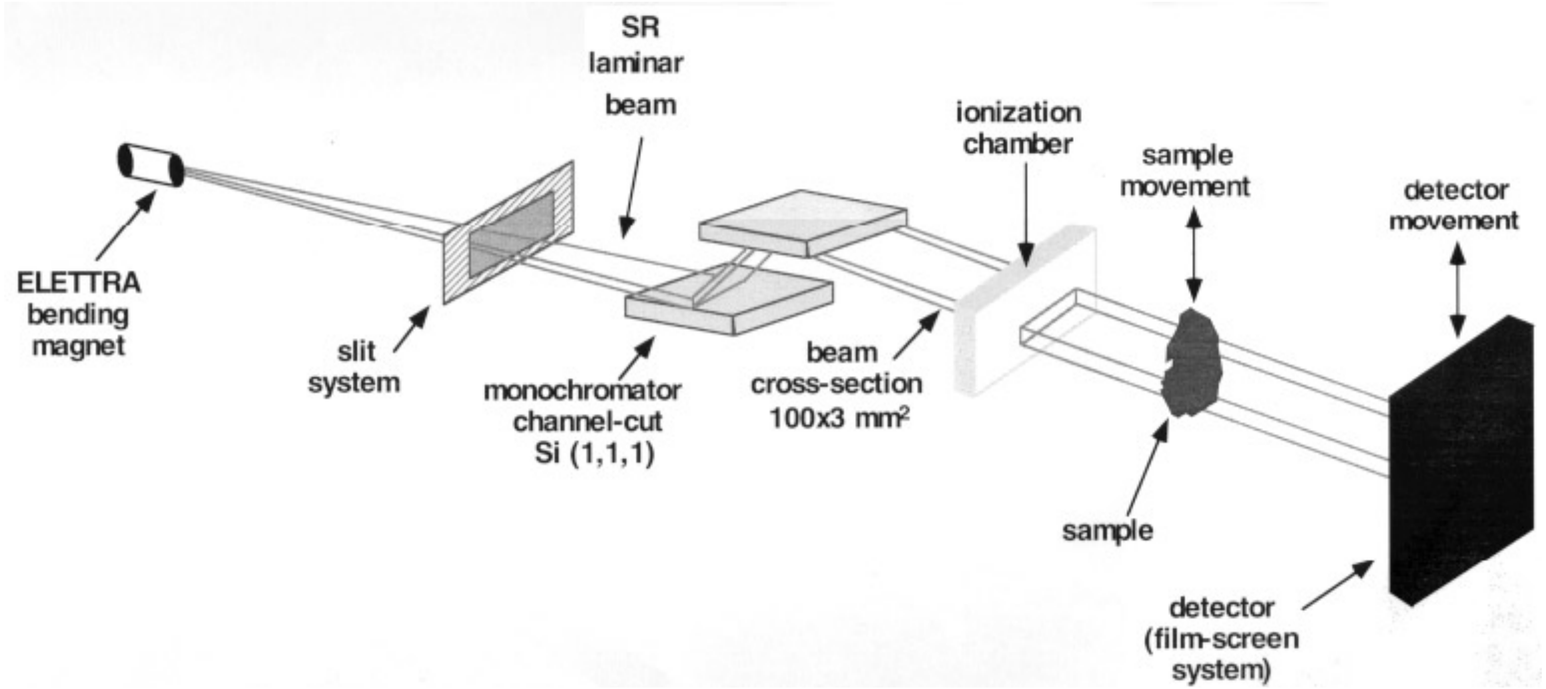

- Spatial coherence because of large source-sample distance
- Tunable (8 – 35 keV) monochromatic beam
- Sample is scanned through a 15cm x 4mm beam

Pani Phys Med Biol 2004 (ELETTRA)

Clinical trial comparing PCI with conventional mammogrpahy

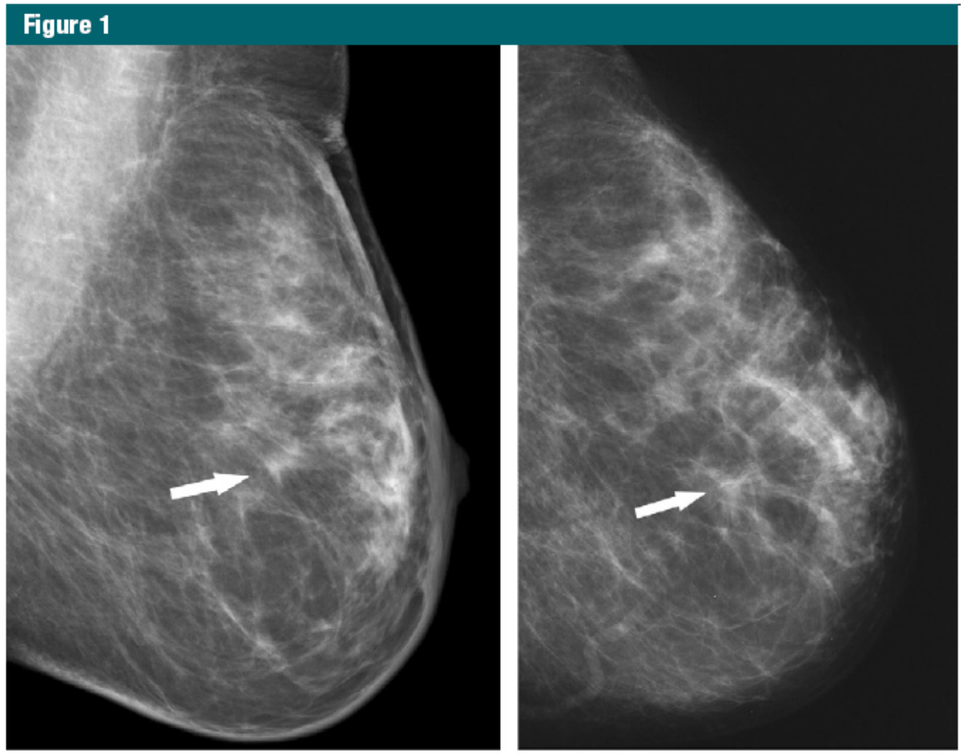

Absorption

Phase contrast

Expert radiologists judged PCI to be higher quality image

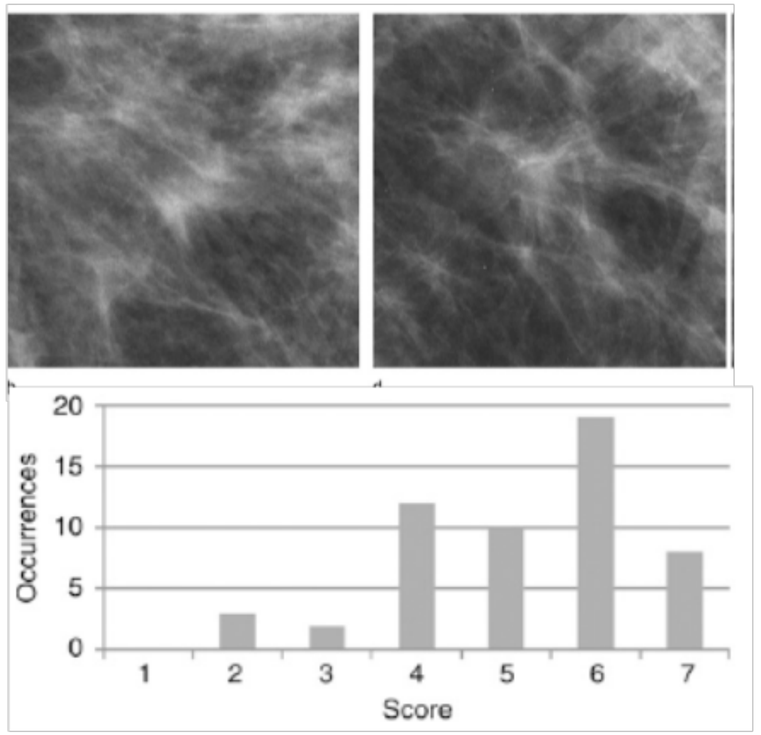

• Looking for spiculated mass with size several 100 microns

1 = conventional better
4 = same quality
7 = PCI better

Castelli Radiology 2011 (ELETTRA)

High repetition rate allows dynamic imaging using synchrotrons

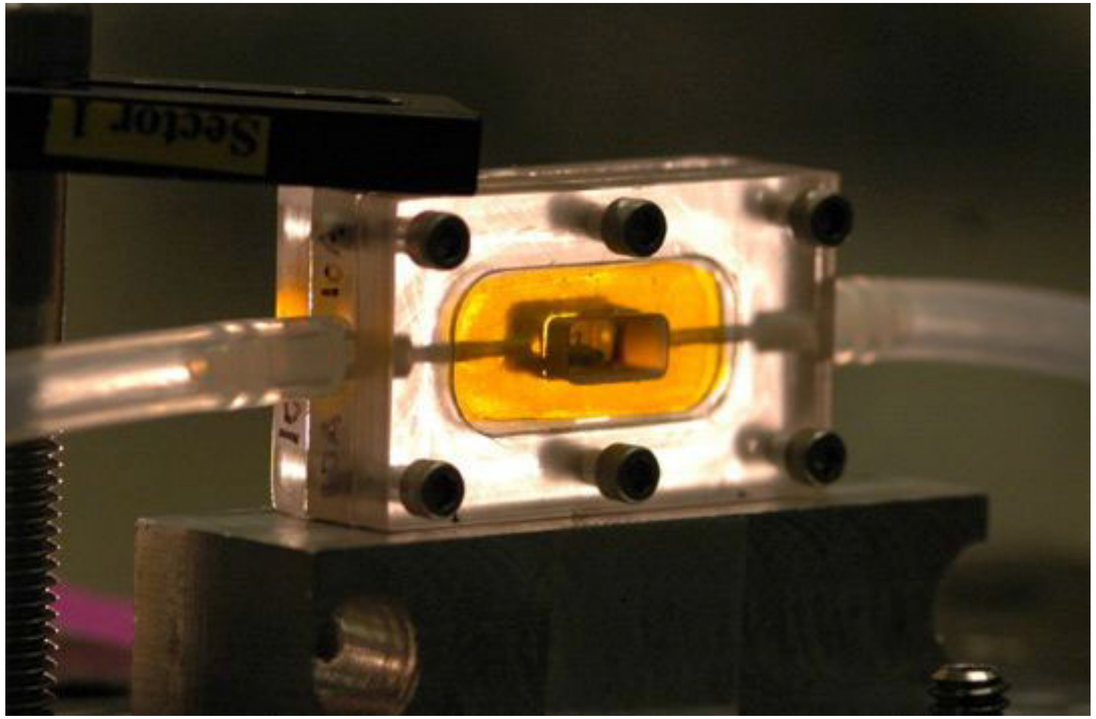

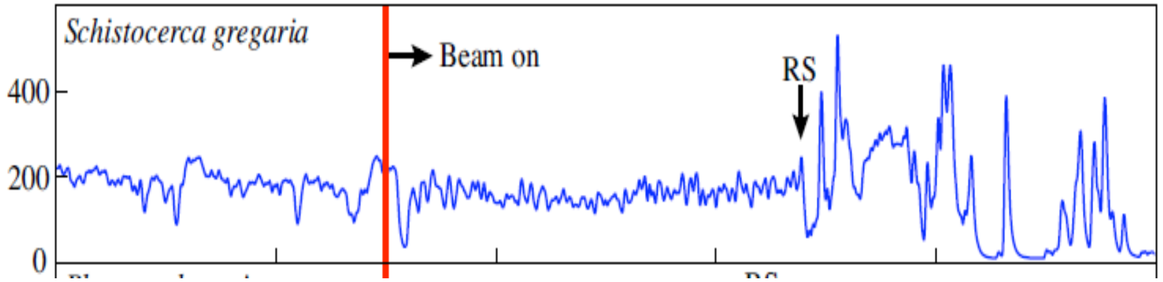

- Insects placed in respirometry chamber
- Grasshopper exposed for about 10 minutes before respiratory signature
- 25 keV x-rays at 88MHz
- Image acquired in 1/60s
- Captured by scintillator and CCD at 30 fps

Socha et al BMC Biology 2007, 5:6

Dynamic imaging using synchrotrons

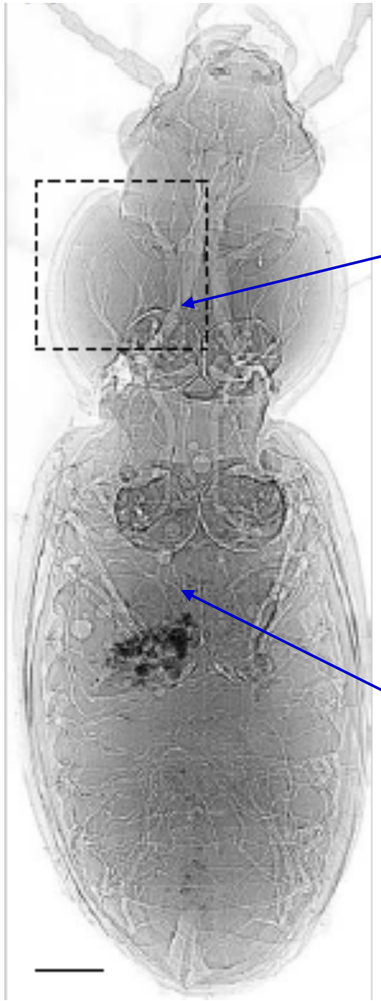

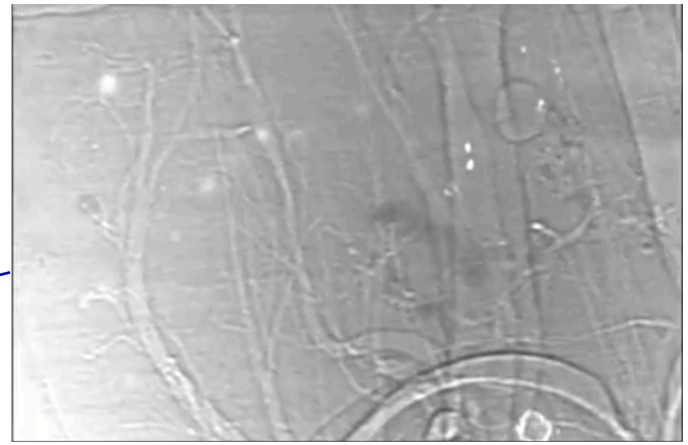

Rhythmic compressive movements in the tracheal system in the carabid beetle Platynus decentis

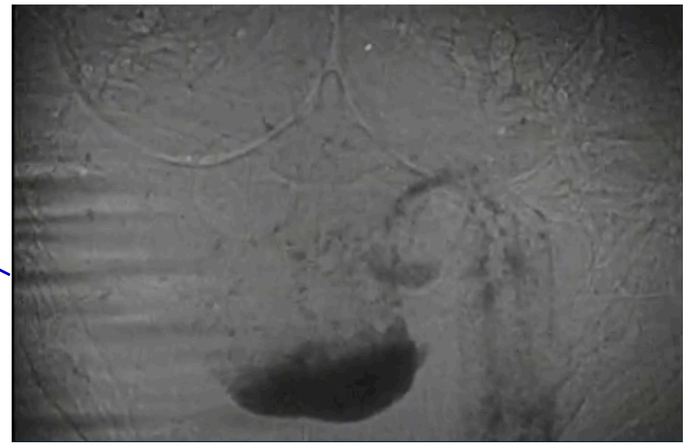

Movements of the foregut and gut contents of the carabid beetle Pterostichus stygicus

High reprate operation of synchrotron sources allows realtime imaging of biological processes

Aerobic chamber allows imaging of respiration and digestion of Beetles

Socha et al BMC Biology 2007, 5:6

Dynamic imaging using synchrotrons

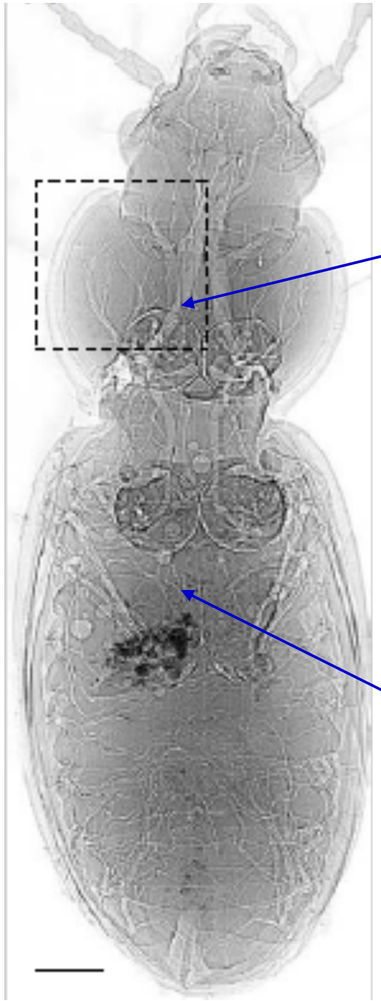

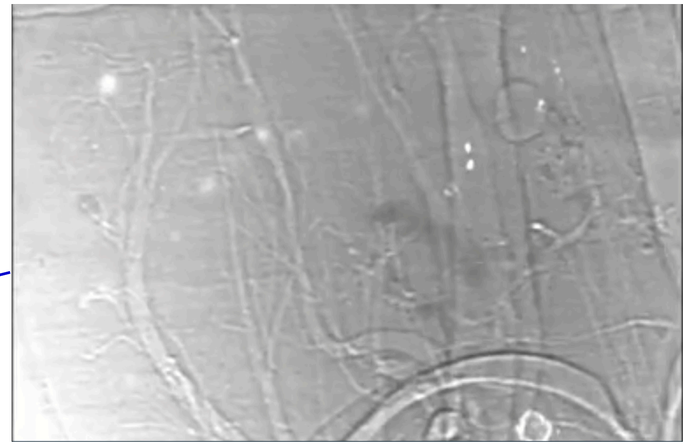

Rhythmic compressive movements in the tracheal system in the carabid beetle Platynus decentis

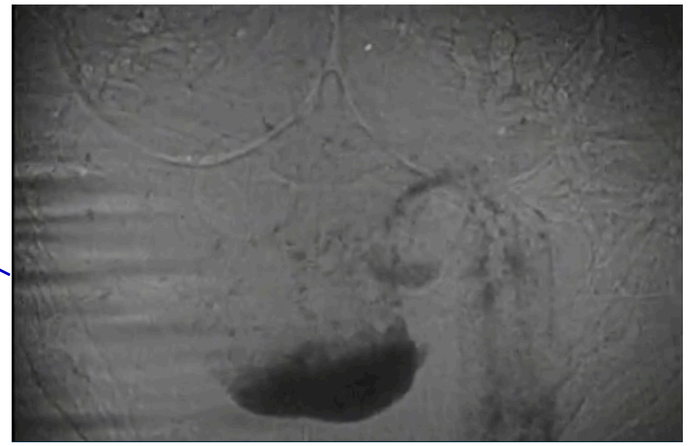

Movements of the foregut and gut contents of the carabid beetle Pterostichus stygicus

High reprate operation of synchrotron sources allows realtime imaging of biological processes

Aerobic chamber allows imaging of respiration and digestion of Beetles

Socha et al BMC Biology 2007, 5:6

Dynamic imaging using synchrotrons

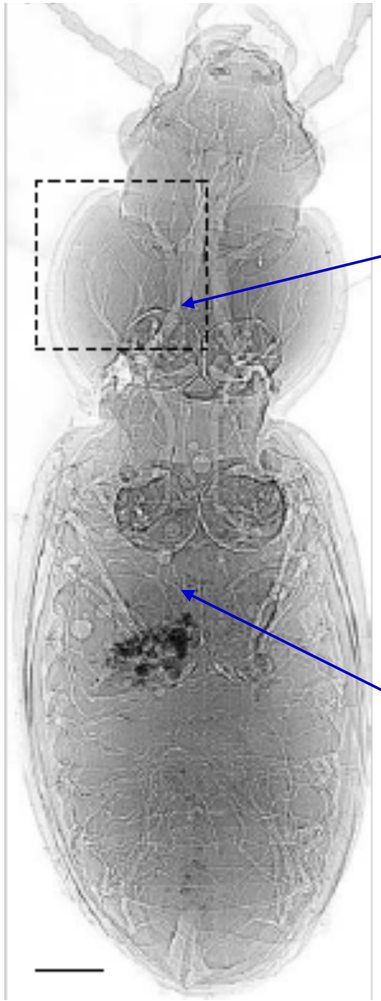

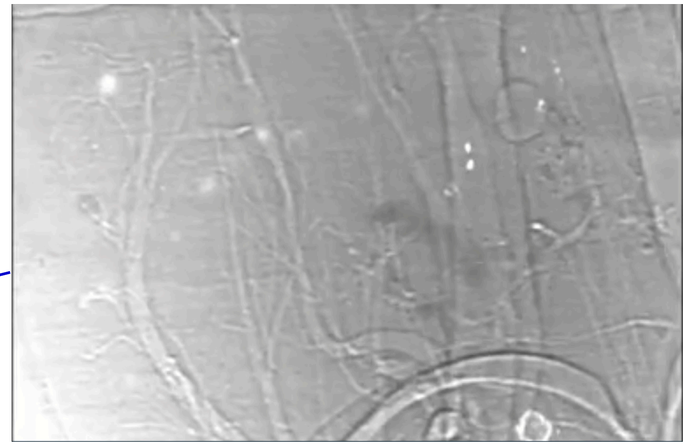

Rhythmic compressive movements in the tracheal system in the carabid beetle Platynus decentis

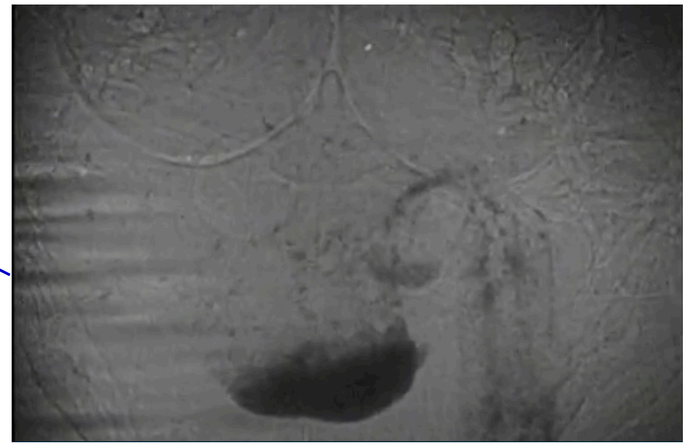

Movements of the foregut and gut contents of the carabid beetle Pterostichus stygicus

High reprate operation of synchrotron sources allows realtime imaging of biological processes

Aerobic chamber allows imaging of respiration and digestion of Beetles

Socha et al BMC Biology 2007, 5:6

Betatron imaging

Imaging of Biological Specimens

X-ray **projection image** of Orange Tetra
Camera & fish at 3 m from source
Camera had to be moved to capture entire specimen
quasi single shot

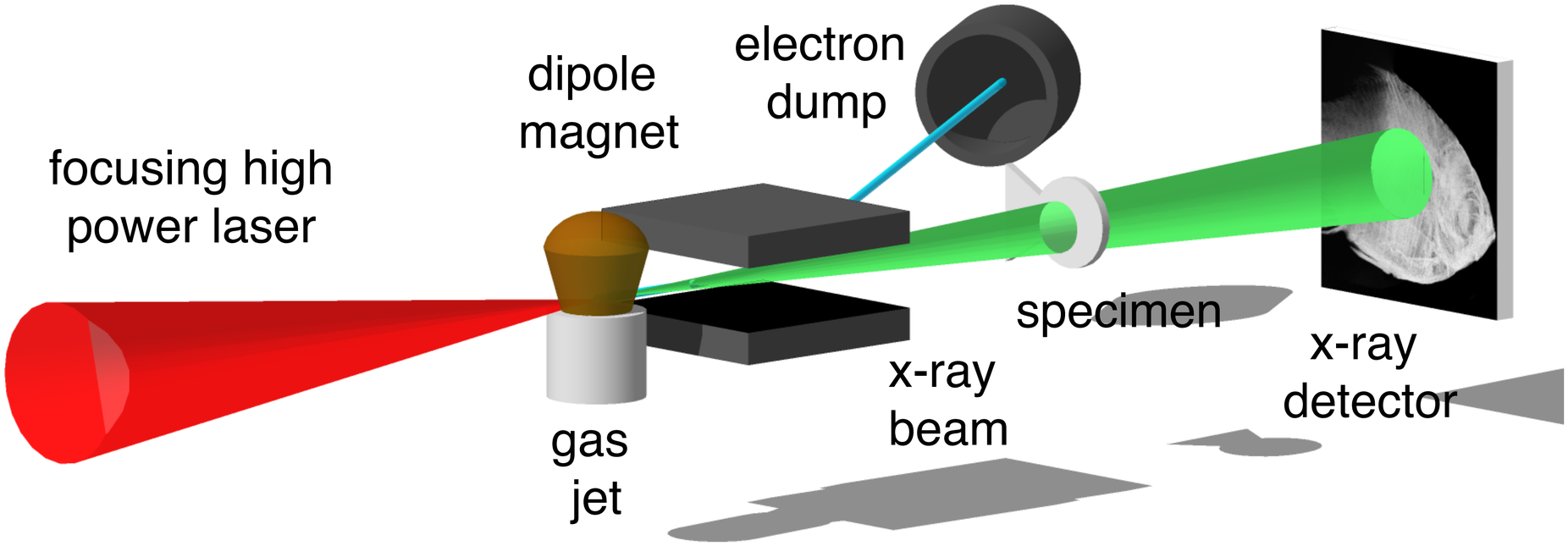

Imaging of Biological Specimens

X-ray projection image of Orange Tetra
Camera & fish at 3 m from source
Camera had to be moved to capture entire specimen
quasi single shot

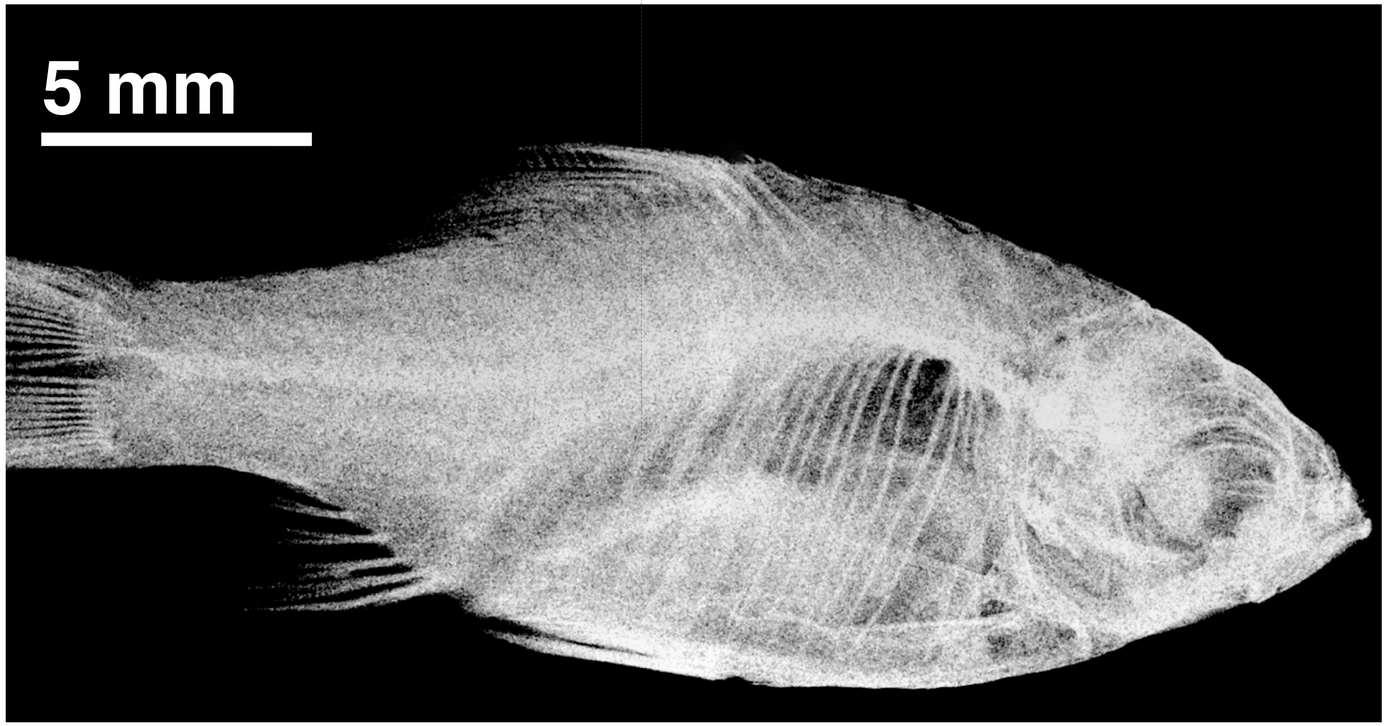

Imaging of Biological Specimens

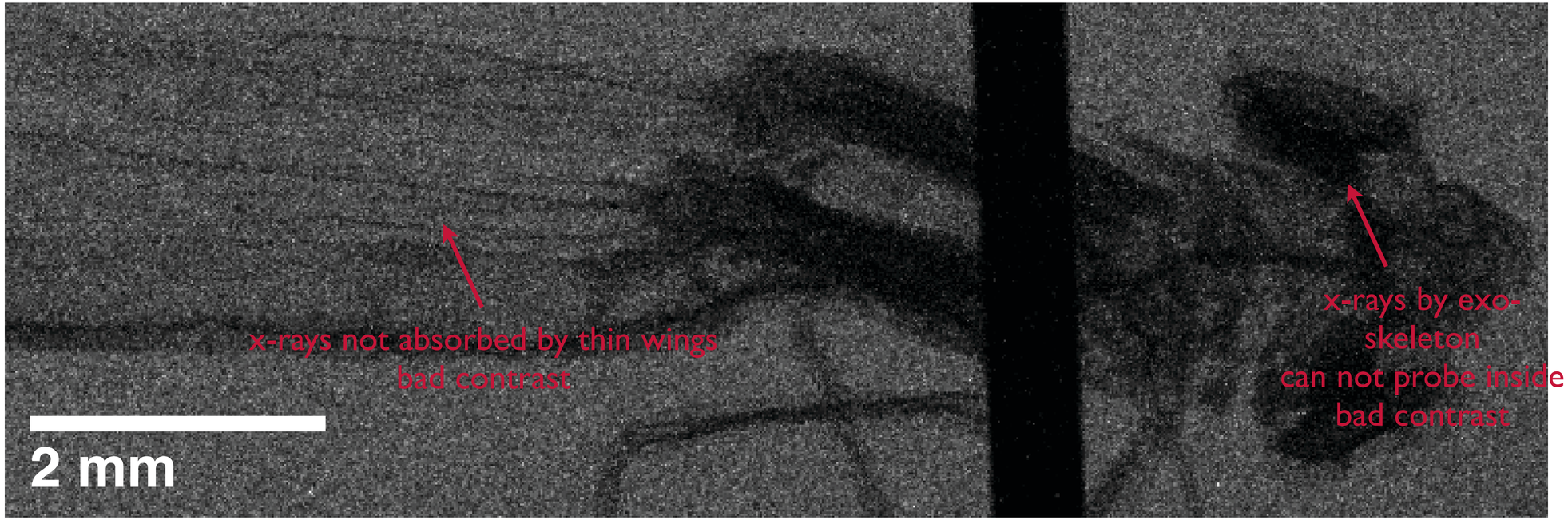

- X-ray **projection** image of damsefly
- Camera & damselfly at 3 m from source
- Camera had to be moved to capture entire specimen
- quasi single shot

Imaging of Biological Specimens

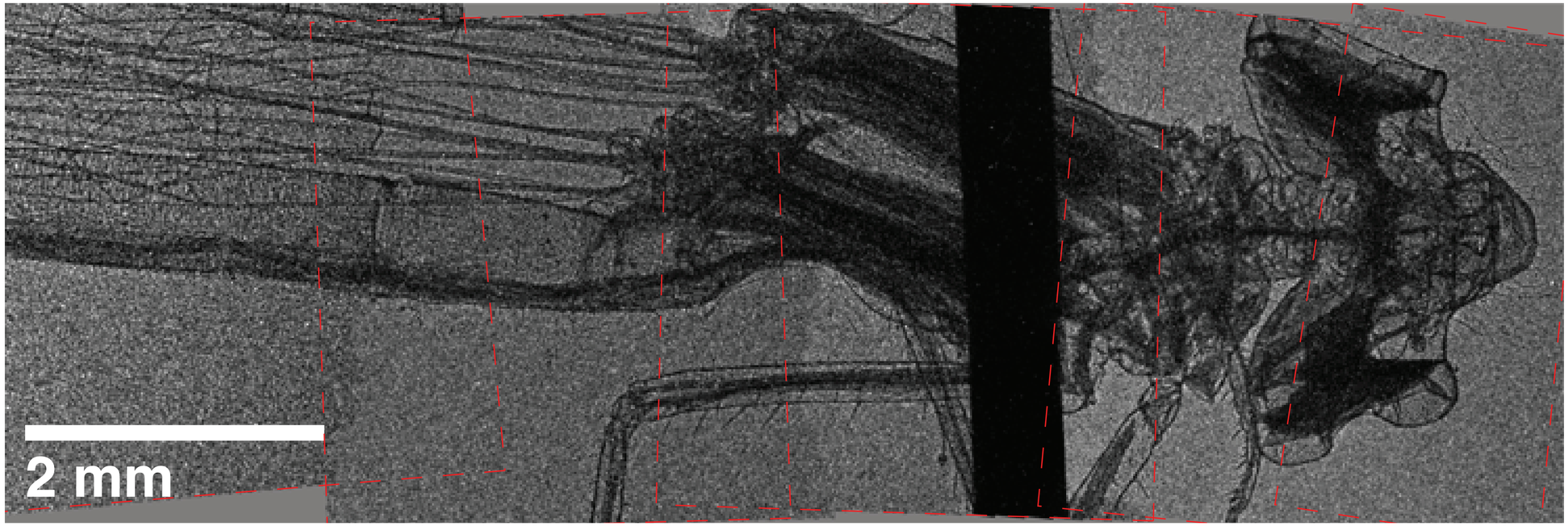

- X-ray **phase contrast image** of damsefly
- Camera at 1.8 m from source, damselfly at 0.5 m from source
- Camera had to be moved to capture entire specimen
- single shot

S Kneip et al., Appl. Phys. Letters. **99**, 093701 (2011)

Phase contrast for soft tissue imaging performed with synchrotron sources

- Absorption contrast is poor for soft tissues since they are uniform
- Phase contrast provides an image of the tissue structures
- Phase contrast imaging of soft tissues showing near histologic quality obtained in synchrotrons

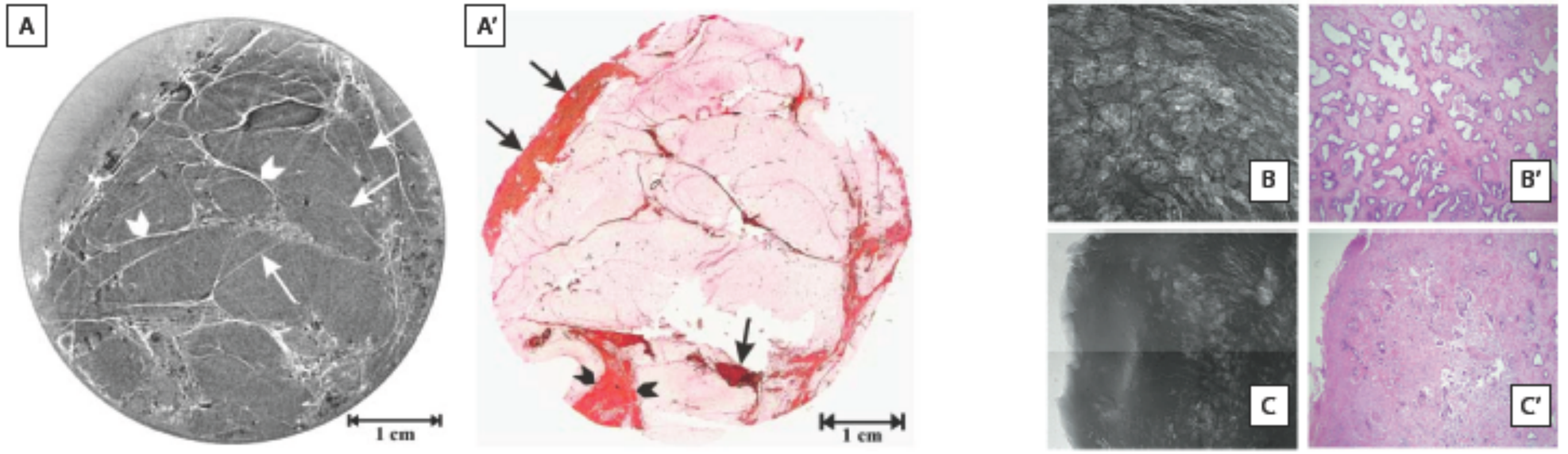

Figure 1: Phase contrast (A, B, C) and histology (A', B', C') of human breast and prostate tissue (taken with conventional synchrotron), showing near histologic image definition in phase contrast imaging [9,10].

C. Y. Yoon et al, Int. J. Urol, **14**, 96 (2007).
J. Keyrilainen et al, Acta Radiol, **51**, 866 (2010).

Soft tissue sample holder

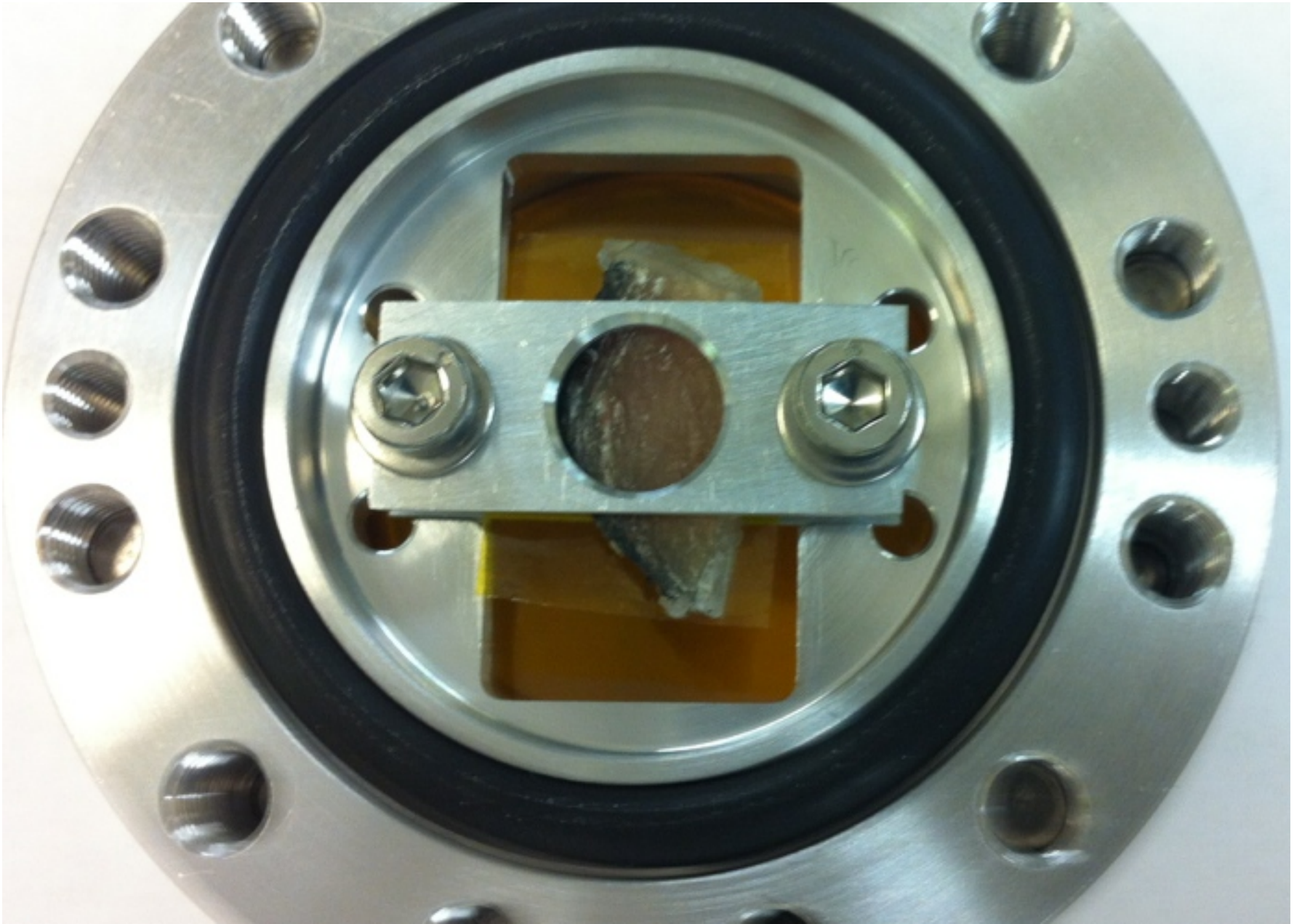

Prostate Imaging with Gemini

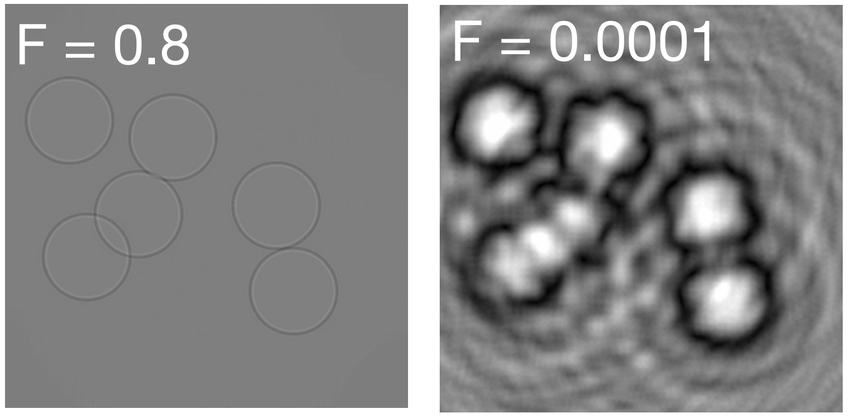

Phase contrast function of Fresnel number *F*

$$F = a^2 E / L$$

Optimal imaging distance proportional to photon energy

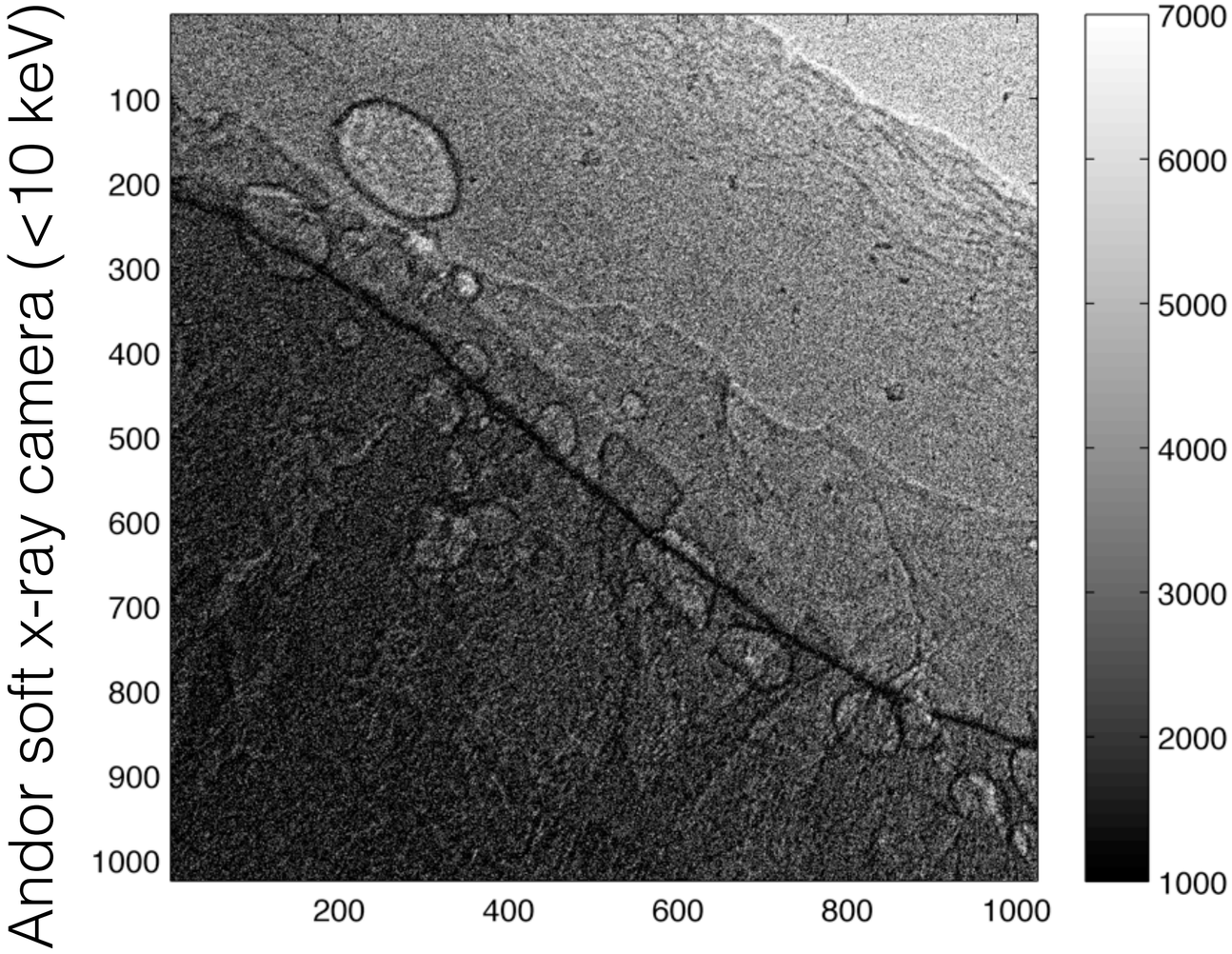

Typical raw x-ray image after denoising

Prostate Imaging with Gemini

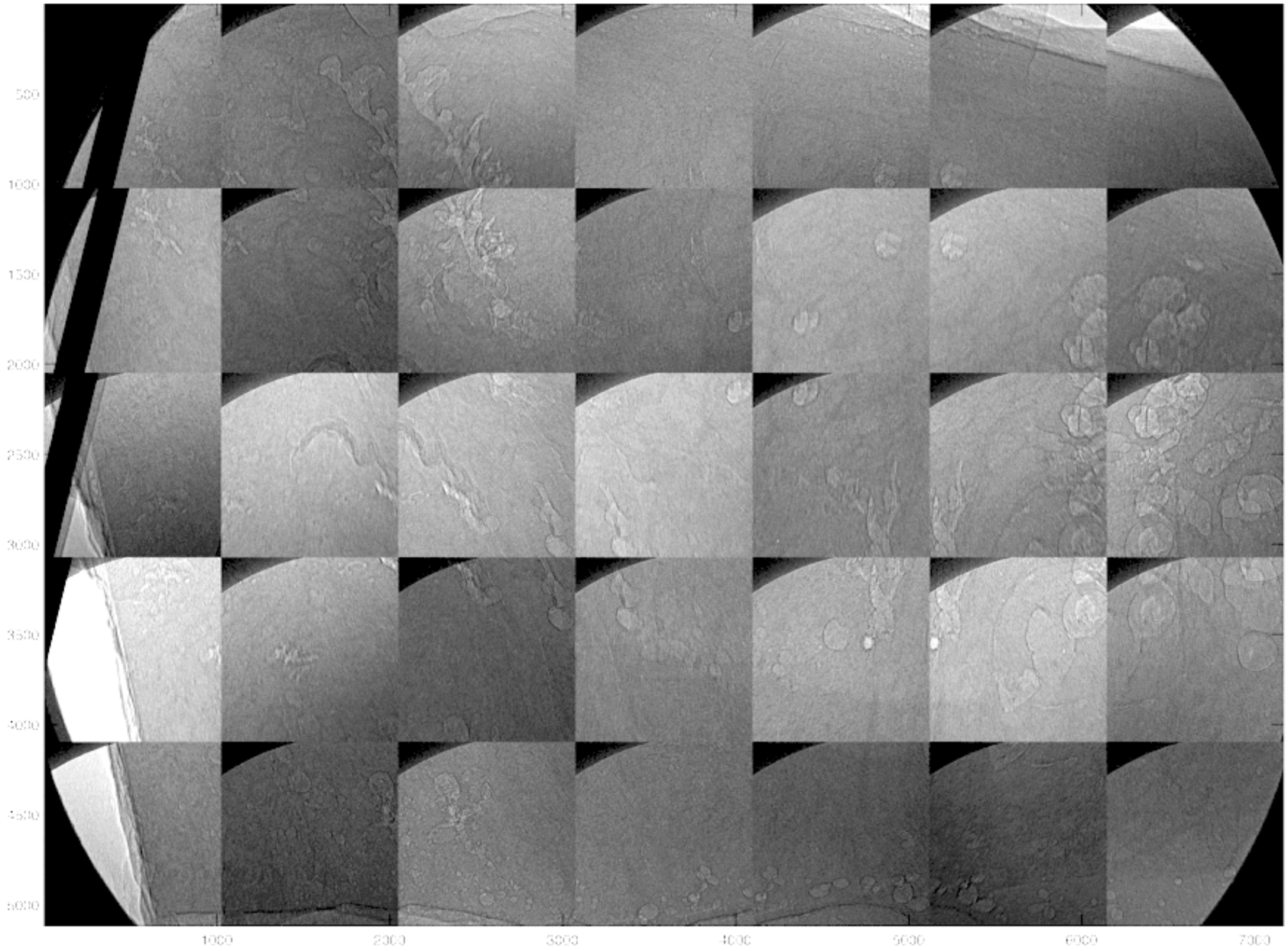

sample CS12 12779 (3 mm)
- High Grade

Prostate Imaging with Gemini

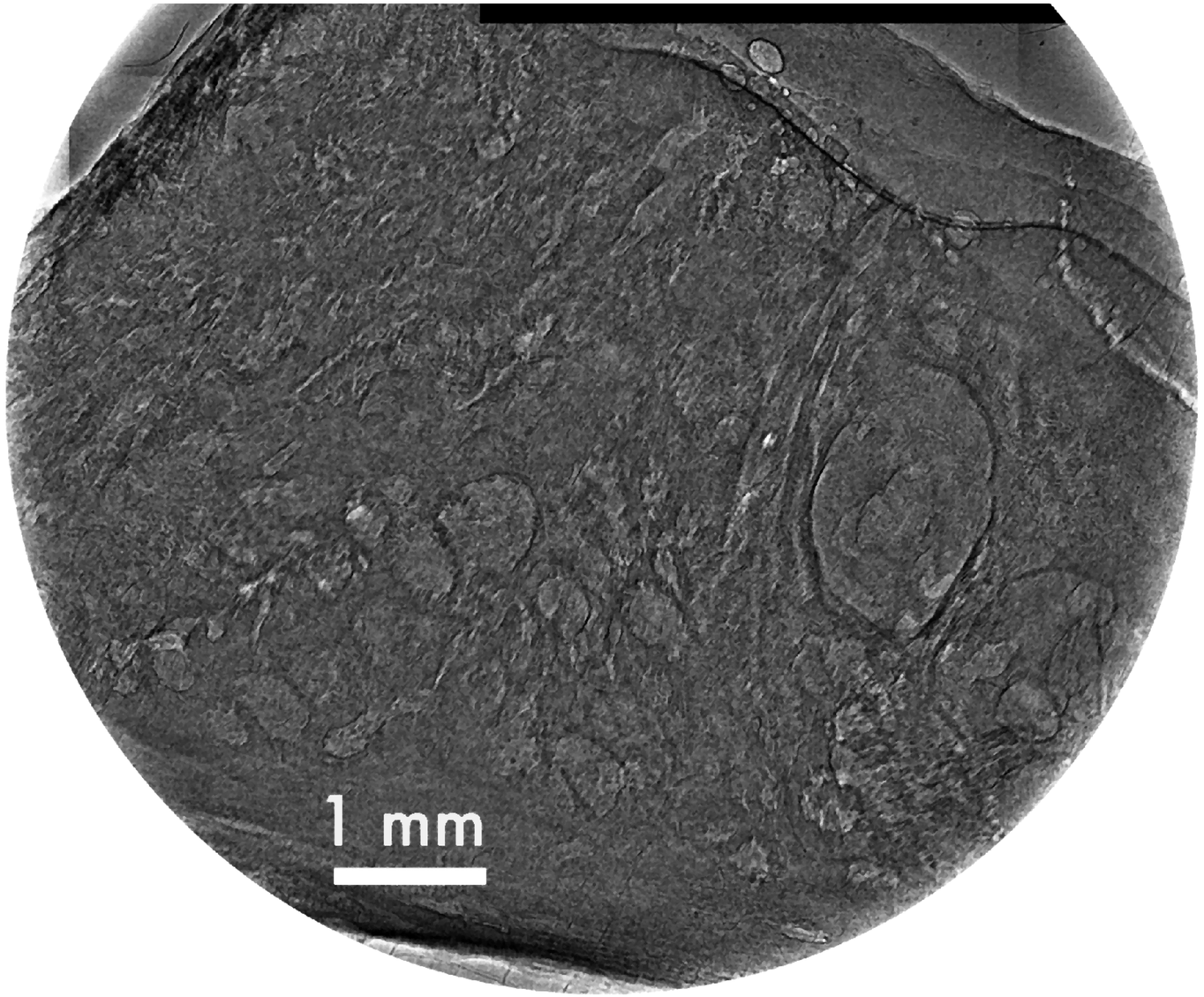

Lopes N. et al. X-ray phase contrast imaging of biological specimens with femtosecond pulses of betatron radiation from a compact laser plasma wakefield accelerator.

Breast tissue Imaging with Gemini

Raw data

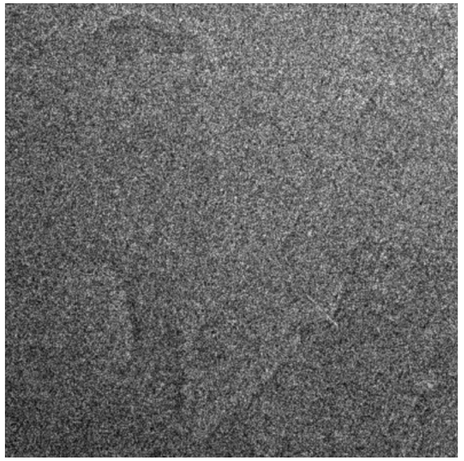

Raster scan + noise reduction

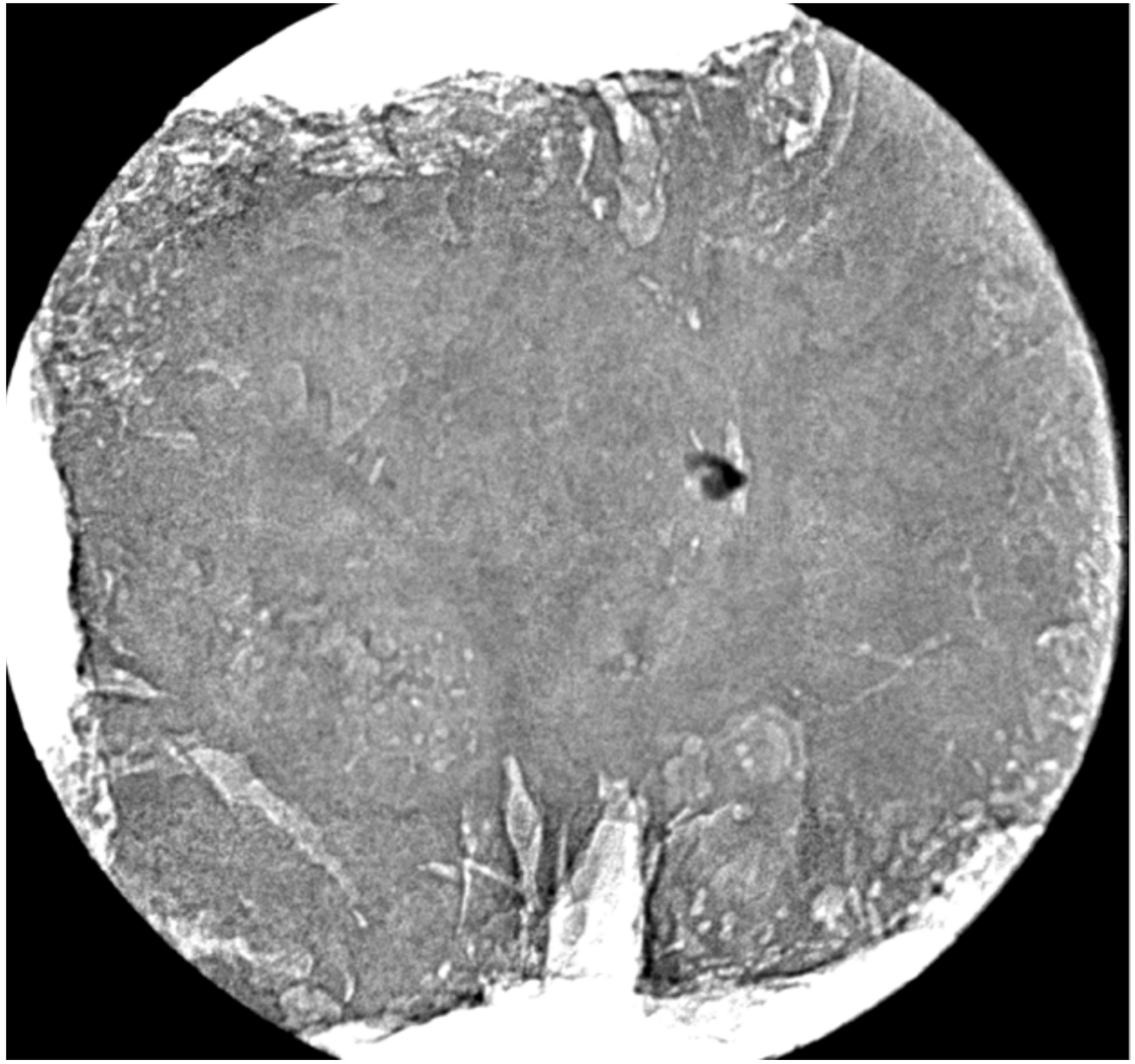

Raw data relatively noisy

Advanced stitching and denoising techniques developed at IC

Imaging bone with Gemini

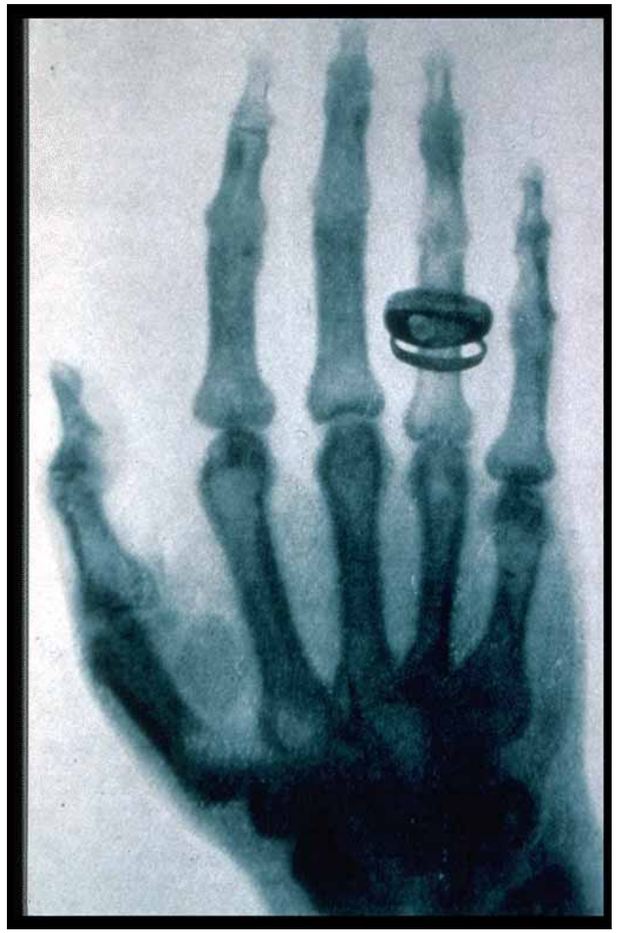

Roentgen 1896

7 mm bone sample transmission

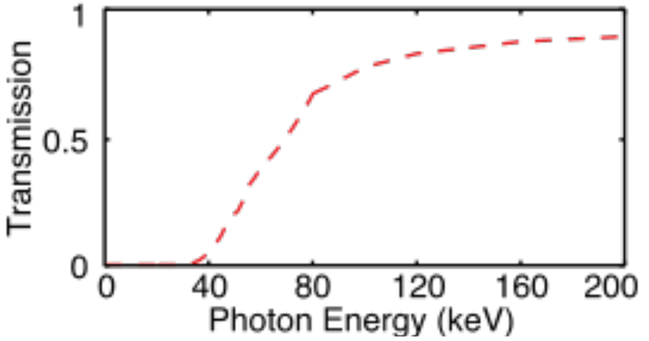

X-ray signal at detector

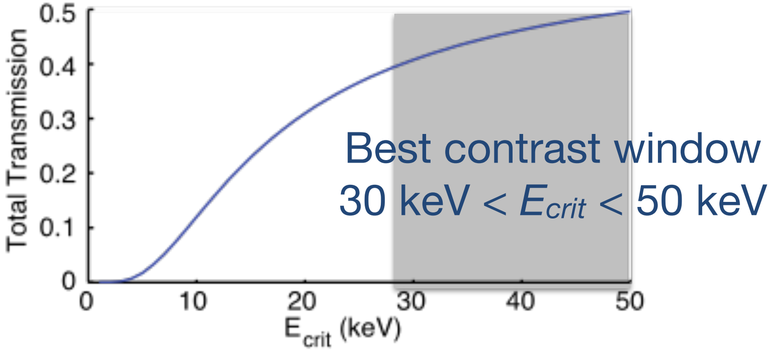

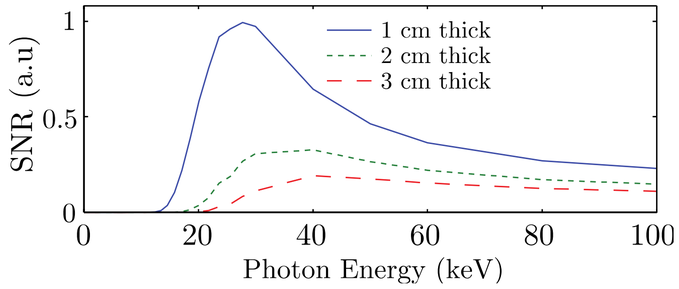

Absorption contrast is sensitive to dI/dE (absorption)

Typical peak in the signal-to-noise ratio (SNR).

Important for reducing dose

Picking the right imaging energy is important

Raw betatron image of trabecular bone after denoising

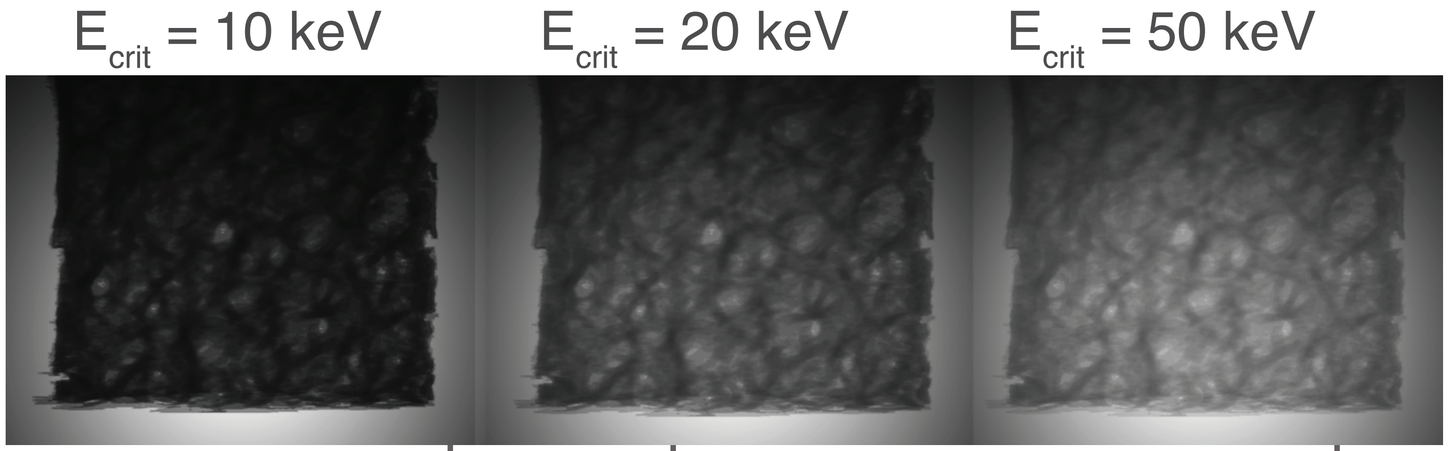

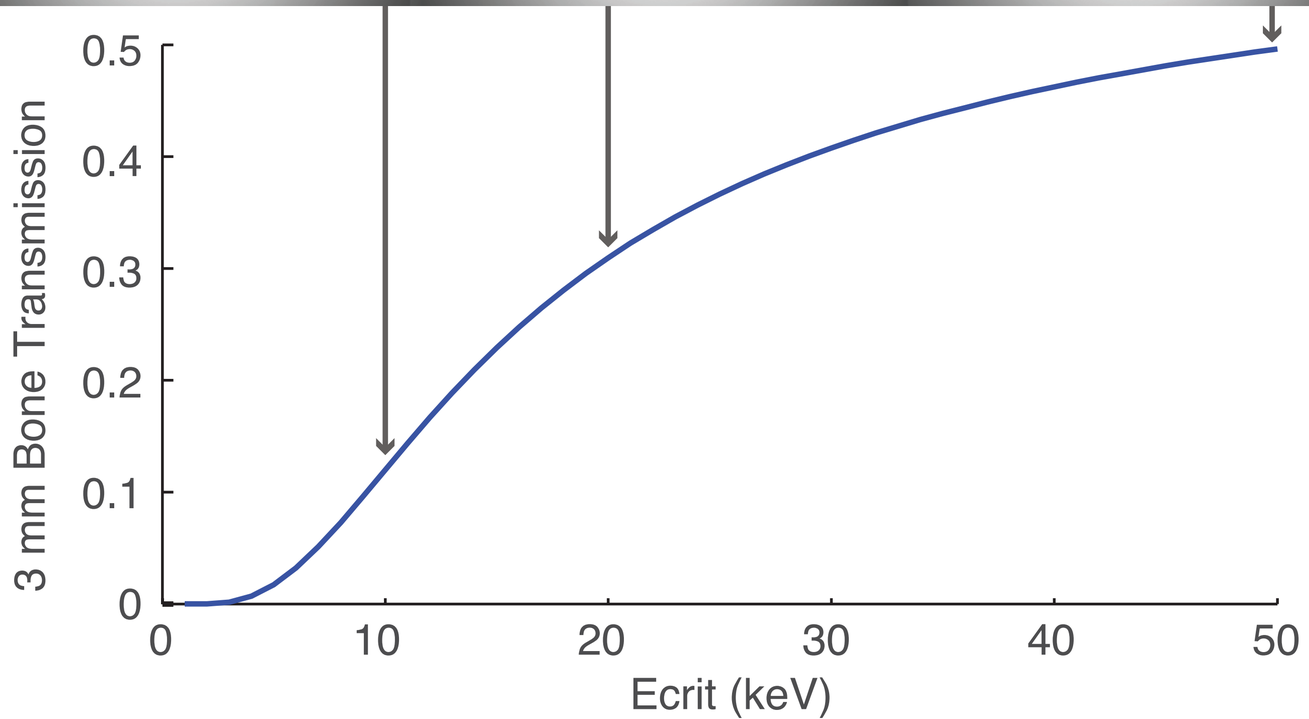

Rotation scan

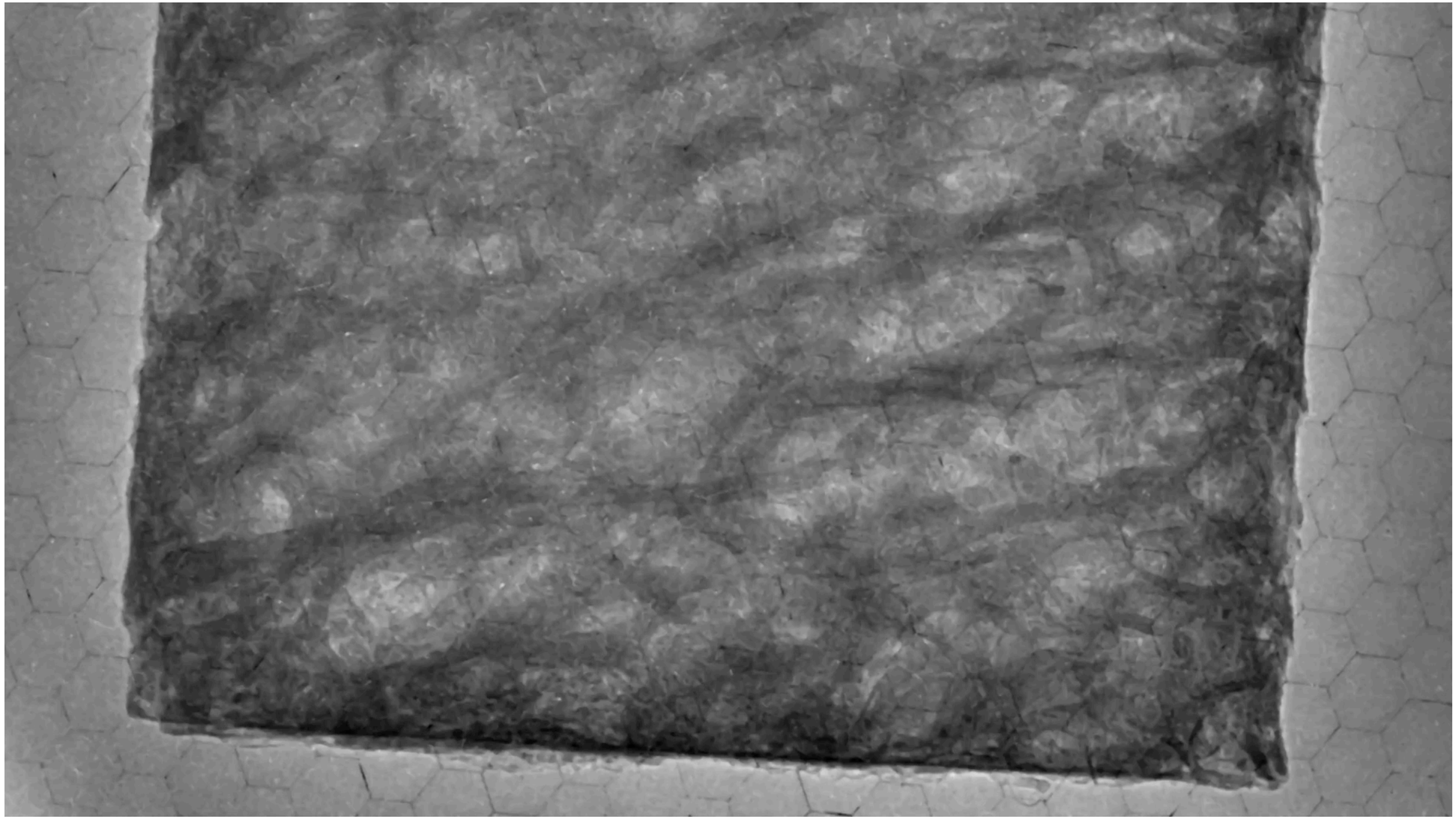

Rotation scan

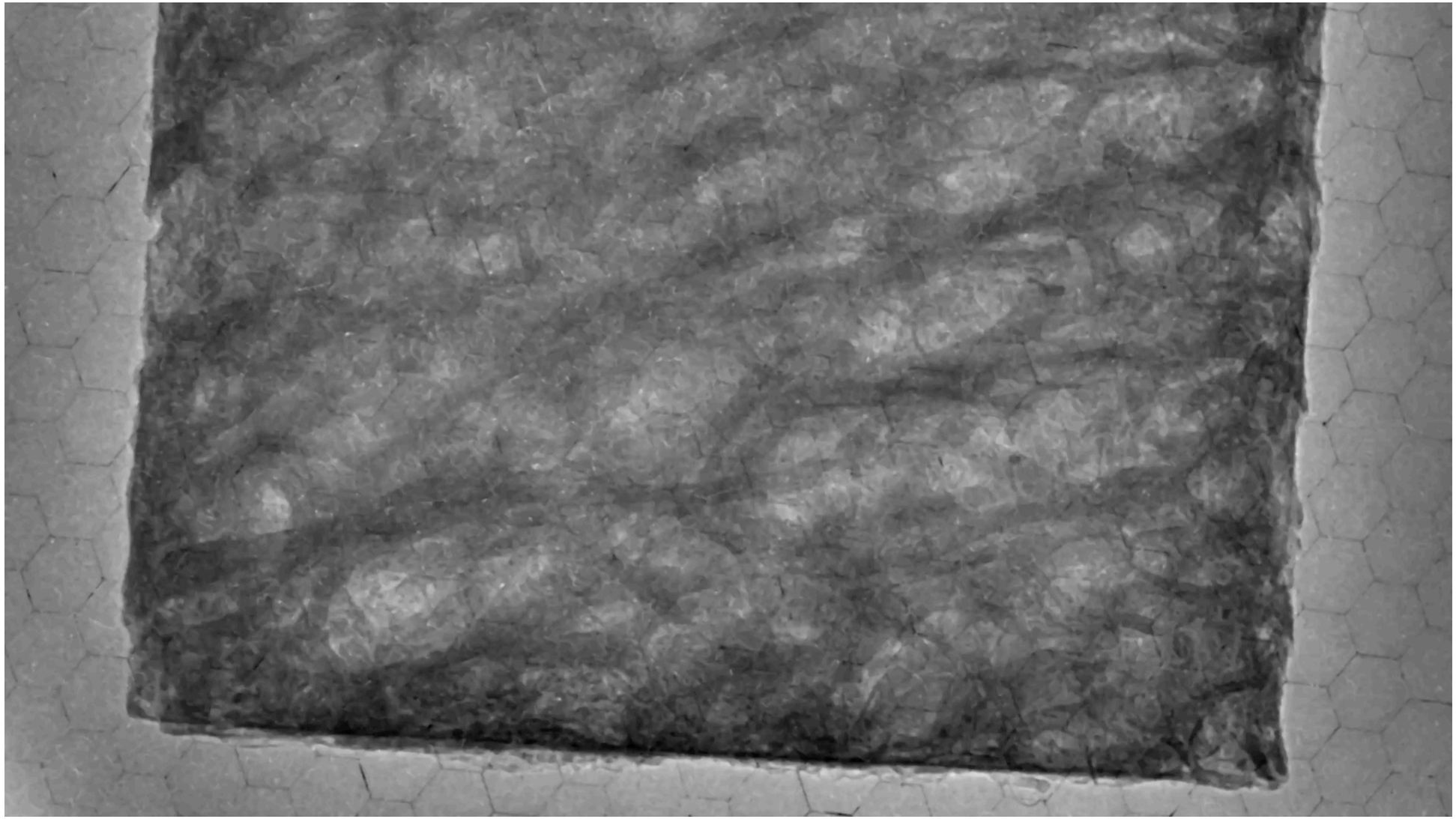

Sonogram from rotation scan

180 projections taken at 1˚ intervals

Inverse Radon Reconstruction

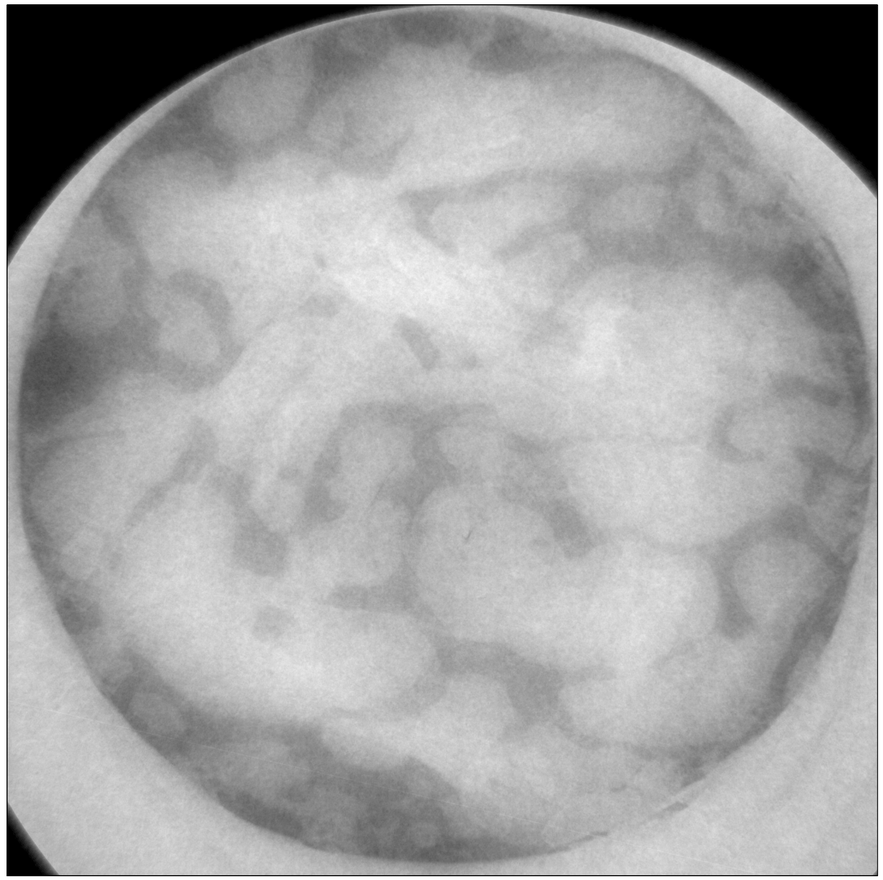

Sinogram

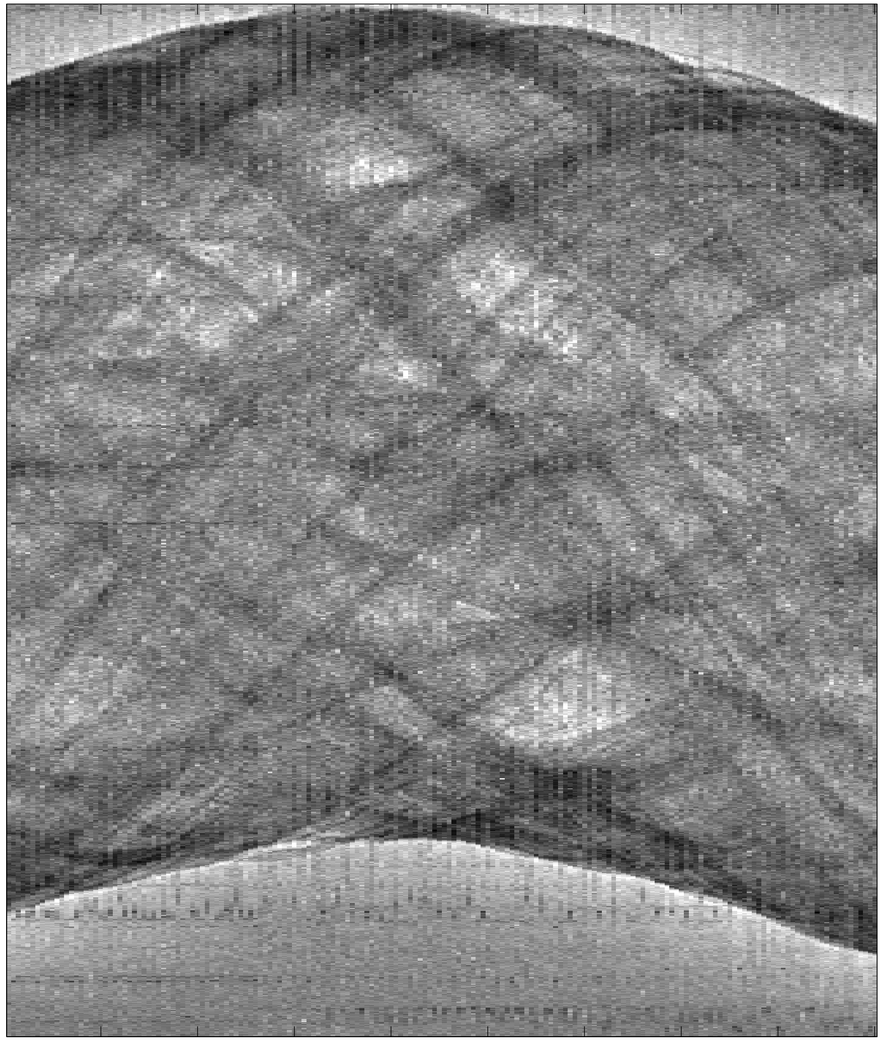

Reconstruct slice from sinogram

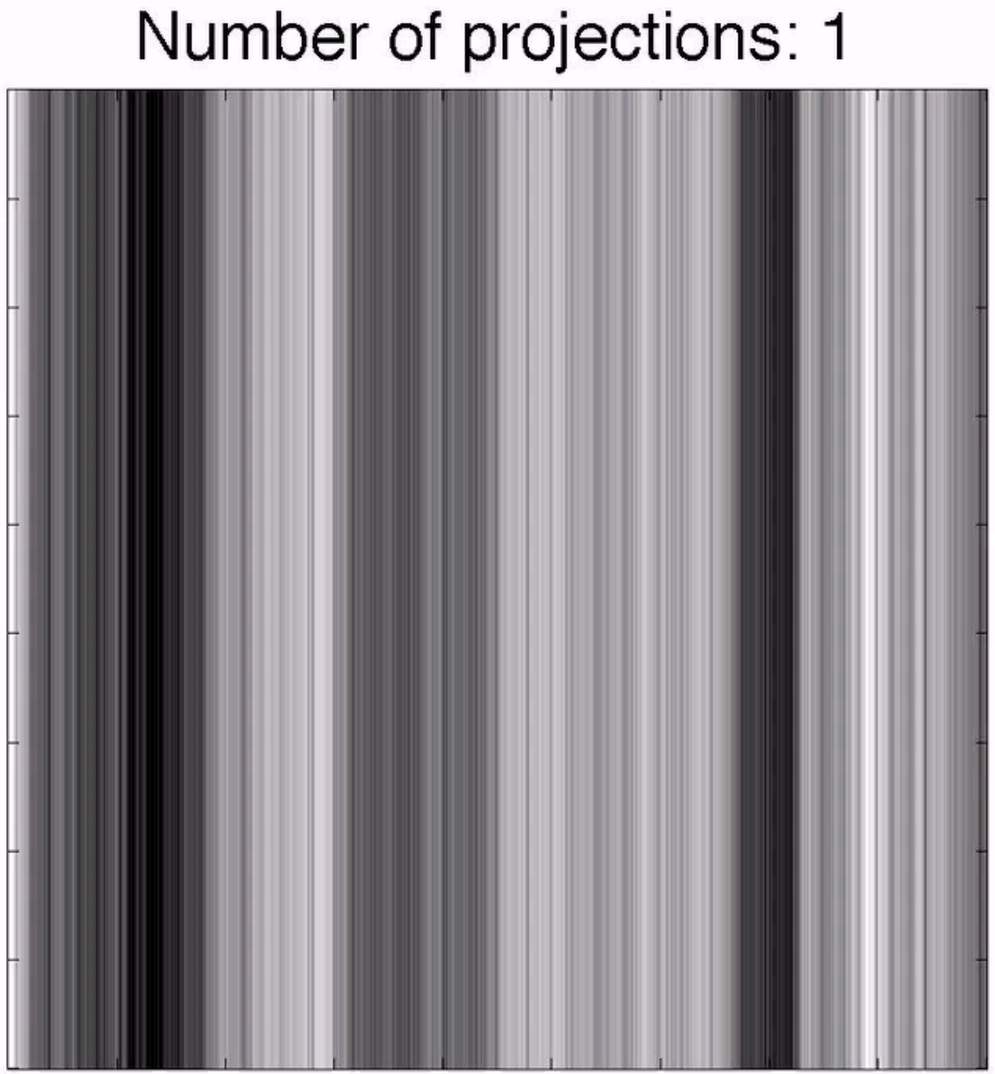

Use the method of ‘filtered back-projection’ – project each image back across the sample volume and add together

Reconstruct slice from sinogram

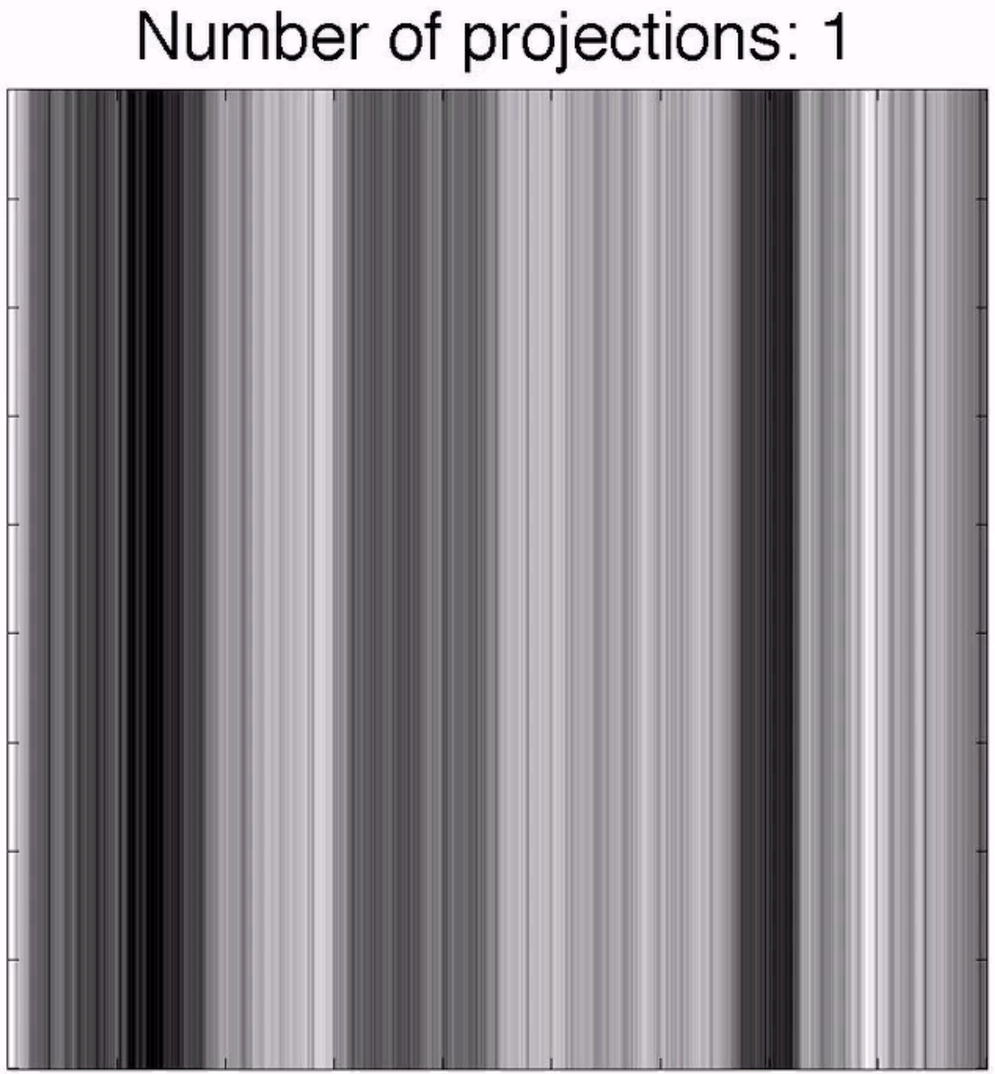

Use the method of ‘filtered back-projection’ – project each image back across the sample volume and add together

Reconstruct slice from sinogram

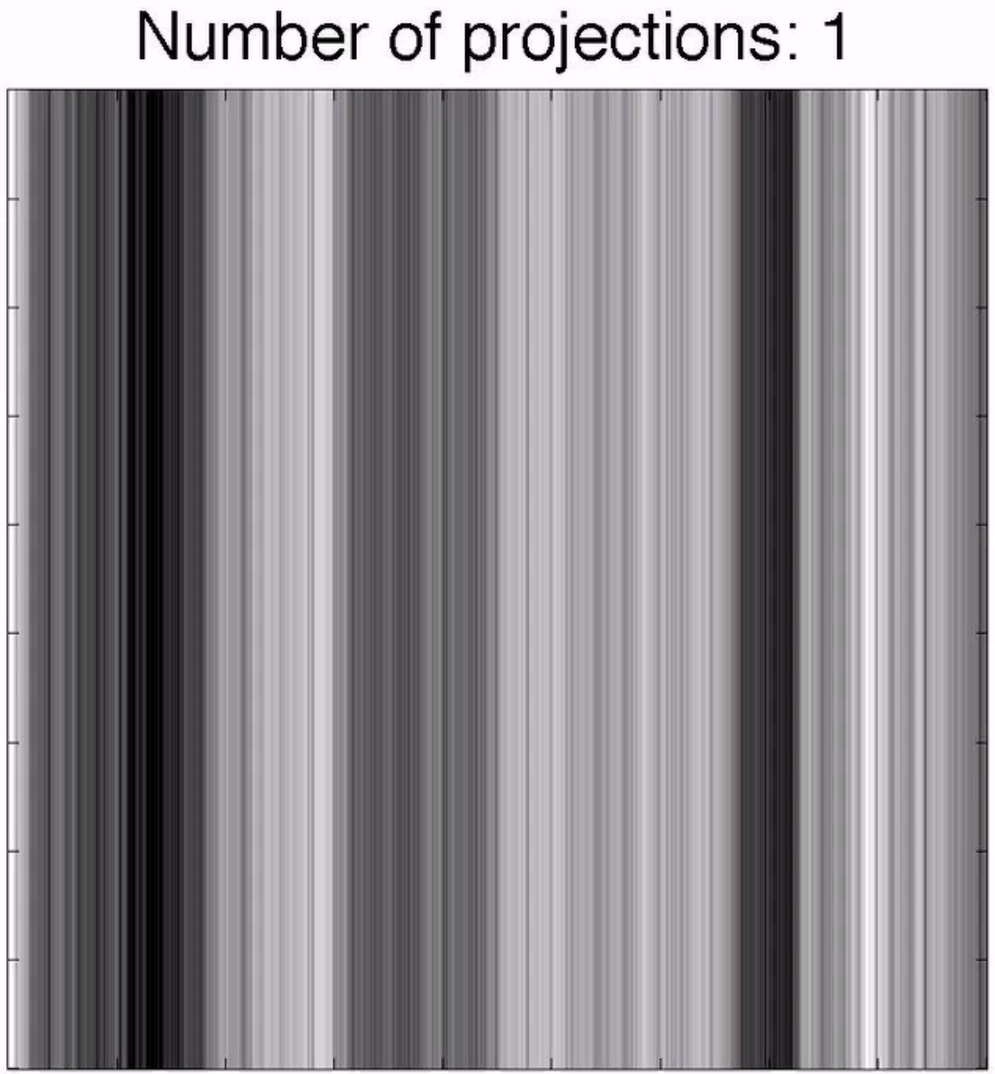

Use the method of ‘filtered back-projection’ – project each image back across the sample volume and add together

Bone tomography

3D reconstruction of the bone sample obtained with voxel size 5x5x5 μm

Cole, J. M. et al. Laser-wakefield accelerators as hard x-ray sources for 3D medical imaging of human bone. Scientific Reports 5, 13244 (2015).

Bone tomography

3D reconstruction of the bone sample obtained with voxel size 5x5x5 μm

Cole, J. M. et al. Laser-wakefield accelerators as hard x-ray sources for 3D medical imaging of human bone. Scientific Reports 5, 13244 (2015).

Bone tomography

3D reconstruction of the bone sample obtained with voxel size 5x5x5 μm

Cole, J. M. et al. Laser-wakefield accelerators as hard x-ray sources for 3D medical imaging of human bone. Scientific Reports 5, 13244 (2015).

Mouse embryonic samples

14.5 day-old embryo

Stained with iodine

Suspended in agarose – important to stop dehydration

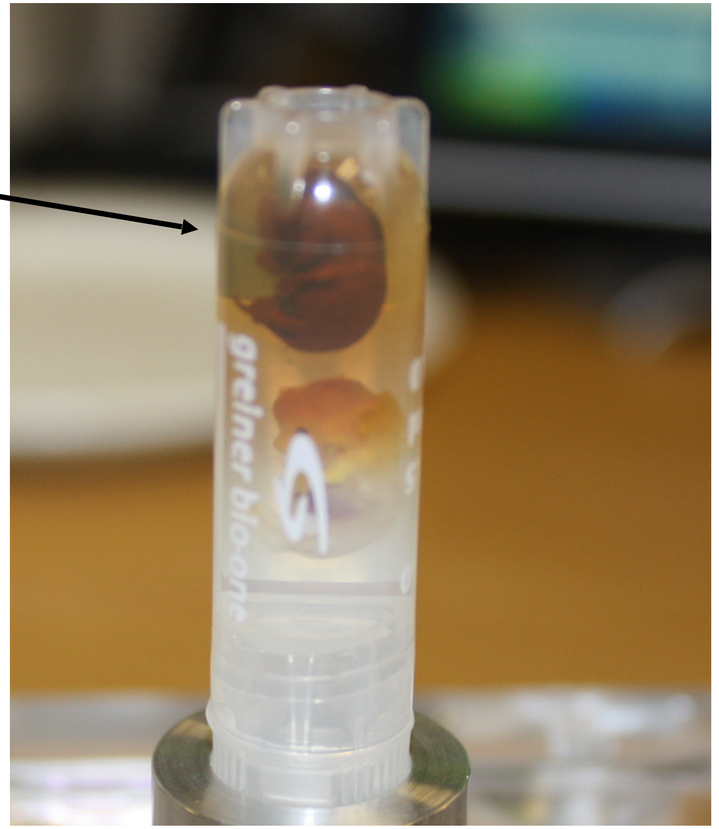

Mouse embryo imaging important in the context of International Mouse Phenotyping Consortium (>$1B project)

Raw image of mouse neonate

Filters for on-shot transmission spectroscopy

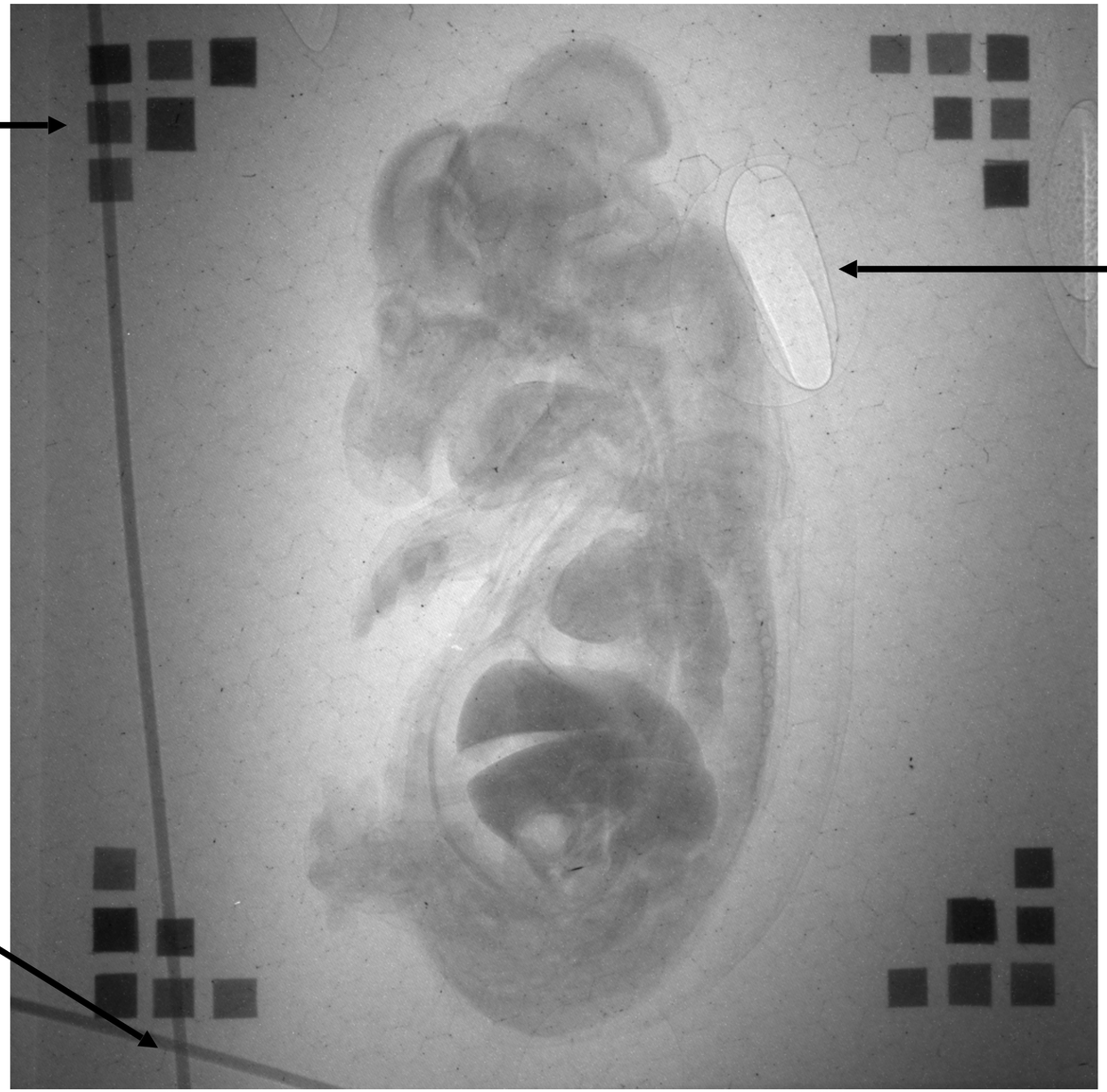

Phase contrast artefacts from bubbles in agarose

(removed for tomography)

Fiducial wires

Mouse neonate at 14.5 day tomography

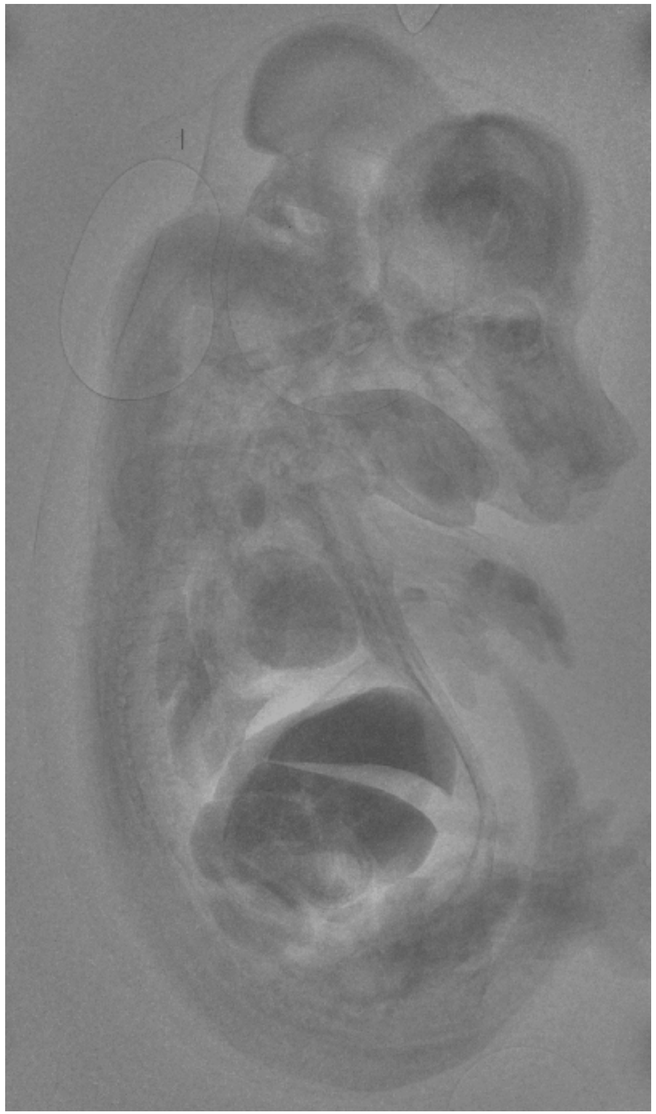

Mouse neonate at 14.5 day tomography

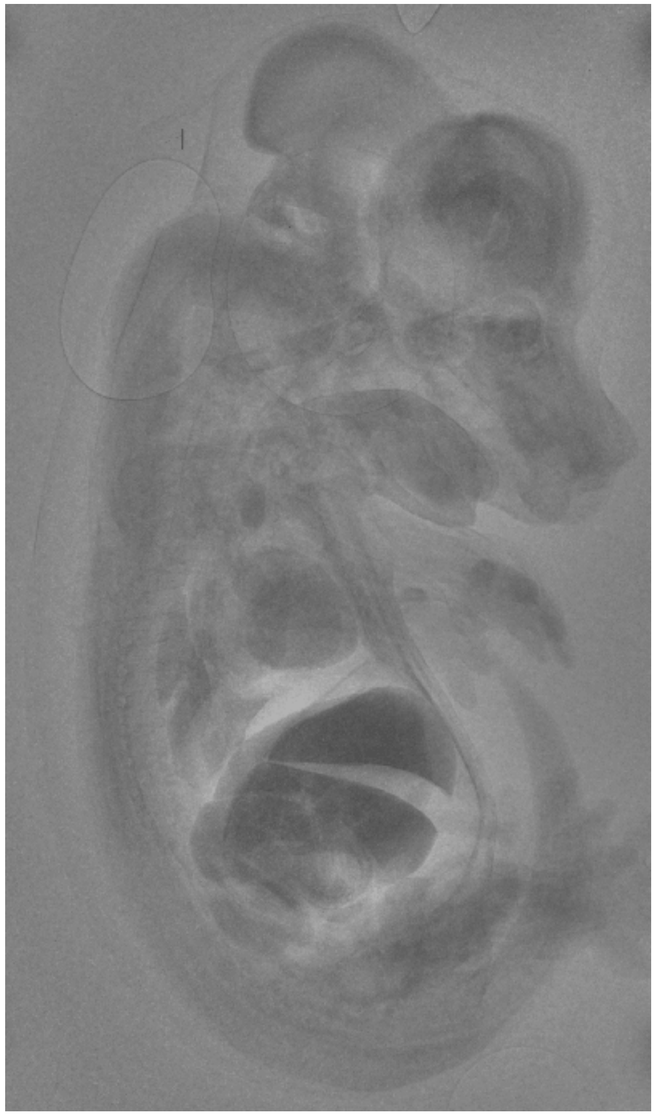

Phase vs. absorption contrast

Phase enhanced (far from CCD)

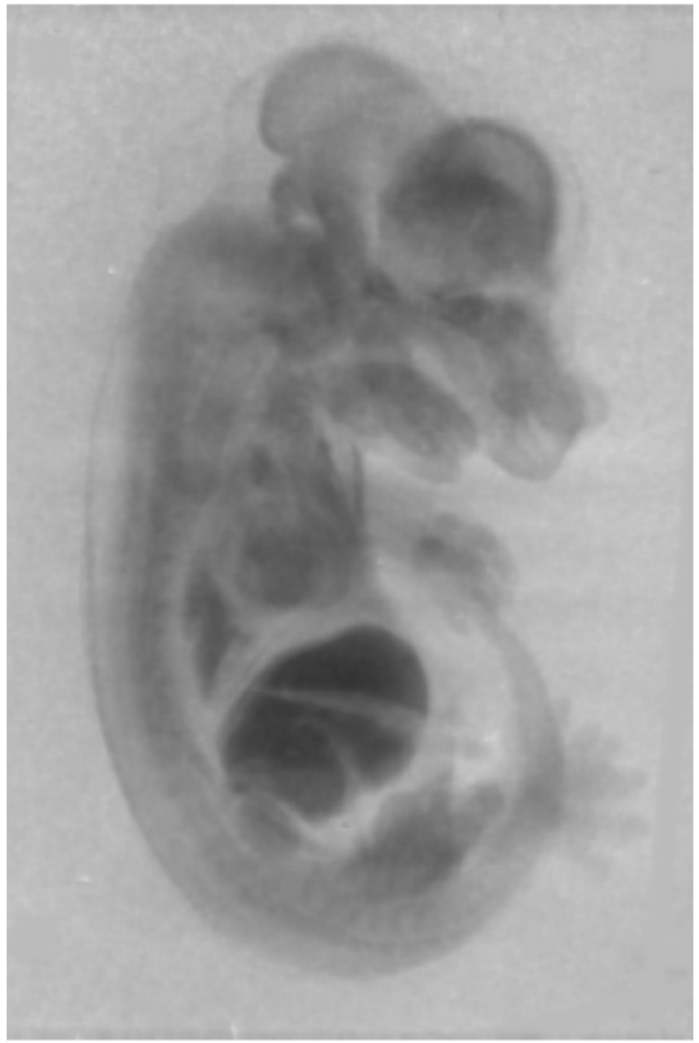

Pure absorption (close to CCD)

Phase vs. absorption contrast

Phase enhanced (far from CCD)

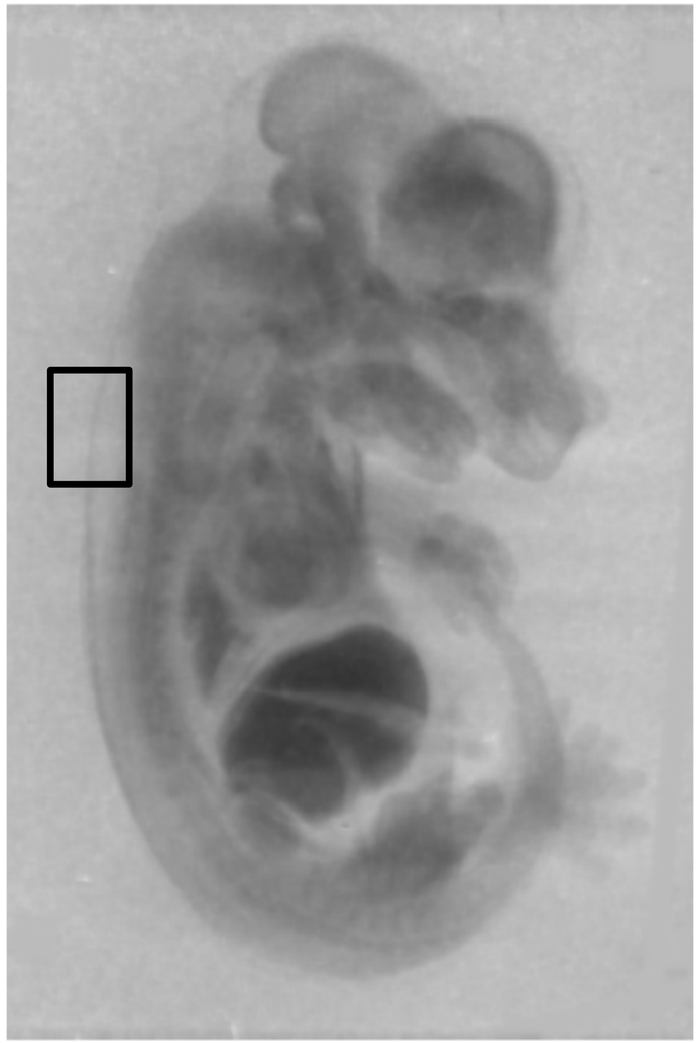

Pure absorption (close to CCD)

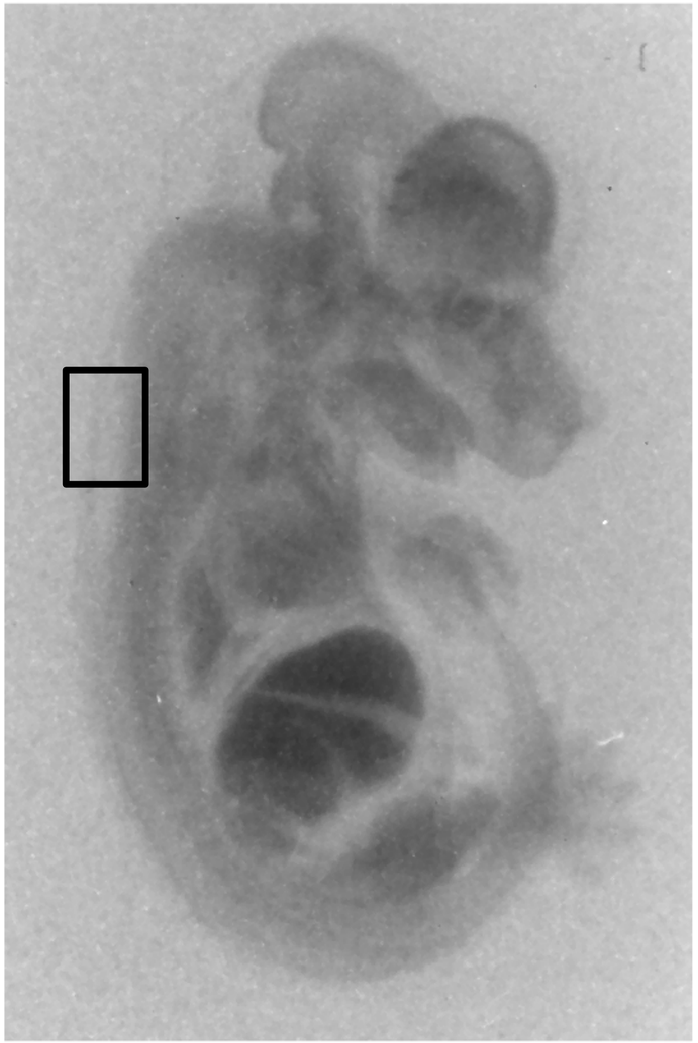

Comparison to μCT

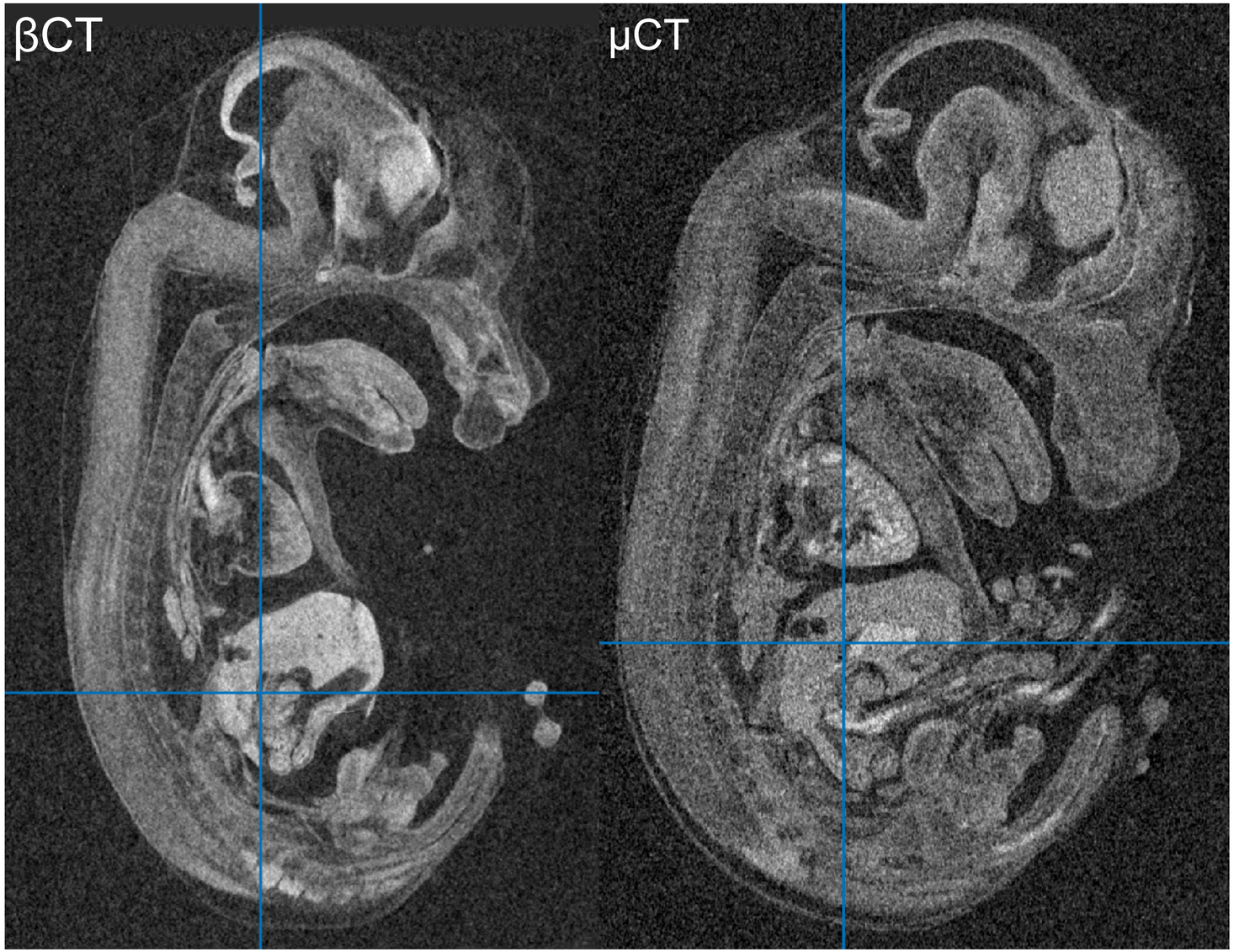

Different samples, but...

Same number of projections

✓ Higher SNR

✓ Higher resolution

✗ Longer scan

14.5 day Mouse Embryo tomography

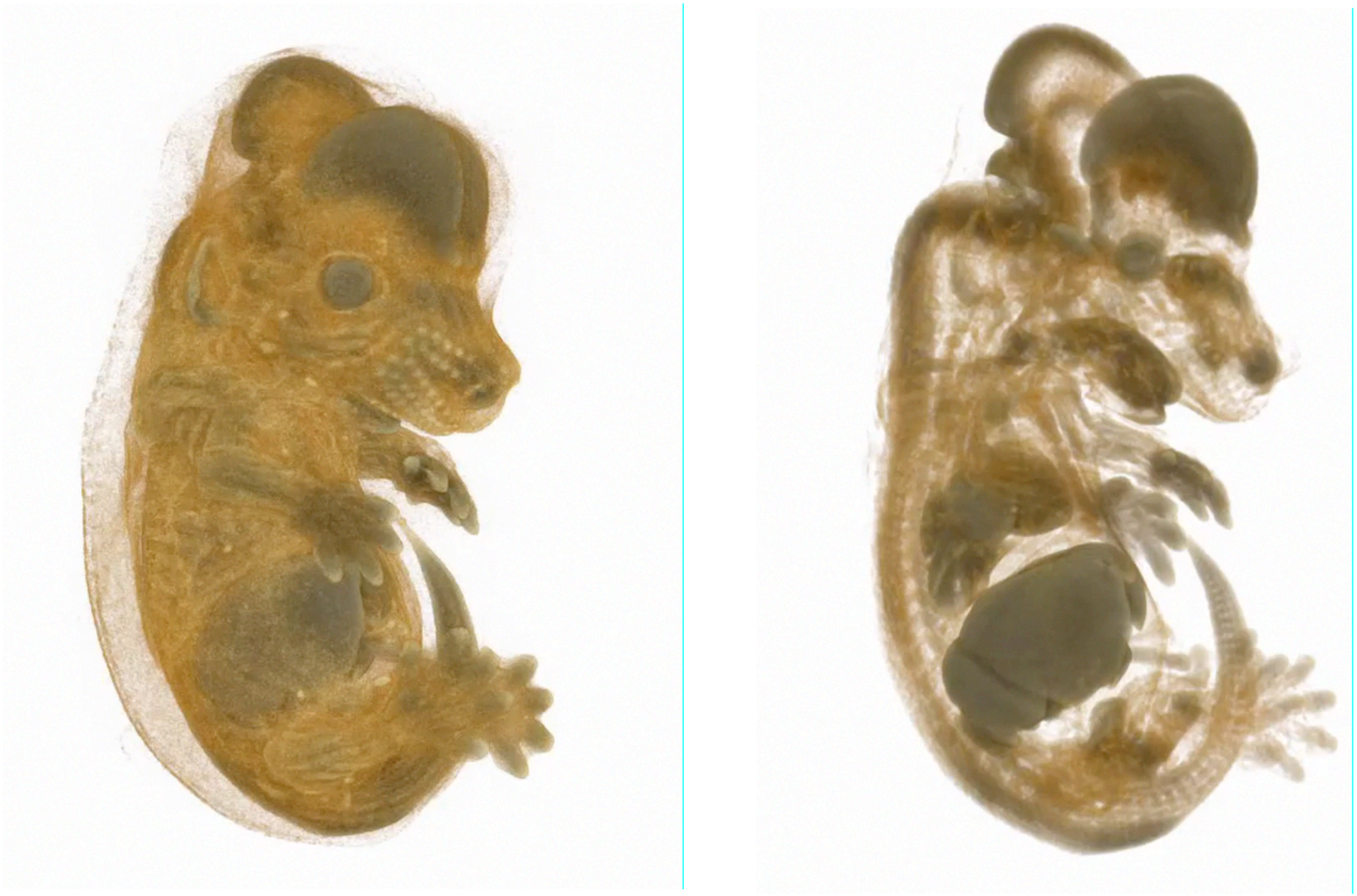

Cole, J. M. et al. High-resolution μCT of a mouse embryo using a compact laser-driven X-ray betatron source. Proceedings of the National Academy of Sciences 115, 6335–6340 (2018).

14.5 day Mouse Embryo tomography

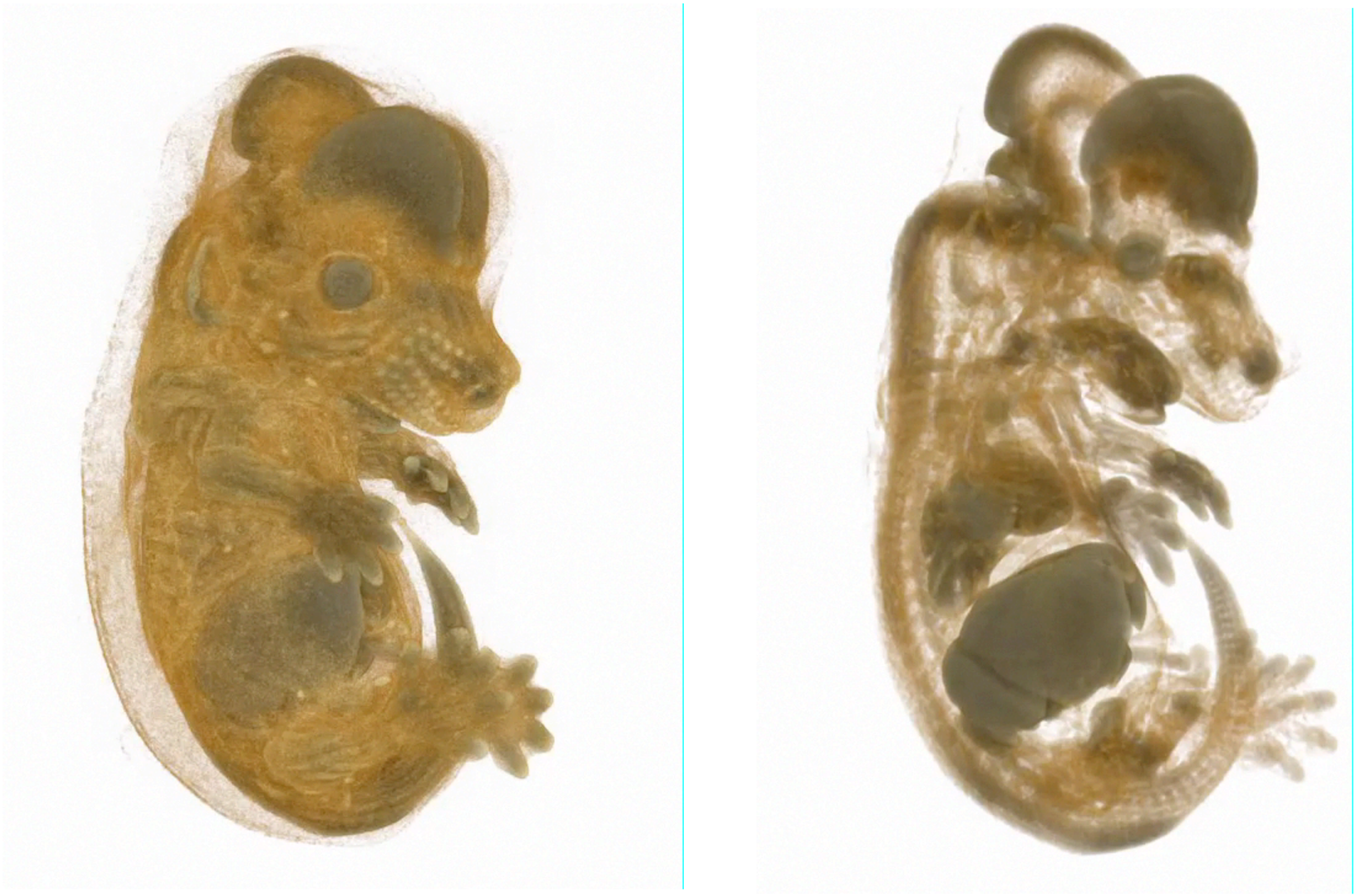

Cole, J. M. et al. High-resolution μCT of a mouse embryo using a compact laser-driven X-ray betatron source. Proceedings of the National Academy of Sciences 115, 6335–6340 (2018).

14.5 day Mouse Embryo tomography

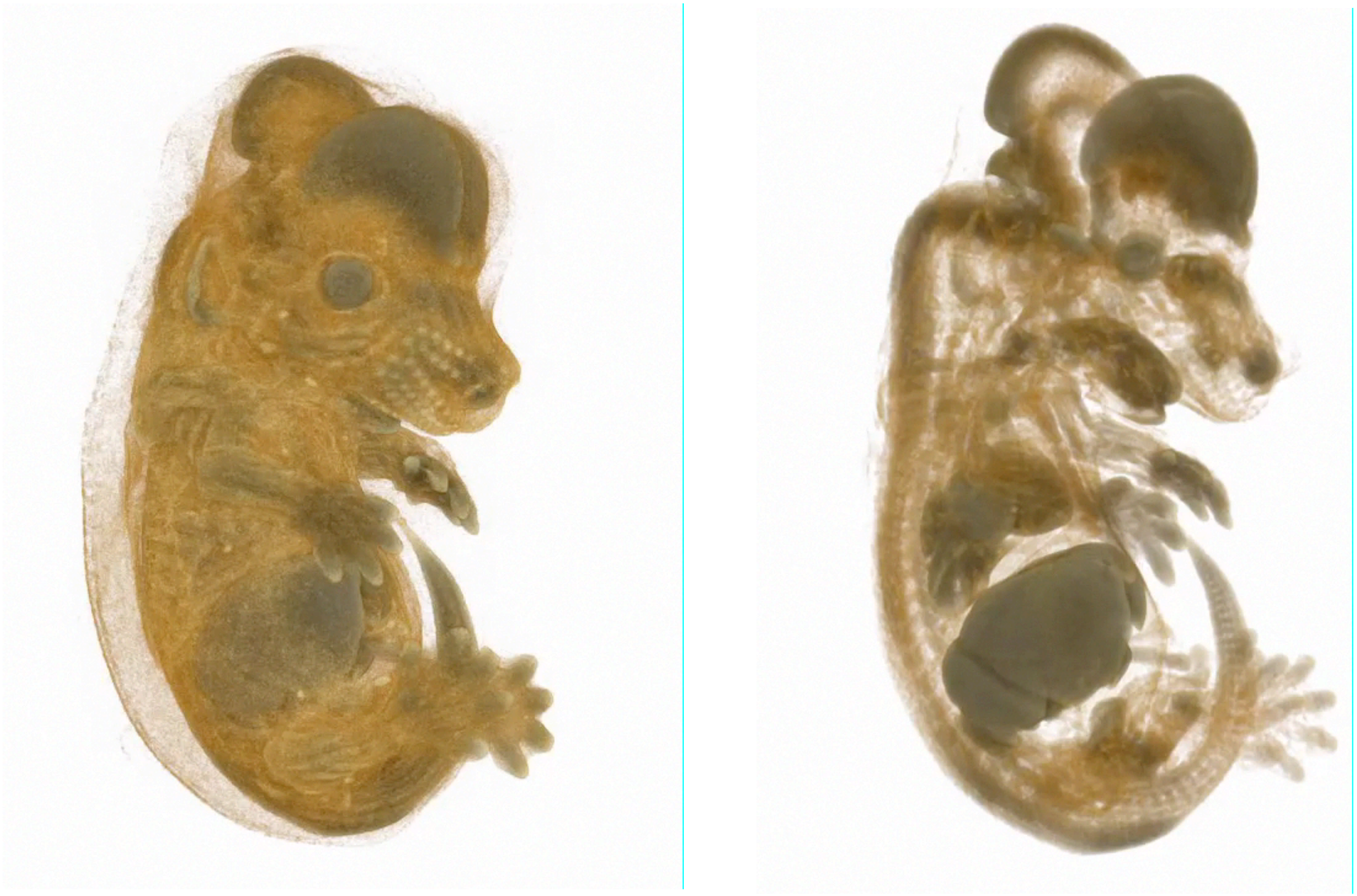

Cole, J. M. et al. High-resolution μCT of a mouse embryo using a compact laser-driven X-ray betatron source. Proceedings of the National Academy of Sciences 115, 6335–6340 (2018).

Comparison with x-ray tubes

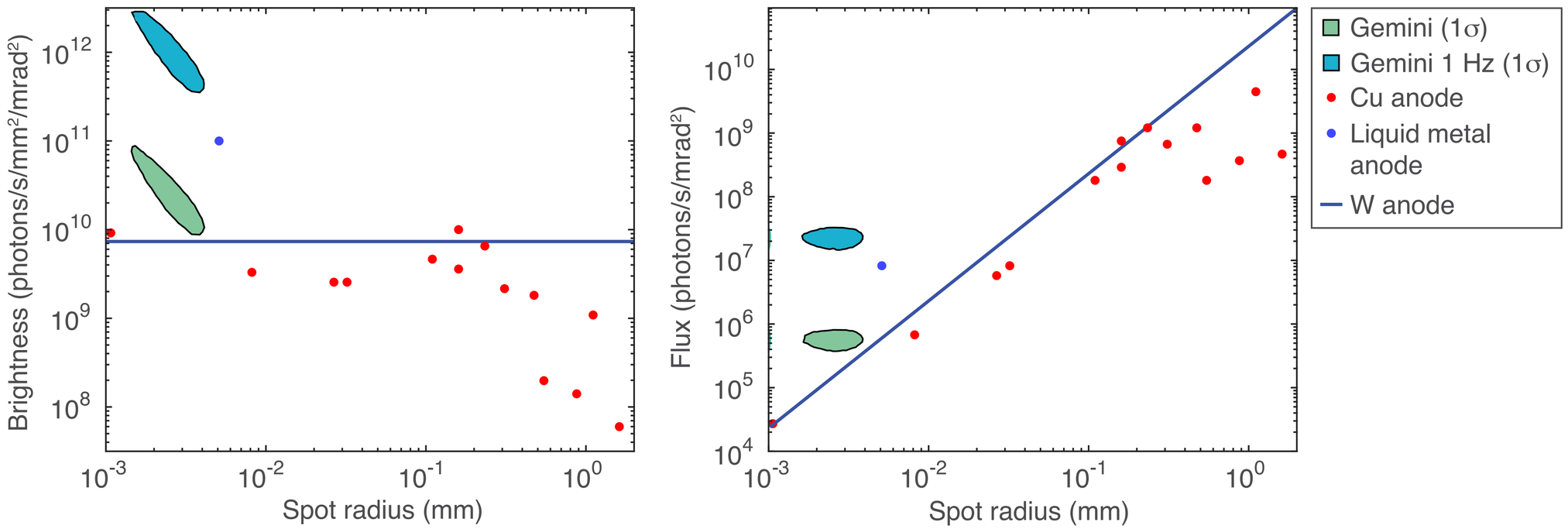

Cole, J. M. et al. High-resolution μCT of a mouse embryo using a compact laser-driven X-ray betatron source. Proceedings of the National Academy of Sciences 115, 6335–6340 (2018).

Shock Imaging Setup

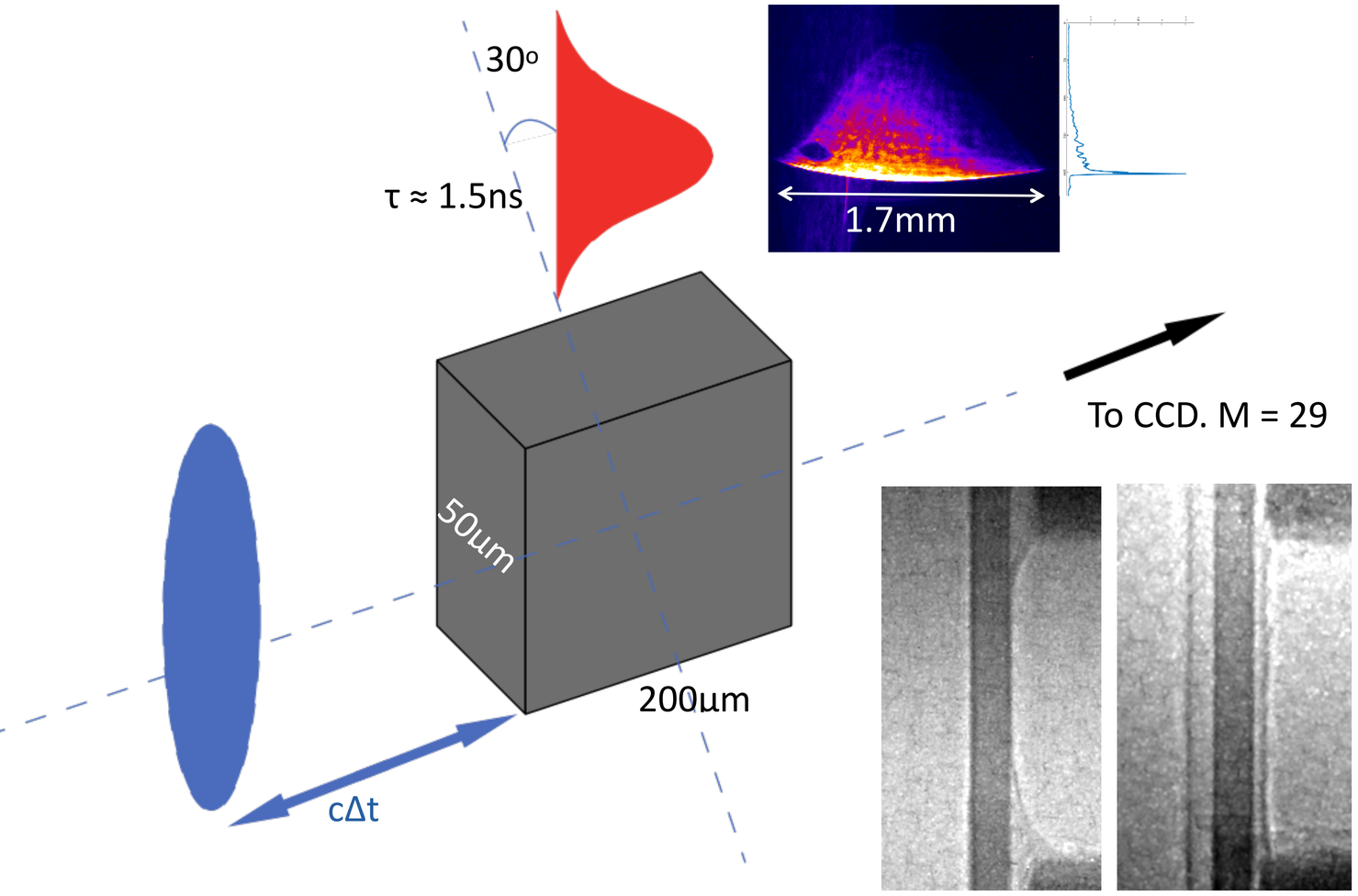

Setup designed to use ultrafast nature of betatron beam ($\tau < 100\,\mathrm{fs}$) to image dynamic interactions

Shock driven by $E_L \approx 10\,\mathrm{J}$, $\tau_L \approx 10\,\mathrm{ns}$ laser pulse into untreated and foam tamped Si targets and imaged transversely by betatron beam.

Time Series: Untamped

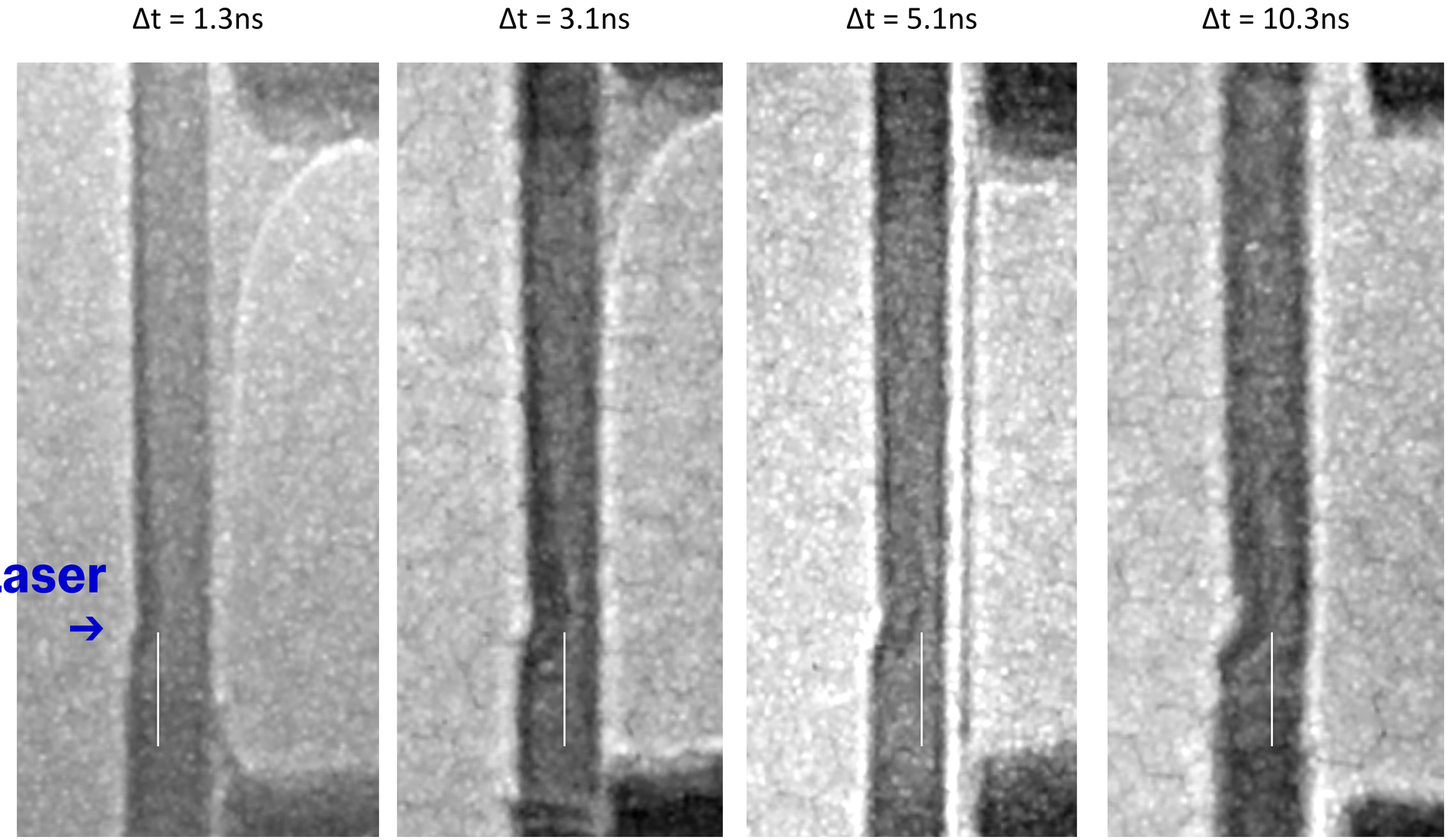

Wood, J. C. et al. Ultrafast Imaging of Laser Driven Shock Waves using Betatron X-rays from a Laser Wakefield Accelerator., Scientific Reports 8, (2018).

Time Series: Tamped

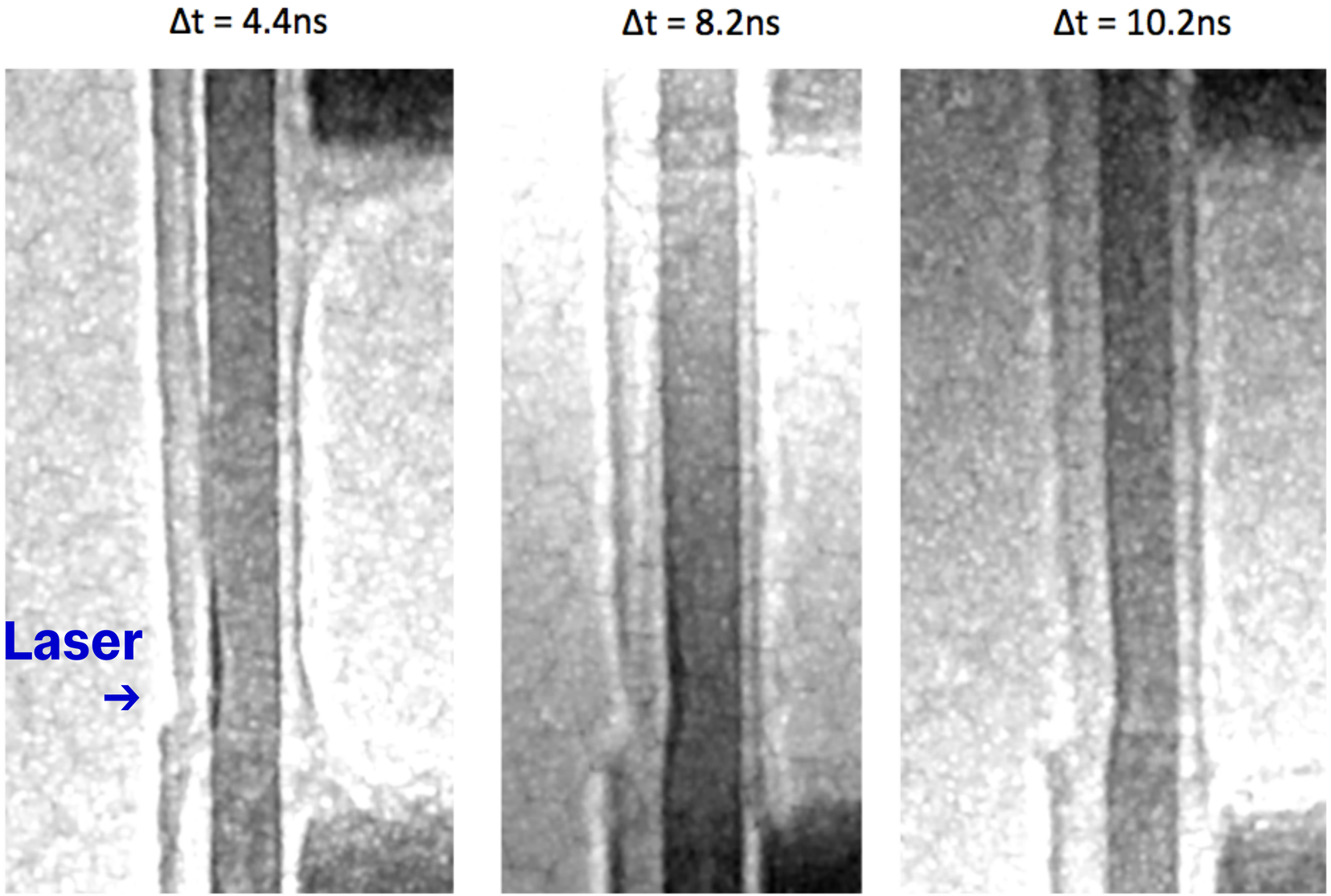

Wood, J. C. et al. Ultrafast Imaging of Laser Driven Shock Waves using Betatron X-rays from a Laser Wakefield Accelerator., Scientific Reports 8, (2018).

Time Series: corrugated target

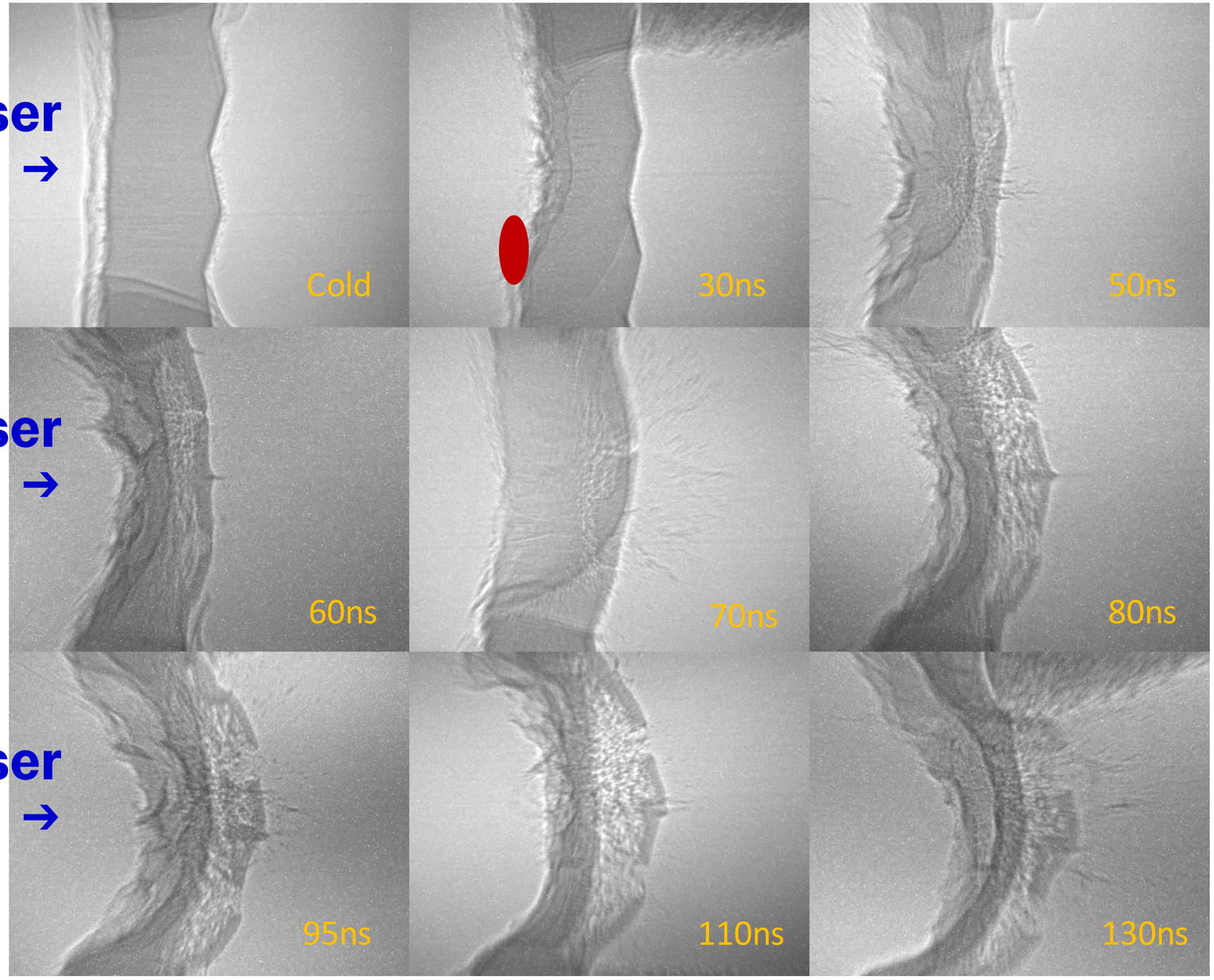

Non-destructive evaluation (NDE) of additive manufacture

Plastic test object with varying sphere diameters, external/internal diameters of cylinders, and plane to plane distances produced for XCT performance verification

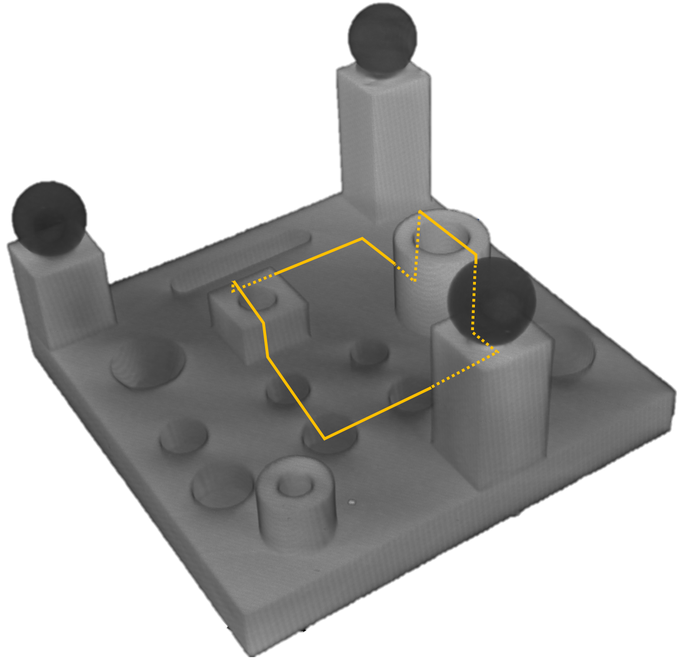

tomographic reconstruction using conventional lab x-ray CT

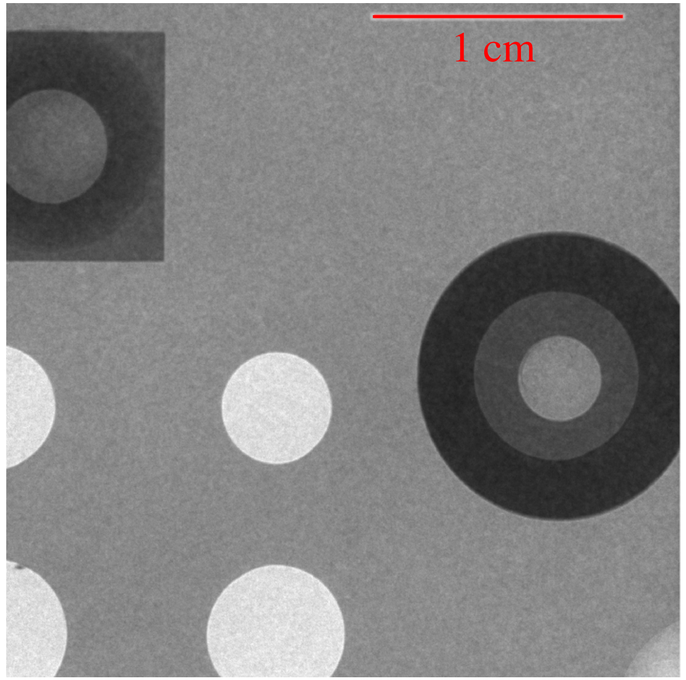

radiograph of the test object obtained with the laser-betatron source

Gruse, J.-N. et al. Application of compact laser-driven accelerator X-ray sources for industrial imaging. NIM A 983, 164369 (2020).

Imaging of novel battery technology

Betatron imaging can be used for inspection of novel lithium battery configurations

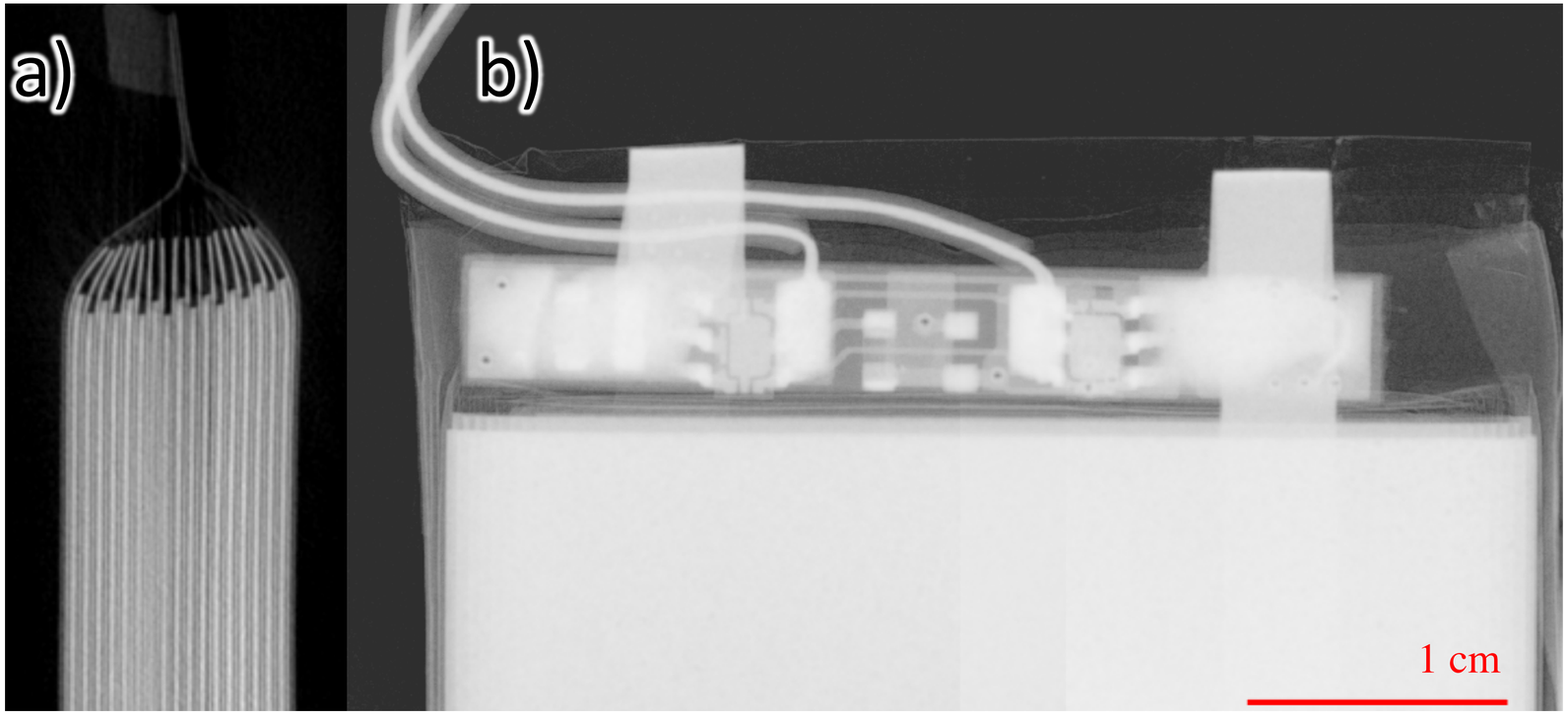

tomographic using conventional lab x-ray CT of a pouch cell of gel layer with alternating cathode and anode layers

radiograph of the tab area of a pouch cell obtained with the laser-betatron source

Gruse, J.-N. et al. Application of compact laser-driven accelerator X-ray sources for industrial imaging. NIM A 983, 164369 (2020).

NDE of novel composite materials

Betatron imaging used for phase contrast imaging of carbon fibre with kink band failure

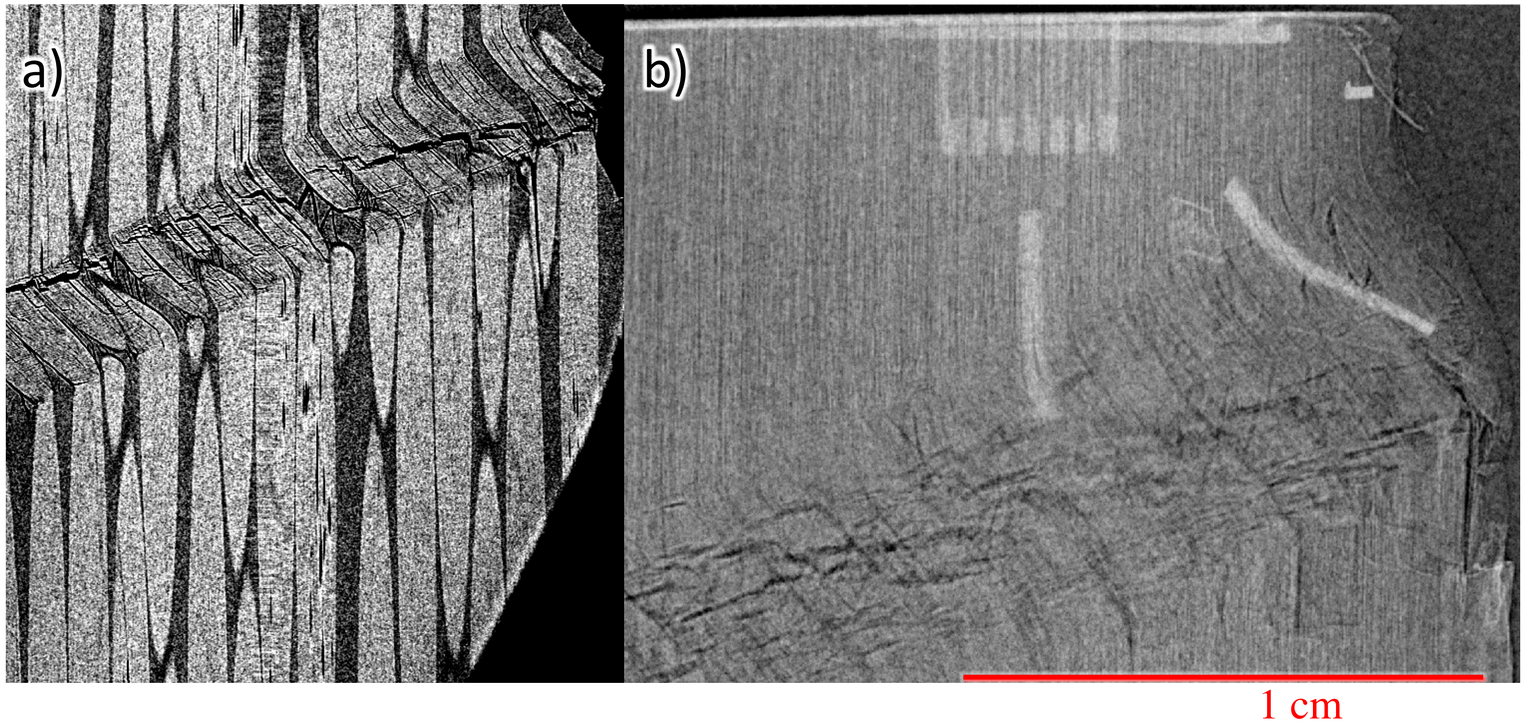

tomographic using conventional lab x-ray CT of defects due to a failure in carbon fibre

radiograph obtained with the laser-betatron source with carbon fibre tows visible

Gruse, J.-N. et al. Application of compact laser-driven accelerator X-ray sources for industrial imaging. NIM A 983, 164369 (2020).

Multimodal imaging performed with betatron source too

Betatron imaging used for multimodal imaging

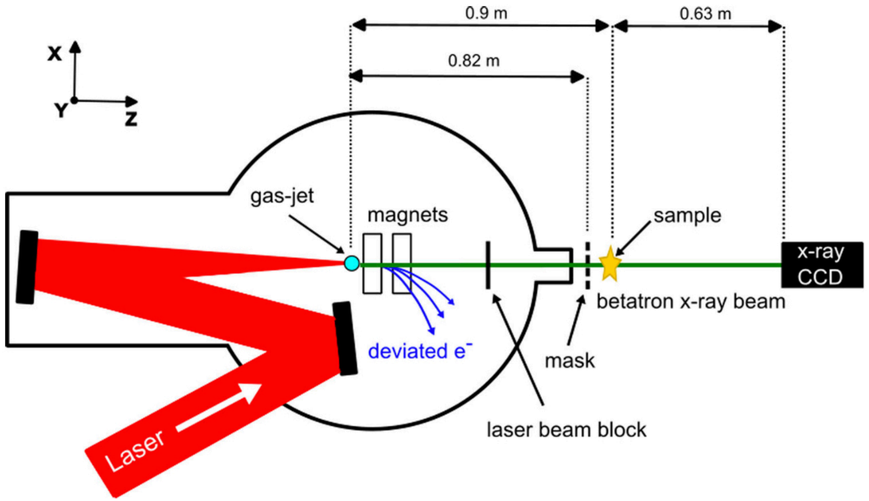

mask is spread is scanned across sample to allow sub pixel resolution and access to small angle x-ray scattering as well as absorption and phase-contrast modes

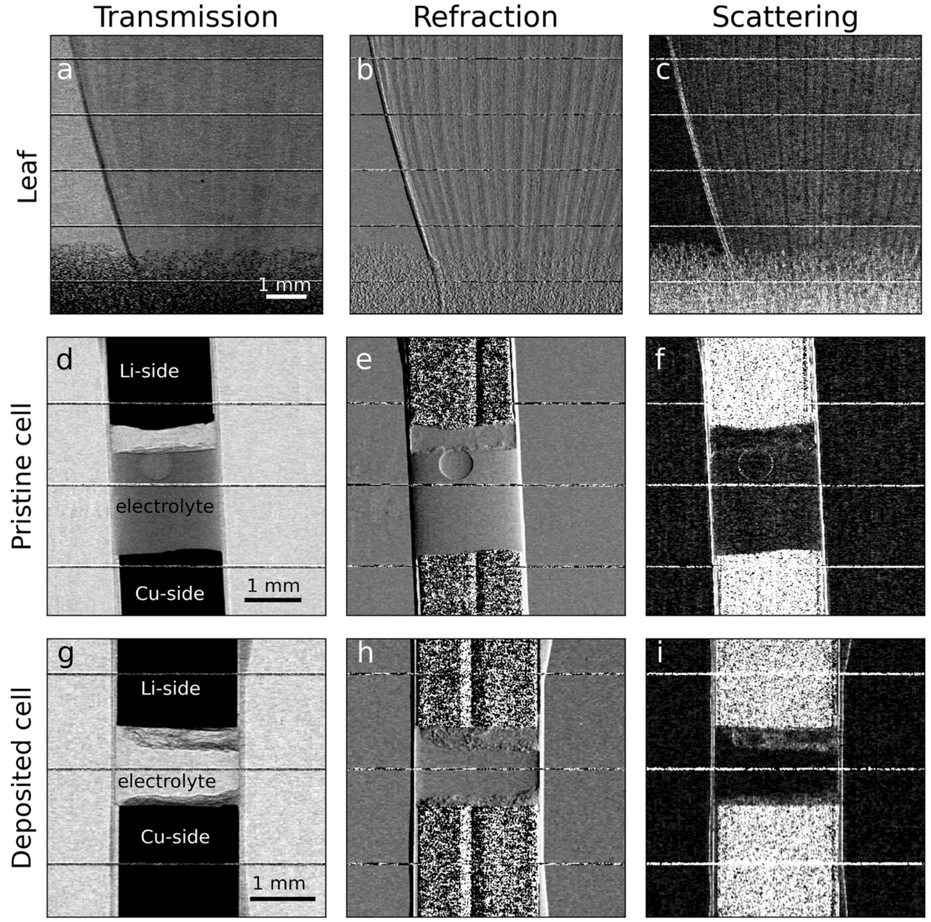

Transmission, refraction, and scattering were retrieved for a leaf (a–c) and two electrochemical samples (pristine, d–f, and after electrochemical deposition, g–i)

Doherty, A. et al. Femtosecond multimodal imaging with a laser-driven X-ray source. Communications Physics 6, 288 (2023).

Betatron Source also ideal for single shot x-ray absorption studies

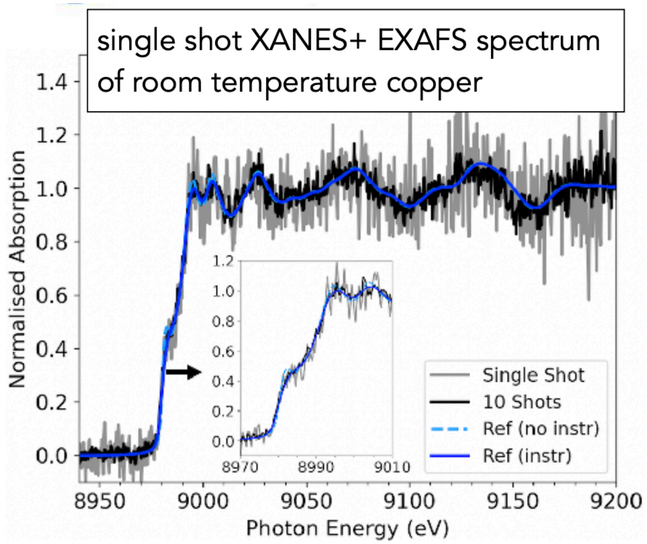

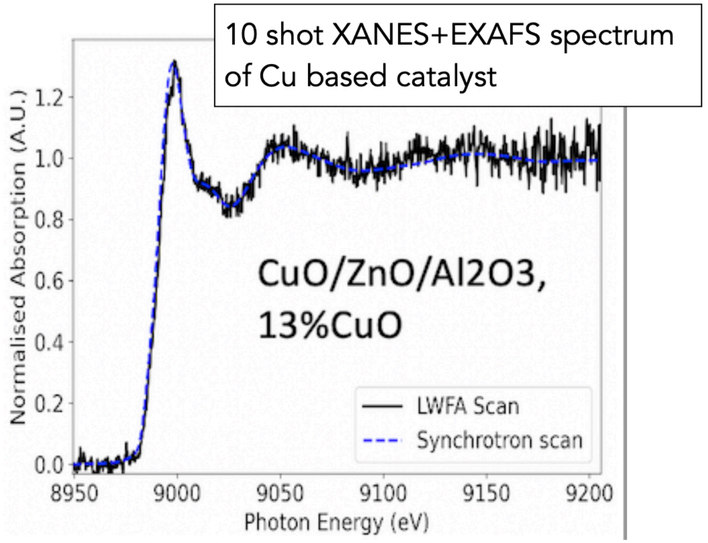

Betatron source can also be used for broadband x-ray absorption

Single shot XANES demonstrated. Ultrafast nature of betatron radiation enables time resolved XANES

- XANES analyzes the transitions of core electrons to unoccupied states above the Fermi level, just above the X-ray absorption edge. This gives insights into the oxidation state, coordination environment, and chemical bonding.

First single shot EXAFS of Cu based catalyst

- EXAFS measures oscillations in the X-ray absorption spectrum due to scattering of ejected photoelectrons from neighboring atoms. These oscillations contain information about the distances and types of neighboring atoms (like the distance between an absorbing atom and its first few neighbors).

Kettle, B. et al. Single-Shot Multi-keV X-Ray Absorption Spectroscopy Using an Ultrashort Laser-Wakefield Accelerator Source. Physical Review Letters 123, (2019).

Kettle, B. et al. Extended X-ray absorption spectroscopy using an ultrashort pulse laboratory-scale laser-plasma accelerator. Communications Physics **7**, (2024).

Developing wakefield x-ray sources

Next generation of Facilities now coming online (ELI-PW, EPAC…)

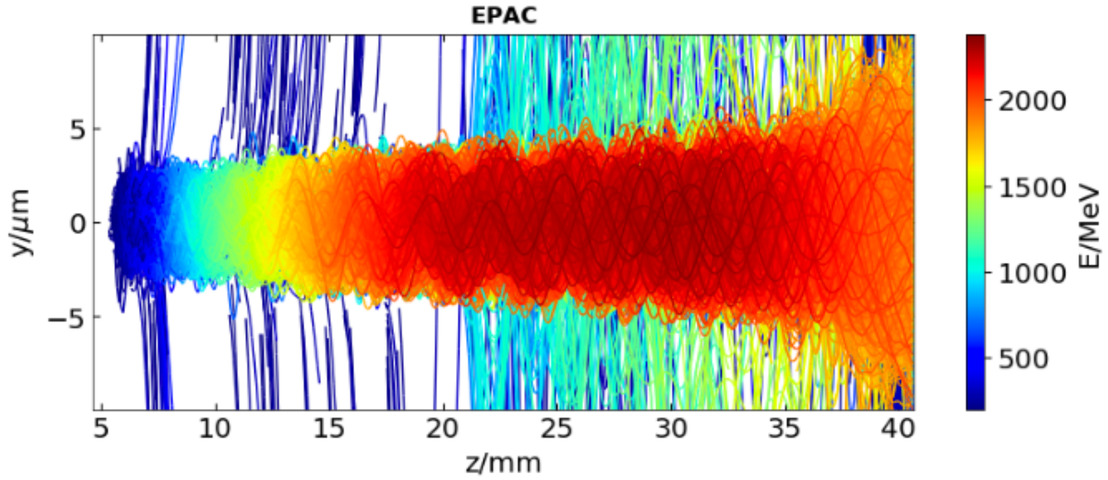

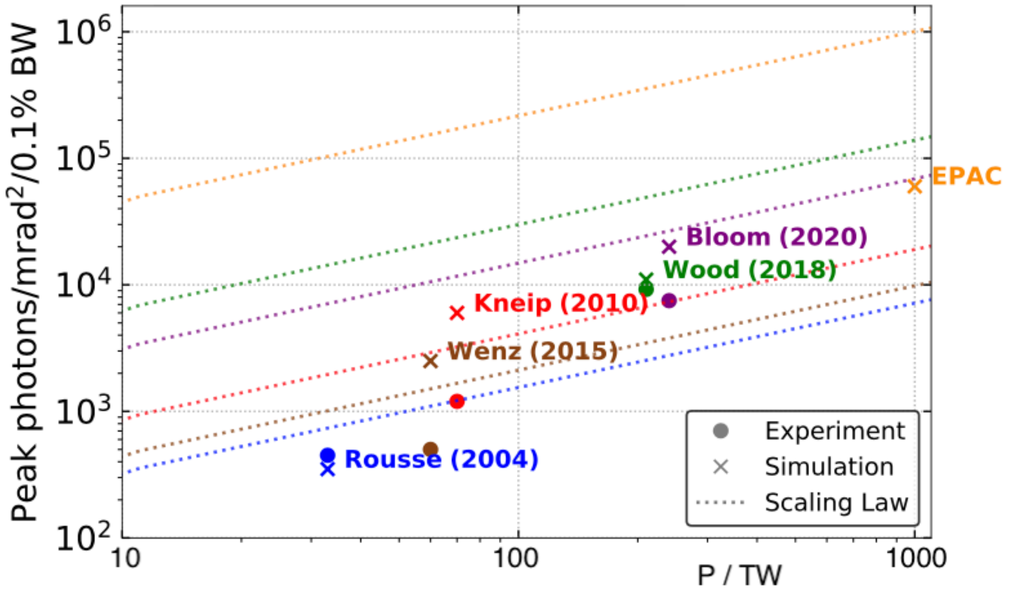

Discovery

- **Driving forward the scientific understanding of laser driven accelerators and sources.**
- Explore matter in extreme environments, usually only found off planet.
- Enable experiments to simulate astrophysical events and study fundamental aspects of the universe.

Innovation

- **R&D for a new generation of compact, super-bright, novel accelerators.**
- Advanced, multi-modal, dynamic and highly penetrating imaging capabilities
- New technologies for advanced sensing in defence and security
- Novel radiobiology for future therapeutic modalitie

Training

- High quality and broad spectrum training for engineers, apprentices, PhD and early career scientists, generating a pipeline of people with expert, high quality skills.

EPAC

Successor to Gemini being built at Rutherford-Appleton Laboratory

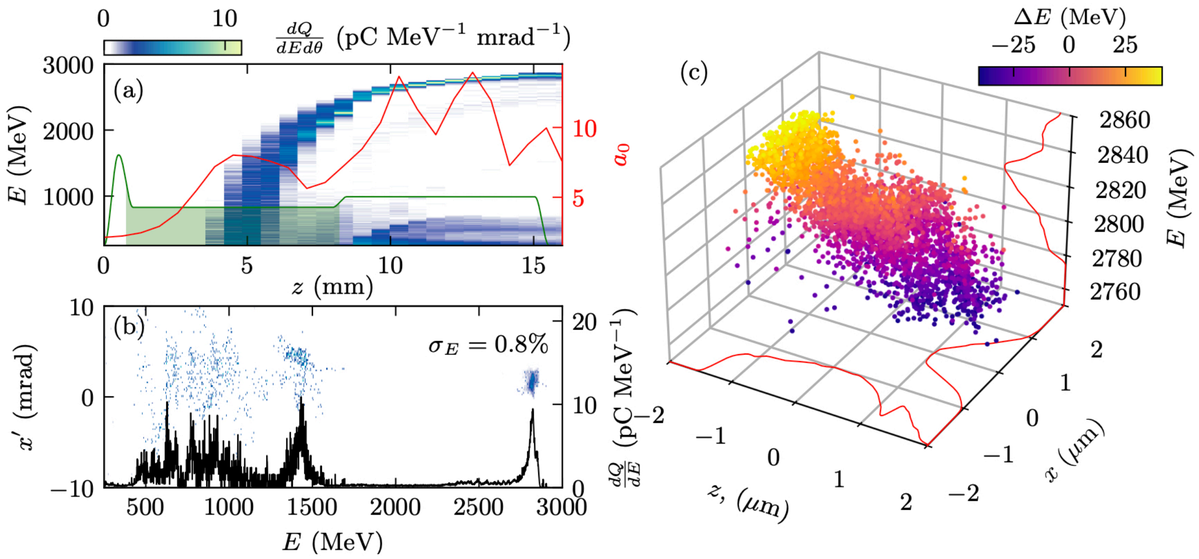

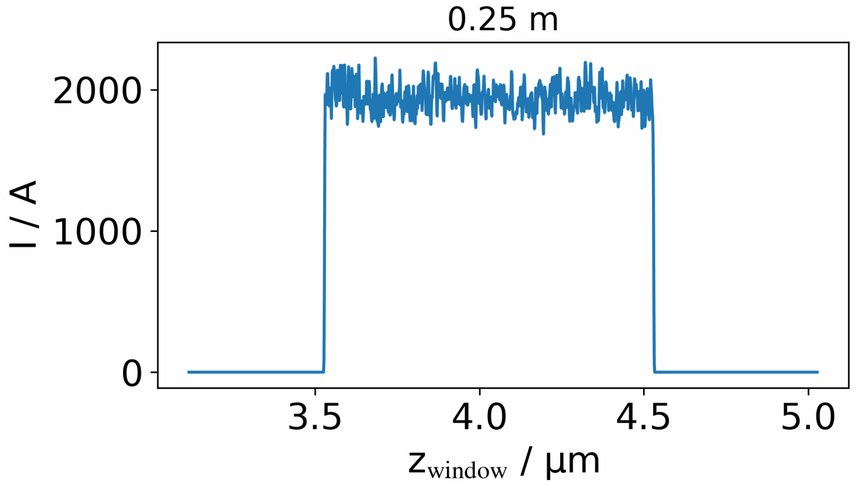

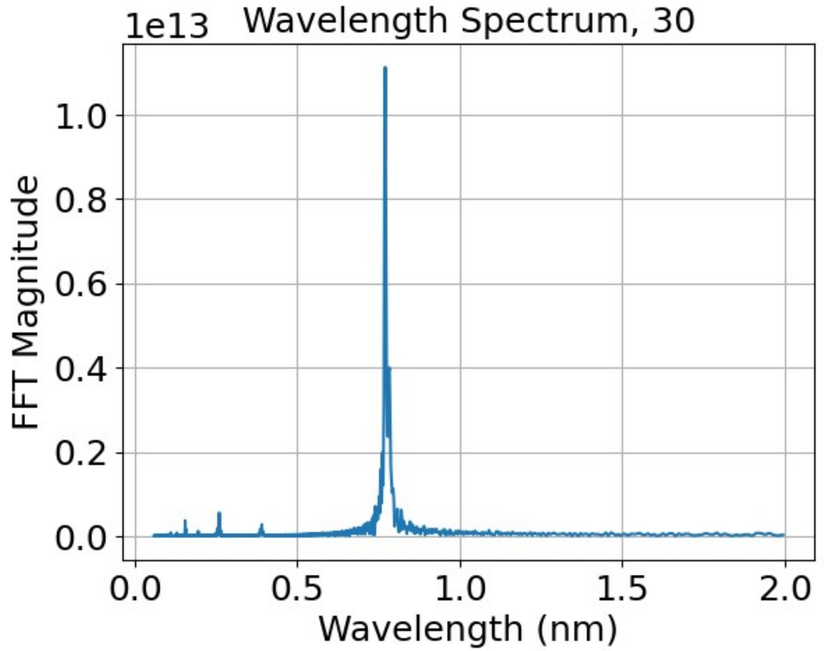

M. Backhouse, Sparse Multi-Task Multi-Objective Bayesian Optimisation for Laser Wakefield Acceleration, Submitted (2025)

Runfeng Luo, X-ray FEL driven by laser wakefield accelerators, In preparation (2025)

Central Wavelength: 0.77 nm

EPAC

Successor to Gemini being built at Rutherford-Appleton Laboratory

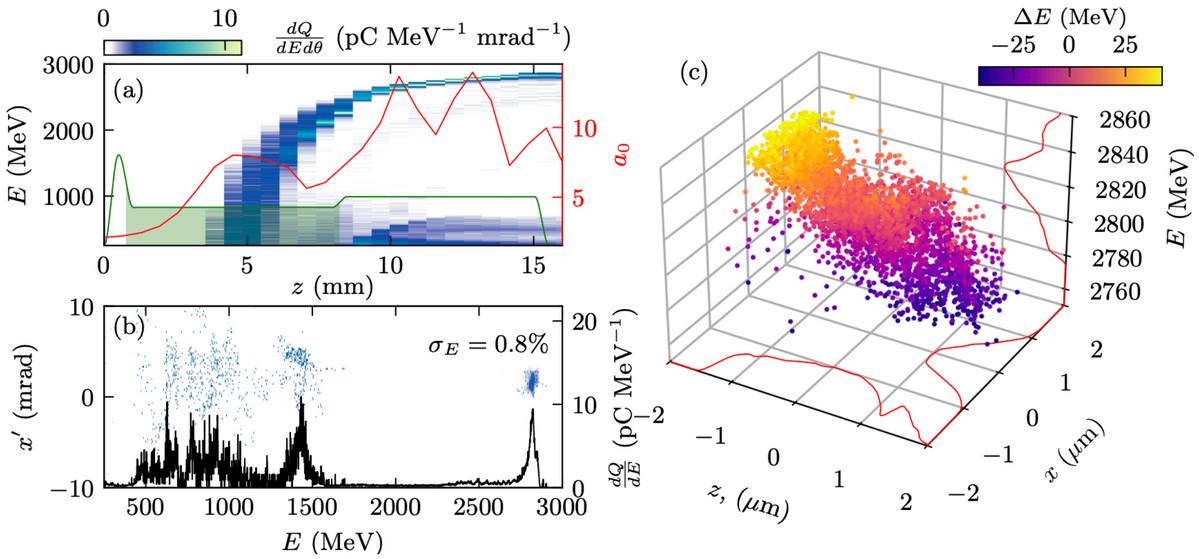

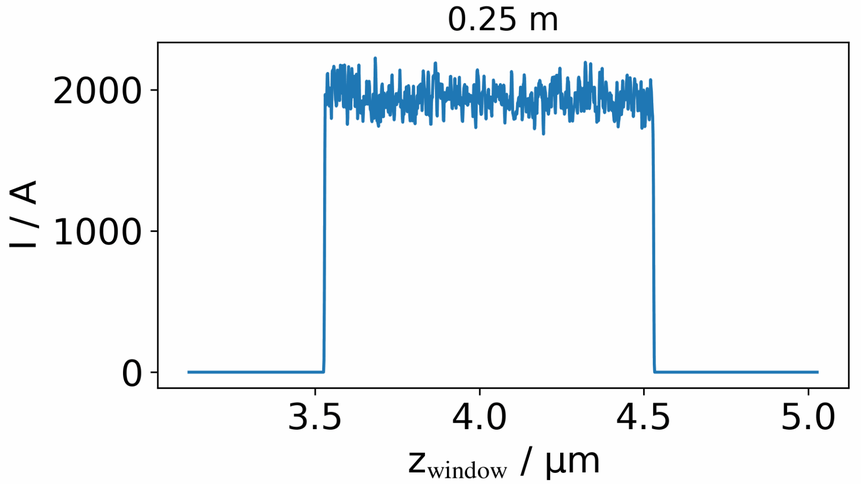

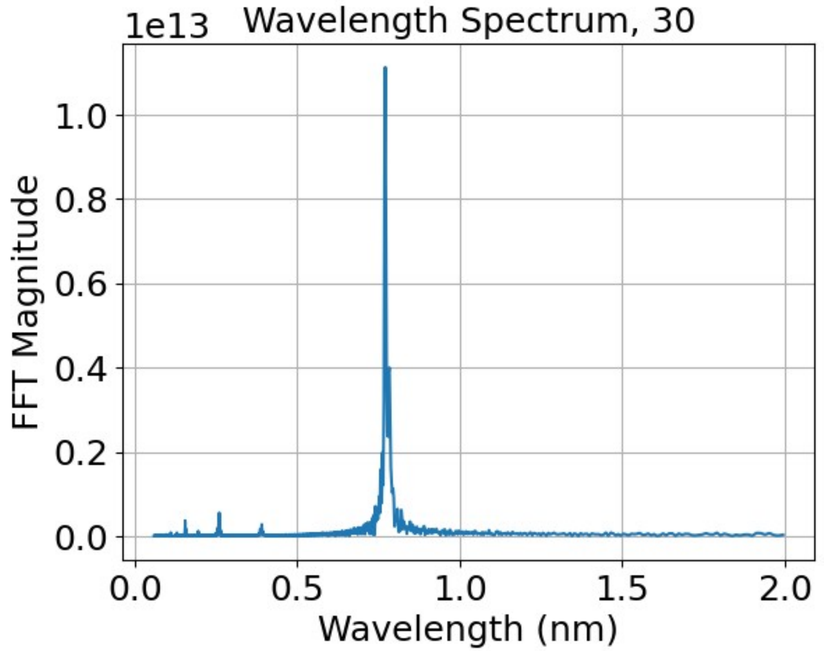

M. Backhouse, Sparse Multi-Task Multi-Objective Bayesian Optimisation for Laser Wakefield Acceleration, Submitted (2025)

Runfeng Luo, X-ray FEL driven by laser wakefield accelerators, In preparation (2025)

Central Wavelength: 0.77 nm

Acknowledgements

P. Abel[2], R. Abel[3], E. Aboagye[2], S. Alatabi[1], C. D. Armstrong[4], C. D. Baird[4,5] , N. Bourgeois[4], C. M. Brenner[4], S. Cipiccia[6], **J. Cole**[1], R. C. Combes[2], D. Dangor[1] , C. D. Gregory[4], **J-N. Gruse**[1] , O. J. Finlay[7], S. Hawkes[4], C. Hooker[4], A. Jin[8], S. Johnson[9] , Y. Katzir[4], L. Kenny[2], A. Lim[10], **N.C. Lopes**[1,12,], S.P.D. Mangles[1], K. Mecseki[1], C. D. Murphy[5], D. Neely[4], N. Ngo[11], Q.D. Nguyen[2], D. Norris[9], R. Pattathil[4], L.R.Pickard[13], **K. Pode**r[1], K.D.Potter[14] , S. Rosario[1], D.R. Rusby[4], J. Sanderson[11], S. Shousha[10], C.Spindloe[4], M. Sroya[11], M. J. V. Streeter[1], D. Symes[4], L. Teboul[9], C. Thornton[4], C.I.D.Underwood[4], J. M. Warnett [15], H. Westerberg[9], M. A. Williams[2], M. Winkler[10], **J. C. Wood**[1]

[1] The John Adams Institute for Accelerator Science, Imperial College London

[2] Department of Surgery and Cancer, Imperial College London

[3] MSK Laboratory, Department of Surgery and Cancer, Imperial College

[4] Central Laser Facility, STFC, Rutherford Appleton Laboratory, Didcot

[5] York Plasma Institute, Department of Physics, University of York

[6] Diamond Light Source, Harwell Science & Innovation Campus, Oxfordshire

[7] Physics Department, Lancaster University

[8] Department of Mechanical Engineering, Imperial College London

[9] MRC Mammalian Genetics Unit, Harwell Campus

[10] NHS Healthcare Trust, Imperial College London

[11] Healthcare Tissue Bank, Imperial College London

[12] GoLP, Instituto Superior Técnico, Lisboa, Portugal

[13] National Composites Centre, Bristol and Bath Science Park, Feynman Way Central, Emersons Green, Bristol

[14] Advanced Composites Collaboration for Science and Innovation (ACCIS) University of Bristol, Bristol

[15] WMG, University of Warwick, Coventry

Future Uses of betatron sources

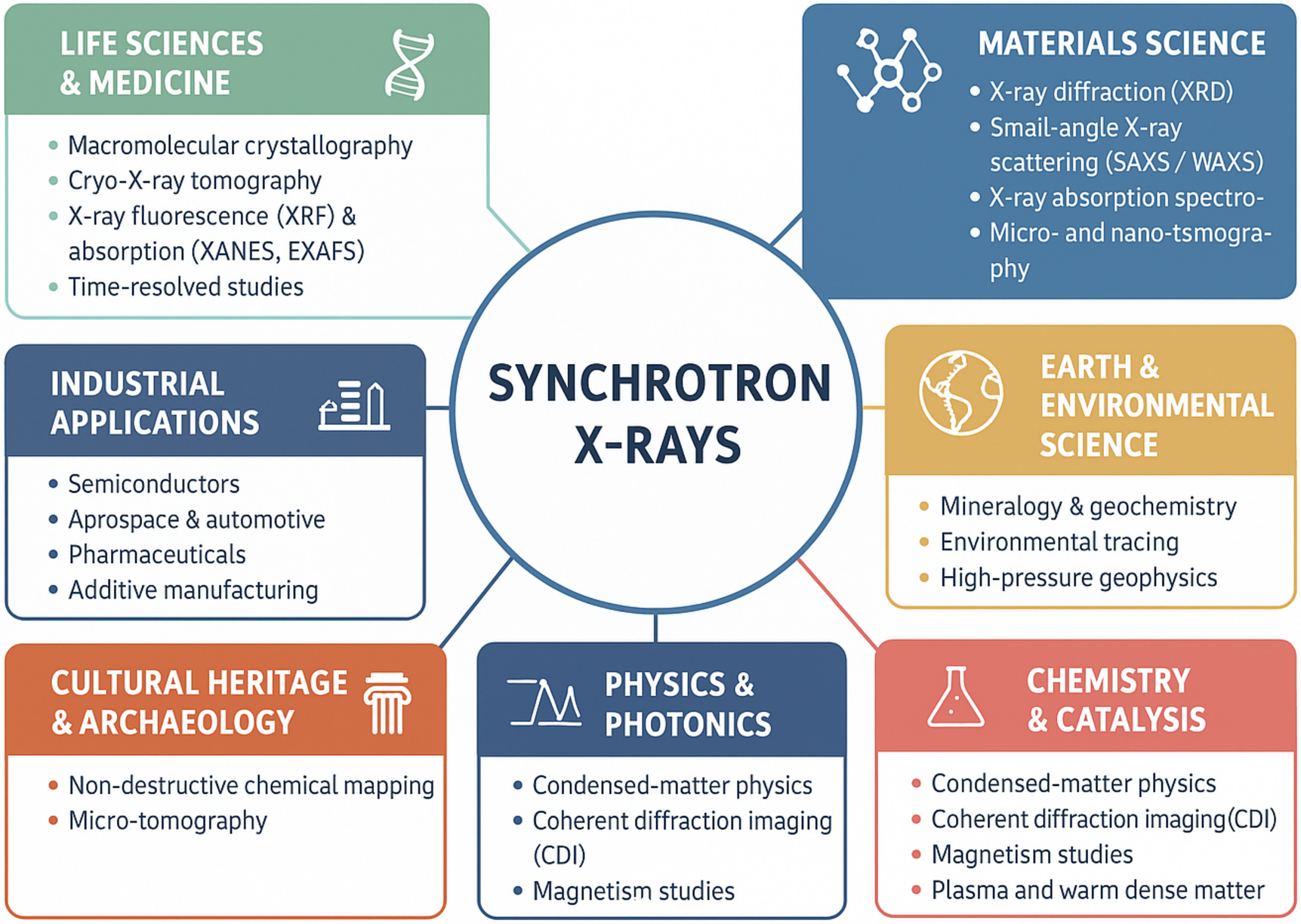

IMPERIAL

Thank you

Betatron Radiation - Applications
07/10/2025

Future Uses of betatron sources